ADAPTIVE CONTROL METHODS FOR NON-LINEAR SELF-EXCITED SYSTEMS

by

Michael A. Vaudrey

Dissertation submitted to the Faculty of the Virginia Polytechnic Institute and State University in partial fulfillment of the requirements for the degree of

DOCTOR OF PHILOSOPHY IN MECHANICAL ENGINEERING

GRADUATE COMMITTEE

William Saunders, Chair

William Baumann

Uri Vandsburger

Harry Robertshaw

Donald Leo

August 28, 2001

Blacksburg, Virginia

Keywords: Adaptive Feedback, Thermoacoustic Instability, Neural Network, Time Averaged Gradient, Least Mean Square Algorithms, Combustion Control

ADAPTIVE CONTROL METHODS FOR NON-LINEAR SELF-EXCITED SYSTEMS

Michael A. Vaudrey

ABSTRACT

Self-excited systems are open loop unstable plants having a nonlinearity that prevents an exponentially increasing time response. The resulting limit cycle is induced by any slight disturbance that causes the response of the system to grow to the saturation level of the nonlinearity. Because there is no external disturbance, control of these self-excited systems requires that the open loop system dynamics are altered so that any unstable open loop poles are stabilized in the closed loop.

This work examines a variety of adaptive control approaches for controlling a thermoacoustic instability, a physical self-excited system. Initially, a static feedback controller loopshaping design and associated system identification method is presented. This design approach is shown to effectively stabilize an unstable Rijke tube combustor while preventing the creation of additional controller induced instabilities. The loopshaping design method is then used in conjunction with a trained artificial neural network to demonstrate stabilizing control in the presence of changing plant dynamics over a wide variety of operating conditions. However, because the ANN is designed specifically for a single combustor/actuator arrangement, its limited portability is a distinct disadvantage.

Filtered-X least mean squares (LMS) adaptive feedback control approaches are examined when applied to both stable and unstable plants. An identification method for approximating the relevant plant dynamics to be modeled is proposed and shown to effectively stabilize the self-excited system in simulations and experiments. The adaptive feedback controller is further analyzed for robust performance when applied to the stable, disturbance rejection control problem. It is shown that robust stability cannot be guaranteed because

arbitrarily small errors in the plant model can generate gradient divergence and unstable feedback loops.

Finally, a time-averaged-gradient (TAG) algorithm is investigated for use in controlling self-excited systems such as the thermoacoustic instability. The TAG algorithm is shown to be very effective in stabilizing the unstable dynamics using a variety of controller parameterizations, without the need for plant estimation information from the system to be controlled.

ACKNOWLEDGEMENTS

I must extend endless thanks to Will Saunders and Bill Baumann, my wife Mandy, and my parents Walt and Sandra. Without any of whom, none of this would have been possible.

TABLE OF CONTENTS

LIST OF FIGURES

LIST OF TABLES

Chapter 1

Introduction

Self-excited systems are open-loop unstable plants whose time response to any arbitrary input increases exponentially until a physical limit is reached. Once that physical limit is reached, typically in the form of a saturation non-linearity, the system will oscillate by entering into a stable limit cycle. Because the system is open-loop unstable, an external input is not the source of disturbance; the disturbance is self-generated from within the plant. Figure 1.1 illustrates a simplified block diagram of a generic self-excited system.

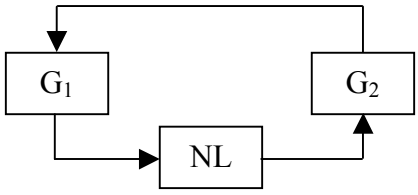

FIGURE 1.1 GENERIC SELF-EXCITED SYSTEM

In this case, G_1 and G_2 may be stable systems themselves, but when their outputs are connected to their inputs, the resulting dynamics generate at least one unstable pole. Because time responses of physically realizable systems do not increase exponentially forever, a nonlinearity (NL) is included to limit the loop gain.

One physical example of a self-excited system is a thermoacoustic instability. Most recently, attempts to reduce pollutant emissions from land-based gas turbines using lean fuel/air ratios have exacerbated this instability problem. Interaction between lightly damped acoustics and unsteady heat release rate generate the closed loop system of Figure 1.1. For relatively moderate levels of heat release, this self-excited system will exhibit non-linear limit cycling behavior, releasing energy in the form of sound pressure. For higher levels of heat release this sound pressure can induce vibrations that can physically damage

the combustor. It is therefore necessary to implement control procedures to permit lean fuel/air ratios while preventing the instability from reaching unacceptable levels.

Figure 1.2 illustrates[1] a generic control approach where acoustic actuation and sensing are the respective output and input to a feedback controller H. In the case of the thermoacoustic instability illustrated in Figure 1.2, G_A represents the acoustic transfer function between unsteady heat release rate and acoustic velocity and G_F is the flame dynamics transfer function whose output is the unsteady heat release rate. This feedback loop can become unstable and is limited by a non-linearity (NL) depending on combustor operating conditions.

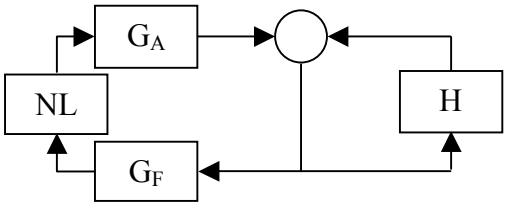

FIGURE 1.2 GENERIC THERMOACOUSTIC INSTABILITY CONTROLLER IMPLEMENTATION

To the controls engineer it will be clear that limit cycle oscillations cannot be globally suppressed without using some form of *feedback* control. Feedforward control can only modify the zeros of a plant. In the case of the self-excited system, the limit cycling oscillations are generated from an unstable pole which must be relocated to the left half plane to reduce those oscillations. System poles can only be affected by using feedback control.

Because of the wide range of operating conditions for gas turbines, passive solutions are hard to achieve and active combustion control is a promising alternative. **This research is focused on the design, analysis, and implementation of a variety of *active* control approaches for designing "H" in Figure 1.2 to achieve stabilizing, or attenuating control of the limit cycling plant**. It is also important to note that the controller designs

[1] Note that all summing junctions in figures throughout this document are assumed to be positive unless otherwise noted with a negative sign on the appropriate terminal.

examined herein are strictly designed to *stabilize an already unstable system*. This is a significantly different problem from the goal of keeping a stable system stable, or actively preventing an instability from occurring. The control methods, simulations, experiments, and conclusions presented in this work *do not* directly address this problem and generally ignore transients between stable and unstable combustor conditions.

The control methods and analysis presented here enjoy a wider berth than the restricted application to thermoacoustic instabilities. The thermoacoustic instability is a physical example of a self-excited, or open loop unstable, system. In fact, the controller design methods presented here are also applicable to the generic self-excited system as shown in Figure 1.3.

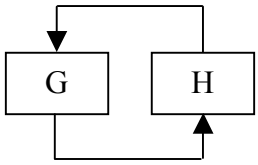

FIGURE 1.3 GENERIC SELF-EXCITED SYSTEM CONTROL IMPLEMENTATION

Figure 1.2 is easily represented by Figure 1.3 by closing the self-excited loop so that

$$G = \frac{1}{1 - G_A G_F NL} \qquad \textbf{[1.1]}$$

where "NL" is a DC gain that can be obtained from the describing function analysis dependent upon the form of the non-linearity. Since the hot acoustics and flame dynamics are both present in the feedback loop when the combustor is operating, the plant of [1.1] is open-loop unstable.

1.1 RESEARCH GOALS

Classical disturbance rejection can add damping to a linear system in the form of a feedback compensator. Such a compensator is designed to have high open loop gain between phase crossover frequencies to ensure low closed loop amplitude where required. This concept also

applies to a self-excited system, but the gain required to completely stabilize the system cannot be known without knowing the exact (linear) location of the unstable pole of [1.1]. This is a difficult task for the combustion modeling community, and is an area of ongoing research.

Further complications in controlling the self-excited system are twofold. First, the operating conditions or power load of the combustor may change causing the plant dynamics to change. If this occurs, the limit cycle frequency may also change, requiring a new controller design for each operating and load condition. Second, the presence of the feedback controller itself may cause changes in the heat release dynamics which will cause changes in the acoustics, and ultimately the system pole locations. Essentially, the static feedback controller designed for the limit-cycling system may not be a stabilizing controller solution for the system after the control loop is closed. This effect presents a very daunting modeling task where the exact behavior of the nonlinearity must be known to predict the controller's impact on the physical system.

The fixed gain feedback controller (dynamic compensator that is not continually updated) has not been found to be a practical solution to this time varying plant. The variation in plant dynamics that occurs over a range of combustor operating conditions prevents even a robust fixed gain controller from achieving stabilizing performance over all of those operating conditions. The next logical step taken by researchers has been the use of adaptive controllers that vary their control parameters in response to changes in the plant. While a relatively large number of researchers in this field have implemented adaptive controllers both in simulation and experimentally, few have appreciated some of the complexities that may be encountered during control.

Some of the deficiencies in prior research and the lack of a robust algorithmic approach to thermoacoustic instability control have motivated this research. Beginning with static feedback control, the robust implementation issues discussed above prevent it from being a viable solution to the control problem. However, as mentioned earlier, all control approaches that hope to stabilize the self-excited system *must* close the loop using feedback control. Previous researchers have met with some success in establishing attenuating control at specific operating conditions using phase shifting feedback controllers. However, many research efforts

described "secondary peaks" when the loop was closed, that prevented significant control. **The first goal of this research was to identify the source and solution to these secondary peaks so that stabilizing feedback control could be enabled**.

The second main goal of this research was to examine in detail, Filtered-X least mean squared (LMS) adaptive control approaches to control of the thermoacoustic instability. The lack of an uncontrollable reference signal makes this problem non-trivial, and necessarily feedback in nature. Previous investigations of adaptive control approaches have met with varying degrees of success, with nearly all describing anomalous behavior. Because of the time varying nature of the plant, it is clear that the successful controller will adapt to maintain stabilizing control. With classical adaptive control considered as a viable solution, it was the goal of this research to fully characterize the performance of (feedback) LMS based controllers and provide any alternate solutions or recommendations.

In addition to solving problems of prior research, an opportunity exists for developing new and innovative controller designs to attenuate the limit cycle instability. **Therefore the final goal of this research was to develop new and intelligent controllers for stabilizing self-excited systems**. Artificial neural networks and time averaged gradient algorithms are offered as new solutions to the active control problem presented by the thermoacoustic instability.

1.2 CONTRIBUTIONS

There have been a variety of contributions made by this research while addressing the aforementioned goals. The most significant contributions to the state-of-the-art are summarized here.

As mentioned above, **fixed gain feedback controller design** (à la "phase shifting feedback control") was plagued by "secondary peaks" and the inability to achieve stabilizing control. This phenomenon was more aptly renamed "controller induced instabilities" as a result of this work. A **system identification procedure** was developed that resulted in the ability to design a feedback controller *a priori* that prevented the formation of controller induced instabilities. While it is not possible to ensure stabilizing control (because the gain of the nonlinearity is

unknown), a specific controller frequency response can be evaluated for effectiveness at attenuation while preventing additional instabilities. More effective controller designs then become apparent as a result of heuristic examination of the system identification.

Building on the feedback controller and system identification technique developed early in this work, an **artificial neural network** was constructed that predicted the open loop plant dynamics based on combustor operating conditions. The resulting open loop frequency response is then used by a rule based design algorithm to continually update the feedback controller. While the real-time implementation demonstrated effective control over a wide range of operating conditions, some researchers may perceive the process to be too cumbersome for practical application. In addition the ANN is not scalable to different combustor rigs without new training data sets. Nevertheless, this control approach was not previously investigated and it effectively solved many of the problems plagued by manual and adaptive feedback controller designs.

The specific method of **adaptive feedback control** examined in this work has not been addressed by prior researchers investigating self-excited system control. The predominant mode of previous adaptive control approaches has been the application of an adaptive IIR LMS controller. Using an appropriate plant identification technique not previously investigated, it is shown that an FIR filter can achieve stabilizing control. A variety of **stability issues** associated with adaptive feedback control are also identified and explained in detail. Two distinct instability mechanisms are identified: feedback loop instabilities and algorithm divergence. Both are shown to generate unexpected loss of control for arbitrarily small plant estimation errors. Yet another **intermittent instability mechanism** is identified and explained with respect to actuator authority and control of the self-excited system.

Finally, the **time averaged gradient** (TAG) algorithm is applied to the self-excited plant. The TAG offers a new solution for adapting both the magnitude and phase of a feedback controller without the need for an estimate of the plant. All LMS based adaptive approaches, as well as neural network approaches, rely on the ability to have an accurate estimate of the control-to-error path. A solution is offered here that can be applied instantly on any combustor

independent of operating conditions. Additional rule based parameters are also investigated to improve the performance of the algorithm for the general combustion plant.

1.3 DOCUMENT OVERVIEW

Chapter 2 summarizes the relevant literature on thermoacoustic instabilities and their control. In general this represents the most seminal papers and most recent work in the areas of adaptive control, neural network control, and time averaged gradient control. There are also sufficient references presented for the reader to obtain an understanding of the thermoacoustic instability and how it can be modeled. This literature is relevant for the model used throughout this work in various simulations.

Chapter 3 is primarily offered as background material to introduce the control of the thermoacoustic instability using fixed feedback controllers. However, it is important that the reader is familiar with the system identification approach described in this chapter since it is referred to throughout the remainder of the work in reference to both adaptive feedback control and the artificial neural network controller. In addition, the fixed gain feedback controller described in Chapter 3 is typically used as a performance baseline to which other control approaches are compared. This is also an important chapter for the reader because it introduces the thermoacoustic instability simulation model used throughout the remainder of the text. Portions of this chapter were published in [16] and [17].

The fourth chapter describes the artificial neural network control approach in detail. The feedback controller design employed by the neural network is described in detail in Chapter 3. The discussion of the neural network is self contained in Chapter 4, presenting the training, design and fuzzy controller update as well as the experimental results. The majority of this chapter was taken from [19]; with the exception of additional material explaining the limitation of controllable operating conditions. Appendix A provides the real-time C-code used for implementing the artificial neural network and associated controller design algorithm.

Chapter 5 presents the application of adaptive feedback control to the thermoacoustic instability. The results of Chapter 5 show stabilizing control using an appropriate plant

estimate proposed by this work. In addition, an intermittent searching condition is identified and shown to be due to actuator authority limitations. Although a majority of this chapter has been submitted in [57], additional evidence of the searching phenomenon is included here. Appendix B provides the MATLAB simulation code that was used to demonstrate the effectiveness of the proposed identification technique for adaptive feedback control.

The detailed stability analysis of the adaptive feedback controller used in Chapter 5, is presented in Chapter 6. Analysis of the loop instability and algorithm divergence is presented as a function of magnitude and phase error in the control-to-error path estimate required in Filtered-X formulations. Although robust stability can never be guaranteed, a new method for a weighted online system identification is presented that can reduce some of the errors encountered in initial system identification. The majority of Chapter 6 is taken from the submitted article [58]. In general, Chapters 5 and 6 can be read independently from each other and from the other chapters herein.

Finally, Chapter 7 presents the design and implementation of the time averaged gradient control algorithm. Simulation and experimental results are provided that illustrate its effectiveness on a variety of platforms. Appendix C provides a MATLAB code that can be used to simulate the TAG algorithm for control of a self-excited system. Since the majority of Chapter 7 was taken from [59], it can be read independently from other chapters in this text.

Although somewhat modular, this document presents a variety of different controller designs that are all used to accomplish the same goal: adaptive control of a self-excited system. The TAG algorithm is shown to provide the most robust and effective performance of all control methods examined. The neural network approach provided acceptable control over a variety of operating conditions, but requires a training procedure that is difficult and time consuming, and is not portable to combustors of different geometries. Adaptive feedback control methods utilizing the filtered-X LMS algorithm were shown to be effective at controlling a single operating condition, but have significant stability limitations preventing stabilizing performance over a wide range of operating conditions. Because of inherent controller design differences, some of the chapters can be read alone, without loss of generality. However, taken as a whole,

the reader can better appreciate the difficulties encountered in designing self-adaptive controllers for unknown self-excited systems.

Chapter 2

Review of Germane Literature

This chapter provides a review of the state-of-the-art in the areas of adaptive control and control of the self-excited combustion plant; and more specifically, the use of adaptive control methods in controlling the thermoacoustic instability. These areas of the literature are (and have been) very active for several years. Well known researchers continue to examine different adaptive techniques in hopes of finding a robust and practical solution to the problem of controlling the self-excited system. Because of the large amount of literature existing in these research areas, only the most relevant articles are addressed directly while others are included as references.

In order to provide the reader with an appreciation of the available literature and the progression of adaptive control techniques applied to thermoacoustic instabilities, a brief review of the general literature is presented first. This will address accepted practices in combustion instability modeling and feedback control considerations used throughout this work. The remainder of the literature review is divided into two sections that separately cover the application of adaptive control methods to combustion instabilities and adaptive control theory as it applies to this work. Throughout this discussion the deficiencies of the prior art are pointed out with respect to the primary contributions made by this work.

2.1 COMBUSTION INSTABILITY MODELING AND CONTROL

Thermoacoustic instabilities in combustors occur as a result of a self-excited feedback loop between unsteady heat release rate and acoustic pressure. For relatively moderate levels of heat release, this self-excited system will exhibit non-linear limit cycling behavior, releasing energy in the form of sound pressure. There have been a multitude of papers published and presentations given on developing models of this self-excited feedback loop through coupling

of an acoustic model with that of an unsteady heat release rate forcing function [1,3-7]. Most of these approaches generally result in a reduced order model that can be used to represent the pressure/heat release rate interaction. In [2], Annaswamy developed a feedback model of the combustion instability process that was represented by a lightly damped acoustic mode in a feedback loop with a low pass filter. With an appropriate cutoff frequency and gain, this closed loop system will generate an unstable pole which can be limited by some arbitrary saturation non-linearity. This establishes the precedent for the system model used exclusively in simulations throughout this work.

As long as combustion instabilities have presented vibration and acoustic problems, researchers have sought to control them. While both passive and active control techniques are viable solutions, the bulk of research has focused on active control due to the potential for limited sized components and tracking through changing operating conditions. Dowling (among others) in [10] provides a brief overview of the concept of feedback control to suppress the instabilities encountered in the combustion process. The fundamental concept of feedback control (and ultimately all control methods for this system) is to apply enough negative gain at (generally) a single frequency so that the unstable pole is stabilized. Barring that, enough damping is added to at least reduce the limit cycle amplitude to acceptable levels. Fixed gain feedback control has been accomplished with varying degrees of success in [13-15]. Earlier experiments were often plagued with what some researchers called "secondary peaks". From the literature, it was clear that many experimentalists did not realize that these were actually controller induced instabilities caused by excess gain at out-of-band phase crossover points when the controller formed a second feedback loop (the first being the unstable combustion loop). This was later explained in detail in [16-18].

Early feedback control design techniques used a fixed (or sometimes manually adjustable) gain and a manually adjustable phase delay to drive an actuator. These "phase shift controllers" are actually very simple feedback controllers, using a measurement of the unsteady heat release rate or pressure fluctuation to drive the controller. More sophisticated feedback controller designs were employed in [11] and [12]. However, compared to an intelligent loopshaping design technique as in [16], it is difficult to justify the more complex (and inaccurate) model based

techniques for single-input single-output control systems. (Further background information on the design of feedback controllers for the self-excited system is provided in the following chapter).

The relevance of the type of actuator used in these control systems should be addressed. There are typically two types of actuation that are used in control of combustion instability: acoustic (or air flow) actuation and fuel flow actuation. In practice it is considered more practical to use fuel flow actuation because fuel injectors require less drive power and space than acoustic actuators delivering equivalent control power. In practice, acoustic drivers (speakers) cannot reasonably supply the required power to control the potentially high sound pressure levels in a relatively confined space; acoustic pressures inside limit cycling combustors will typically exceed 150 dB SPL. There are many discussions of the application of fuel flow modulation to the suppression of combustion instabilities including [8] and [9]. However, the precise mechanism of the interaction of the modulated fuel with the primary flame is still a topic of current and future research. Simulation of acoustic actuation versus fuel actuation only requires a change in the input location of the control signal. This will not significantly affect the controller designs or their performances as presented in this work.

The contributions of this work include the development of new controller designs and analyses that will be useful in the control of combustion instabilities. While actuator power and practical implementation of that actuator is always a consideration in control system design, that is not a focus of this research. The simulations used to test the control techniques assume acoustic actuation. Although the majority of the experiments described in this work use an acoustic actuator coupled directly to the combustion chamber, a number of tests have been performed using a fuel injector as the actuator. The performance characteristics of the various control strategies that have been developed should not vary as a function of the actuator, since all are designed to reduce the pressure to an (ideally) stable operating point.

2.2 APPLICATION OF ADAPTIVE CONTROL TO THE SELF-EXCITED COMBUSTION INSTABILITY

Within this work there are three general adaptive approaches examined: artificial neural network based feedback control, adaptive filtered-X based control methods, and time averaged gradient control methods. Therefore, there are three main areas of the literature that are relevant to the respective techniques investigated. It is interesting to note that very little prior work has been done in either the area of neural network control of combustion instabilities or the use of time averaged gradient control. In fact, these are the two methods that hold the most promise for providing repeatable and comprehensive control of the self-excited system.

2.2.1 NEURAL NETWORKS IN COMBUSTION CONTROL

Blonbou and Laverdant in [20] provide the only notable application of a neural network toward the control of combustion instabilities. Their discussion is not detailed enough to fully understand the exact implementation of the multi-network approach. It appears that one neural network is used as a model of the plant transfer function while the other is used to provide a control output. The control results appear to stabilize the combustor over a variety of operating conditions. The specific structure of Blonbou's application of a neural network is very different than the structure presented herein. This research presents a single neural network used to generate a complex valued frequency response function representing the unstable combustor FRF. This is then used with a rule based algorithm that designs a feedback controller using a loopshaping technique [19]. It is interesting to note that the results from the technique of Blonbou and the neural network application presented here, were made public at precisely the same time in two different parts of Germany. The performance characteristics of stabilizing control over a variety of operating conditions are consistent between both methods of controller implementation; this is a characteristic that is not typically seen in other types of adaptive control.

2.2.2 LMS BASED ADAPTIVE CONTROL IN COMBUSTION CONTROL

Given the popularity and ease of implementation of Widrow's LMS adaptive algorithm [49], it is not surprising that LMS based control methods are most commonly applied to combustion

instabilities. Many times however, these algorithms are applied blindly without regard to the application because it is simply assumed that "adaptive feedforward control" is synonymous with stable control. This section provides references and brief discussions of the prior art in the area of applying adaptive control to the unstable combustion plant. All of these approaches are based on a variation of the commonly known filtered-X LMS algorithm, called the filtered-U LMS algorithm (or adaptive IIR filtering) [48].

Billoud's [22] application of the filtered-U algorithm to the combustion instability problem is referenced by most adaptive implementations that follow it in the literature. Kuo in [48] provides a discussion of the application of the filtered-U algorithm used by Billoud to noise control problems. He states that because of the inherent ability of the adaptation scheme to adapt the poles of the filter, stability cannot be guaranteed. In addition, because of the lack of persistent excitation and the diminishing reference signal due to feedback interaction, it cannot be stated that the filters approach their optimum values. Given this, it is not surprising that Billoud finds divergent behavior for some combustion control experiments using the filtered-U LMS. Adding to the uncertainty of his application, he does not attempt to find an accurate system identification, required by the adaptive filter to ensure stable convergence. Instead he uses a gain and phase delay to represent the control-to-error dynamics. (This is also the case with [30]). The method of adaptive control examined in the present research is shown to be convergent and stable for cases where no error exists in the plant estimation. It differs from the filtered-U because the reference signal is derived directly from removing the influence of the control signal from the error signal. As the plant estimate approaches the actual plant, this is identical to purely feedforward control.

Other researchers following Billoud's work have incrementally added features to the filtered-U approach. Kemal in [25] presented very similar results to that of Billoud using almost the same control architecture. He compares the IIR performance to that of a simple FIR implementation in a purely feedback system. Again it is not surprising to find that neither controller worked admirably (IIR because of adapting poles and FIR because the feedback loop was not accounted for). Further advancements in the automation of the system identification process have been discussed in [27-29]. The results of these studies are mixed:

some are model based simulations giving exceptional control and others are practical implementations exhibiting some amount of controller induced instability. There are inherent problems in this particular control approach that are either ignored or accepted by each of the studies:

- Potential instability of feedback loops created when control system is engaged
- Inherent instability of adaptive IIR filter from adaptation of poles
- Sensitivity to the error in the plant estimate
- Inappropriateness of online ID of a closed loop system when only the control-to-error path is required

Each of these issues are addressed in this work.

A notable class of adaptive filtering techniques has departed slightly from the standard filtered-X LMS based approaches. Self tuning regulators as discussed in [24-26] are model based control approaches that attempt to adapt to a stable control solution using certain model parameters of the combustion process. As the name implies, these are model based approaches and hold little practical appeal until combustor models accurately predict thermoacoustic instabilities.

Several experimentally motivated researchers have reported varying results of controlling combustion instabilities using adaptive controllers [30-33]. These publications are primarily focused on reporting the results of tests on actual combustion systems rather than explaining the details of the controller design. In [30], Mohanraj and Zinn use the same adaptive IIR structure proposed by Billoud, using a tunable delay as the plant estimate. They also reinforce statements made by Billoud concerning the inability of an FIR filter to control the combustion plant, but neither author discusses why this is the case. In fact, the FIR filter can be (and in this work is) used to stabilize the combustion plant if proper conditioning of the error signal occurs. In [31] Ziada and Graf use a commercially available "black box" feedforward controller from Digisonix to stabilize a household burner instability. They have no discussion of the details of the controller design but it exhibits exceptional results, clearly stabilizing the

plant. Finally, Johnson et. al. in [33] presents results of instability control using an adaptive controller and real time observer that is stated to be proprietary. Two statements clearly differentiate this approach from the gradient search (to which it most closely seems to relate): "A first step towards the development of an adaptive scheme was an online identification process that utilized the observer to determine the optimal control phase in an already unstable combustor" and "Future development of the adaptive algorithm will include adaptation of the control gain in addition to the control phase…". It is clear that they are not adapting both gain and phase and that they still require a plant estimate.

The most recent literature in the area of applying adaptive control to the unstable combustion plant continues to ignore some critical elements of performance. Most researchers focus on the application of the filtered-U LMS algorithm (an adaptive IIR filter) to the combustion plant. Some publications describe effective model based control approaches, but rely on inherent knowledge of the combustion process. All researchers in this area seem to have ignored several key elements that are contributions made by this work:

- The feedback loops generated from closing the loop with a controller can become unstable during adaptation, independent of the LMS algorithm convergence.
- An adaptive feedback approach using a measured estimate of the plant can stabilize the combustion system using an FIR adaptive filter. No one has applied this approach to the combustion plant.
- The system identification that is typically carried out can result in large errors between the estimated plant and the actual control-to-error path. These errors are significant in both ensuring algorithm convergence over a wide band and reducing the effect of potentially unstable feedback loops.
- On-line system identification during closed loop control, using the filtered-U approach is generating an incorrect representation of the plant dynamics.
- Stable convergence using the filtered-X based adaptive feedback controller cannot be guaranteed because of the inability to accurately know the actual control-to-error dynamics for the closed loop system.

2.2.3 GRADIENT BASED ADAPTIVE METHODS IN COMBUSTION CONTROL

The time averaged gradient approach developed as part of this work permits adaptation of both magnitude and phase without the need for an estimate of the plant dynamics. It is a simple algorithm based on perturbing weights and measuring the resulting gradient. There is only one instance in the combustion control literature where a similar algorithm has been developed. Presented in May 2000, Banaszuk et. al. in [34] discussed results of a "triangular search algorithm" as a self-exciting adaptation algorithm, not requiring external probing as in extremum seeking controllers. They reference the description of the algorithm to an article by Zhang [36]. The triangular search algorithm updates the control signal directly and requires no external probing to identify the direction of the gradient. The algorithm is not designed to alter different feedback controller parameters because it updates the control signal and not a control filter; this limits its applicability to multivariable and parameterized control. Similar to extremum control, this algorithm has not yet been altered to adapt both phase and magnitude. The time averaged gradient algorithm presented here accomplishes a similar goal of minimizing the error without a plant estimate, but can do so through a variety of parameterizations and control design structures.

2.3 ADAPTIVE CONTROL LITERATURE

Distinct from the application based literature, the stability and performance characteristics of adaptive controllers in general have been studied. However, as rigorous as many of these publications can get, only one mentions the potential instabilities associated with feedback loops during adaptation of adaptive controllers applied to feedback systems. Leboucher et.al. in [53] describes the existence of feedback loop instabilities for filtered-U adaptive controllers. However, she attempts to provide a well-defined measure to analyze the stability of any system as a function of the adaptive parameters. The difficulty here is that all systems are different and loop stability cannot be categorized by a uniform index. Most studies provide varying approaches to examine the effect of choosing the appropriate convergence parameter on fast adaptation, or the effect of model errors in simple feedforward arrangements.

In [37], Feintuch presents the first adaptive recursive filter structure in the literature. The stability of the IIR adaptation is not addressed until later publications such as [42] and [51]. (Other stability analyses and algorithm modifications of the filtered-U approach exist in the literature but are not presented here).

There are multiple analyses available including [39-41] that present the commonly known constraint on control-to-error path identification error of ninety degrees. Each derive the solution using different methods but come to the same conclusion. However, the 90 degree stability criteria has only been proven for sinusoid inputs and special sampling constraints. Broadband algorithm stability has not been shown to adhere the popular 90 degree rule although simulations and experiments continue to support it. Because each approach focuses on the standard filtered-X form of the LMS algorithm, no feedback loops are present. Therefore, in the purely feedforward sense, only the algorithm can lead to exponentially unstable behavior. This can be caused by an error in the plant estimate transfer function (as noted above), or by an inappropriately large choice of convergence step size. This is addressed in detail in [47] and again in [43]. Neither address the creation of feedback loop instabilities because they are dealing with the adaptive filter performance itself rather than the controlled system. A convergence analysis of the filtered-U algorithm is presented in [42]. This holds little relevance to the current work because the assumptions made by the analysis prevent practical application to non-minimum phase systems.

Research involving the time averaged gradient algorithm and its performance on dynamic systems is limited. The most significant contributions are by Clark et. al. in [52], Gibbs and Clark in [44], and Kewley et. al. in [45]. The primary focus is on the description of the algorithm itself and its application to harmonic control. It is explained in [45] that the desired perturbation size is a function of the desired mean squared error, since a perturbation from the optimal generates a time varying error away from the optimal. In addition, the perturbation must be large enough to provide an accurate measure of the gradient. These are primarily heuristic arguments because the uncertainty of a measurement cannot be known *a priori* for a physical system. A "new" gradient based algorithm is discussed in [55]. Presented as a least

squares gradient approach to adaptation, the algorithm is nearly identical to the time averaged gradient approach based on the method of steepest descent.

The literature presented in this section covered the state-of-the-art in adaptive control of thermoacoustic instabilities. It is apparent that there are still contributions to be made in the analysis and application of alternative, and potentially more useful, adaptive control strategies. The neural network control strategy presented herein has not been discussed prior to [19], published by this author. The potential for performance has been confirmed simultaneously and independently using an alternative approach in [20]. The filtered-U algorithm holds distinct disadvantages in control because of the adaptation of potentially unstable poles. Application of this to an unstable or lightly damped plant enhances the possibility of an unstable pole being generated. Nevertheless, combustion engineers continue to apply it to the combustion instability problem with widely varying results. The adaptive feedback approach presented here offers a more direct application of the filtered-X concept that can be analyzed in terms of the plant estimation error. Nevertheless, it has distinct disadvantages discussed in this work that limit it's potential for practical implementation. Time averaged gradient descent approaches may be the next logical step for combustion instability control, since they do not require a plant estimate and are easy to implement. To date, this approach has not been discussed in the combustion control literature.

Chapter 3

Feedback Control of a Thermoacoustic Instability

Static feedback control of thermoacoustic instabilities (also referred to as "phase shifting control") is a common choice among researchers for demonstrating effective control over the self-excited system. As a result, some of the material presented in this chapter is considered to be prior art, though unique contributions have been made in the areas of system identification and predictable and robust design of feedback controllers for the thermoacoustic instability. In addition to the new contributions, the motivating factors for the inclusion of this background material are threefold:

- This section attempts to familiarize the reader with the most rudimentary form of control that is typically employed in self-excited system control.
- The fixed gain feedback control technique serves as a reference point for measuring the relative performance and effectiveness of the various adaptive methods presented in subsequent chapters.
- The effective design of a feedback controller for the self-excited system must be well understood before a) the neural network design can be appreciated and b) the loop stability analysis of the adaptive feedback controller can be explained.

Feedback control system design, for general single-in-single-out (SISO) applications, requires accurate knowledge of the loop transfer function. Active combustion control design is usually implemented using such SISO architectures, but is quite challenging because the thermoacoustic response results from a relatively unknown, self-excited system. In addition there are non-linear processes that must be understood before learning the gain/phase relationship of the system precisely at the instability frequency. However, experiments and analysis presented here have shown that it *is* possible to obtain accurate measurements of the

relevant loop frequency response functions at frequencies *adjacent* to the instability frequency. Using a simple tube combustor, operating with a premixed, gaseous, burner-stabilized flame, these loop frequency response measurements have been used to develop a methodology that leads to 'test-based predictions' of the absolute phase settings and 'best' gain settings for a proportional, phase-shifting controller commanding an acoustic actuator in the combustor.

The contributions of this methodology are twofold. First, manually searching for the required phase setting of the controller is no longer necessary. In fact, this technique allows the exact value of controller phase to be determined without running the controller. To the author's knowledge, this has not been previously reported in the literature. Second, the 'best' gain setting of the controller, based on this new design approach, can be defined as one that eliminates or reduces the limit cycle amplitude as much as possible without generating controller-induced instabilities. Controller induced instabilities result from excessive gain applied by the controller at open loop phase crossover frequencies resulting in amplification in the closed loop system. Excessive gain can cause this amplification to become unstable. It is shown that the tradeoff in limit cycle suppression and avoidance of controller-induced instabilities is actually the well-known tradeoff in the sensitivity/complementary sensitivity function for feedback control solutions.

3.1 LIMIT CYCLE CONTROL AND SYSTEM STABILITY

Determining the stability of a physical system can be difficult in practice. Without an accurate model, it cannot be stated with any certainty whether a system is unstable, or very lightly damped. The time and frequency responses between a lightly damped (stable) complex pole and a linearly unstable, limit-cycling instability can look identical. Whether a system is limit cycling or oscillating due to lightly damped dynamics, does not govern the decision to apply control. Instead, an accurate measure of a thermoacoustic system requiring control is based on an unacceptable noise level or vibration level generated from a particular operating condition. In general, this work has assumed that an unstable plant exists when harmonics of a fundamental frequency appear in the pressure spectrum. In fact, this is only an indication of a non-linearity, and still does not confirm the exact linear system pole location.

Ultimately, the question of stability is not critical if the system requires control. The controller designs presented throughout this work are not strictly dependent on whether the system is unstable or simply lightly damped. This can be more easily understood by considering two linear systems. The first has a stable complex pole in the left half plane, but very near the imaginary axis, that dominates the time response and generates unacceptable acoustic or vibration levels. The second (linear) system has a complex pole in the right half plane. A nonlinearity exists in this system such that the time response will not increase without bound. We can assume that this nonlinearity limits the oscillatory response to the same magnitude as that of the lightly damped stable system. The open loop dynamics of these two systems are illustrated below in the complex plane

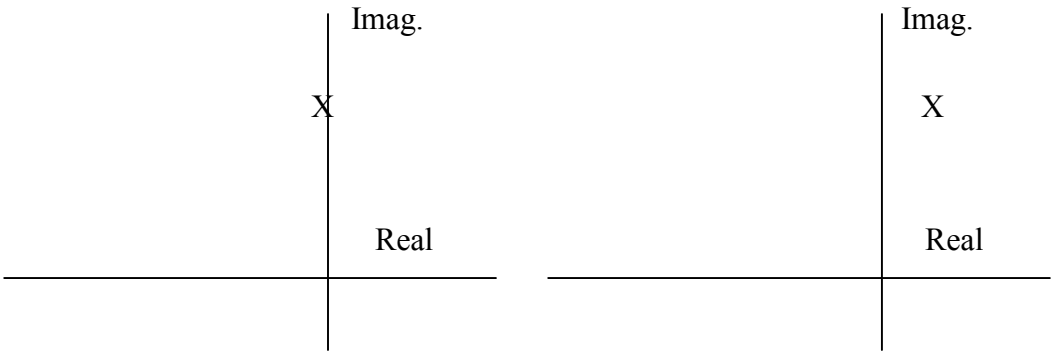

FIGURE 3.1 STABLE AND UNSTABLE SYSTEM DYNAMICS

The time responses and power spectra of the two systems (after a brief transient) will appear almost identical with the possible exception of harmonics in the limit cycling system.

Now consider a rudimentary controller design for the stable system that has the goal of reducing the damping, and thus the oscillation amplitude. Such a controller might have a complex zero in the left half plane to generate a more heavily damped closed loop pole. The same controller design applied to the unstable system (with the proper gain adjustment) will stabilize the unstable pole and create the desired damping on the closed loop pole. The root locus of each system is shown below for clarification of these points. (Note that two real poles were added to generate a causal controller and only the positive frequencies are illustrated).

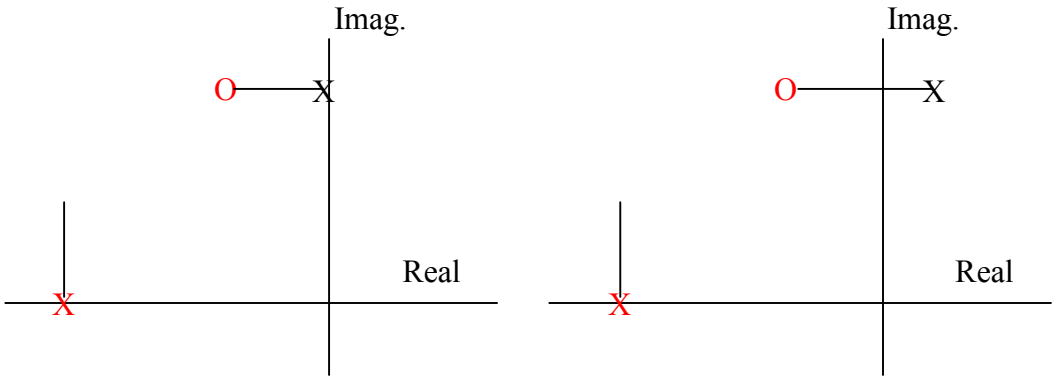

FIGURE 3.2 STABLE AND UNSTABLE SYSTEM CONTROL

The same feedback controller design applied to a stable and unstable system can accomplish the same desired goal of adding damping and reducing the oscillation. For the thermoacoustic instability, a single complex pole typically dominates the time response and this type of control strategy is employed. It is therefore irrelevant to the feedback controller design as to whether or not the system is stable or limit cycling, as long as the design goal remains: to reduce the oscillations.

It should be noted that feedforward control cannot alter system dynamics. Feedforward control is typically well suited to disturbance rejection for stable plants. It can add an out of phase signal to an existing disturbance, thereby reducing the oscillation and altering the zeros of the plant. However, strictly feedforward control is not capable of altering system poles and therefore is not well suited for adding damping to either stable or unstable systems where the disturbance is generated from within the plant. As will be shown, all practical implementations of adaptive schemes in the control of thermoacoustic instabilities are necessarily feedback in nature.

3.2 FEEDBACK CONTROL REVIEW

There are several linear control analyses that can be used to predict closed-loop performance from the open-loop transfer function [50]. One very useful tool for frequency-domain feedback controller design is the frequency response function (FRF). The frequency response of the open-loop transfer function, which includes both plant dynamics and the controller

dynamics, can be used to predict both closed-loop stability and performance by examining the gain and phase margins. It may be successfully argued that Nyquist plot representations, which supply identical stability/performance information for a feedback system, could be used for the following discussions. However, the author believes that the combustion community will benefit from the relative simplicity in understanding the FRF plots and Bode gain/phase rules versus the more challenging Nyquist diagrams.

In general, for negative feedback, a designer attempts to ensure that the open-loop gain (in log units) is less than -10dB at all phase crossover points (±180° multiples) and the open-loop phase is greater than 20 degrees away from the ±180° phase crossovers when the gain equals 0 dB. If these criteria are not satisfied at every frequency, an *increase* in amplitude of the closed-loop frequency response is predicted at those frequencies. This is sometimes termed "spillover", but is more aptly named "controller induced instabilities" in the following discussions [16]. In fact, a "controller induced instability" is not truly unstable, but has the potential to become unstable if the controller gain is continually increased; nevertheless this terminology has been adopted and is used throughout this work to describe increased closed loop frequency response amplitude due to controller dynamics. (It should be noted that this discussion also applies to positive feedback control, requiring only a shift of 180° in the stated phase margins).

For negative feedback systems, suppression of the noise entering the loop is achieved when the open-loop FRF gain is positive (decibel levels greater than zero, i.e. greater than unity magnitude) at frequencies having 0° phase values. The more positive the gain, the higher the suppression of those frequencies in the closed-loop frequency response. For plants with significant amounts of phase delay, closed-loop suppression will be limited to very narrow frequency regions. Fortunately, active combustion control only requires suppression of a very narrow bandwidth, making the feedback controller design a relatively easy task. The most common method of designing acoustically actuated feedback controllers for combustors has been to use a bandpass filter in conjunction with a manually operated phase shifter. Clearly if the plant were known, a fixed-gain controller could be designed *a priori* to suppress the

instability. However, until now, many researchers have used the phase shifting controller because the open-loop frequency response function has been unattainable; and thus a fixed-gain controller design was impossible. A measurement method that leads to prediction of the phase setting for the controller for any operating condition is discussed following a brief description of the experimental system used throughout this work.

3.3 RIJKE TUBE EXPERIMENTAL SYSTEM

The system used for this study as well as most of the subsequent adaptive experiments was a simple closed-open tube combustor operating with premixed air-methane. Figure 3.3 illustrates the test apparatus.

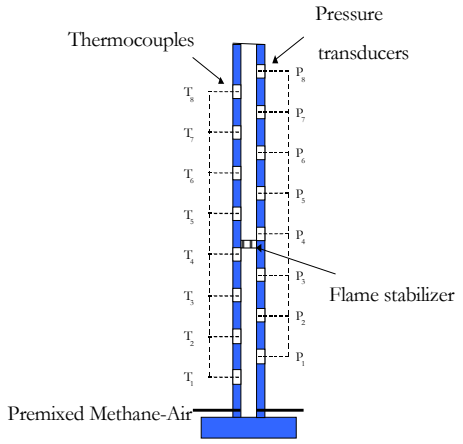

FIGURE 3.3 SCHEMATIC OF TUBE COMBUSTOR RIG

Figure 3.4 shows a picture of the actual Rijke tube combustor experimental setup. The silver cylinder on the side of the tube is the plenum to which the acoustic driver (3" speaker) attaches. This is shown in greater detail as the insert in the upper right corner of Figure 3.4.

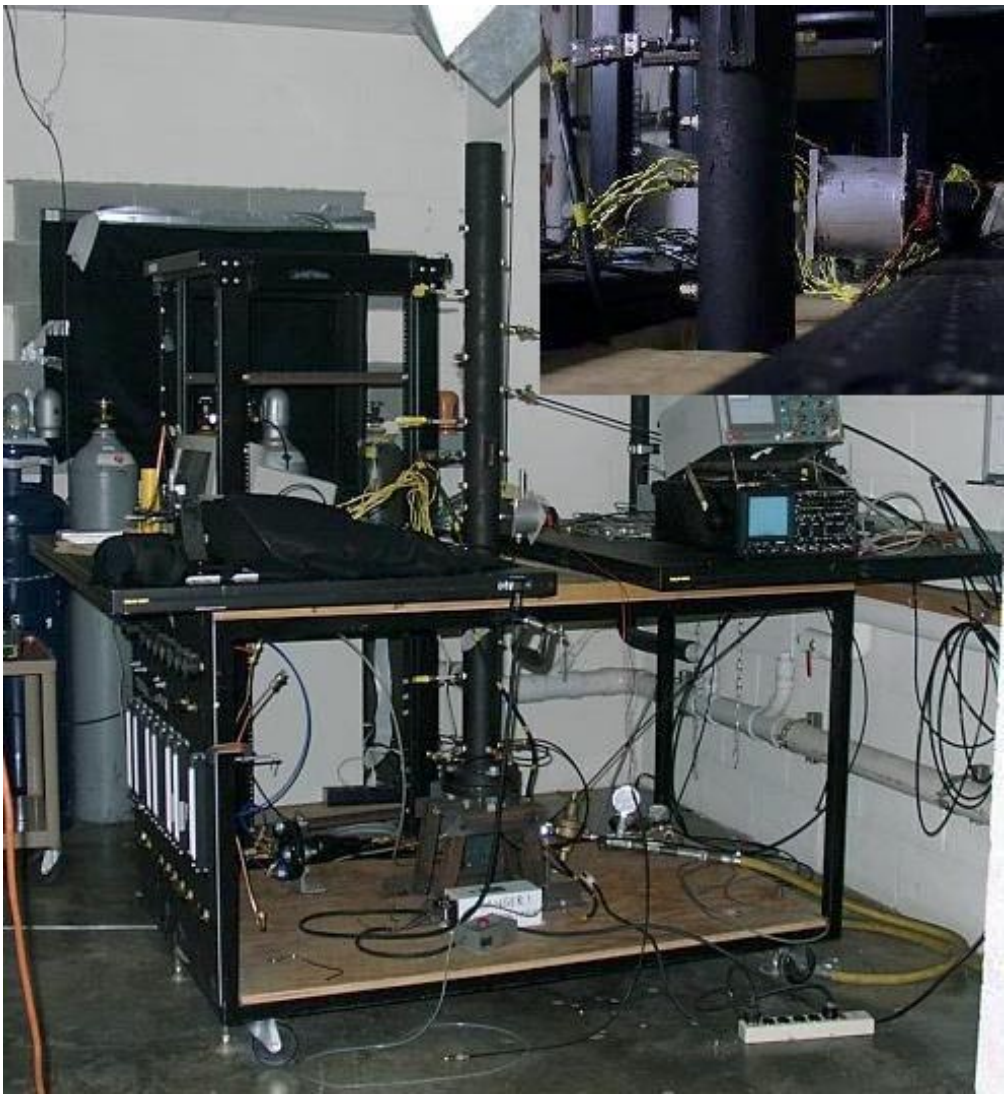

FIGURE 3.4 PICTURE OF RIJKE TUBE COMBUSTOR RIG

A ceramic honeycomb flame stabilizer was situated in approximately the center of the tube. The Rayleigh criteria [4] predicts interaction of the unsteady heat release rate from the flame and the acoustics of the combustor, resulting in an instability occurring for the second acoustic mode (180 Hz) of the tube. Using the same stability criteria discussed above, one could show that the open-loop gain of the self-excited system is greater than 0 dB at the phase crossover point 0° for positive feedback. Experimentally, this is not easily verified since the acoustics cannot be separated from the flame dynamics without breaking the self-excited loop, ultimately

altering both independent transfer functions. The controller loop, however, can be "broken" in order to examine the open-loop transfer function of the controlled system.

The open-loop transfer function (OLTF) block diagram is shown in Figure 3.5.

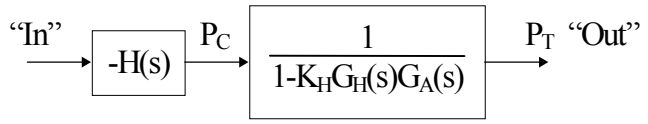

FIGURE 3.5 OPEN LOOP COMBUSTOR CONTROL SYSTEM

H(s) represents the digital feedback controller consisting of the following components in series: an anti-alias filter, A/D converter, digital phase delay, D/A converter, smoothing filter, power amplifier and a speaker. The speaker is attached to a small fitting that connects directly into the tube combustor at a location just below the flame holder (Figure 3.4). The pressure output of this actuator is considered to be P_C. This "controller pressure" then drives the tube which is itself a closed-loop system represented by the second block in Figure 3.5; where $K_H G_H$ represents the dynamics of the flame transfer function and G_A represents the acoustic plant. (Generally, the precise dynamics of the self-excited closed-loop FRF are still largely unknown to the accuracy required for generalized frequency domain controller design because $K_H G_H$ is not known). A pressure sensor at the bottom of the tube is used to measure the output of the path shown in Figure 3.5, consisting of the pressure generated by the self-excited oscillations plus the action of the controller.

Therefore, the plant dynamics shown in Figure 3.5 must be identified before the control design can proceed. It is shown next that the effects of the nonlinear thermoacoustic response are band-limited to a narrow range of frequencies spanning the instability frequency. The input for the system identification process was chosen to be a sine wave for the purpose of frequency-by-frequency identification. Ideally, a white noise source could be used in this case to identify all frequencies simultaneously, simplifying data collection. However, the limited power density available from the actuated random signal and the high amplitude instability from the self-

excited combustor, prevent adequate coherence between the input and output at multiple frequencies.

Many simulations of the thermoacoustic plant were also carried out to investigate various controller designs throughout this work. The general form of the simulated plant was similar in all cases. The acoustic transfer function was taken to be a lightly damped (ξ=0.02) complex pole at approximately 175 Hz (the second mode of the hot acoustics in the experimental setup). The flame dynamics were represented by a single pole low pass filter at approximately 200 Hz. Different levels of gain were added to the loop to simulate higher and lower heat release conditions requiring more or less control authority to stabilize. The nonlinearity was approximated by a hyperbolic tangent function. When simulated in the closed loop, depending on the loop gain, the system would reach a stable limit cycle well within one second. The controllers that were investigated in simulation (and experiment) were not engaged until the limit cycle was established. For the remainder of this work, this simulation format will be assumed unless otherwise noted. The details of several MATLAB simulations are also shown in the Appendix.

3.4 SYSTEM IDENTIFICATION

Because of the uncertainty in previous work concerning the plant to be estimated, the topic of system identification has not been addressed adequately. In [22] Billoud discusses using the Filtered-X algorithm where the plant estimate is either generated from a single tone identification near the limit cycle frequency or by using a gain and phase delay. Kemal and Bowman [23] discuss obtaining an open loop frequency response but do not provide details regarding the exact nature of the transfer function obtained. Ultimately they note that using a gain and delay appears sufficient for tonal control. Koshigoe et. al. [28] among others, have investigated using an online system identification procedure. Because of the feedback nature of the self excited system, the online identification will necessarily include the controller and feedback dynamics. If G_{ACT} is the correct estimate (as will be shown in a subsequent chapter), online identification procedures cannot produce the correct result after the loop has been closed.

The identification problem is to find a stable representation of G_{ACT} when we have access to the input to G_{ACT} but the only measurable output is P_T as shown in Figure 3.6.

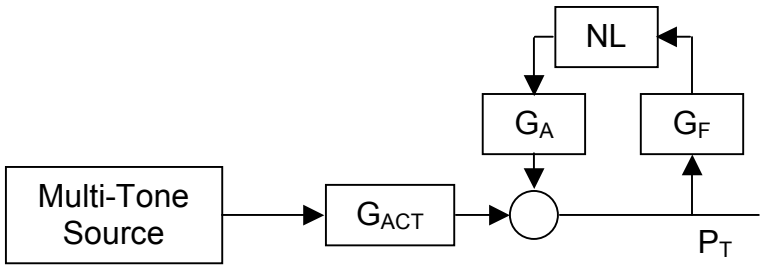

FIGURE 3.6 SYSTEM IDENTIFICATION DIAGRAM

Extinguishing the flame so that the physical feedback loop disappears is not an option since the hot acoustics, which are an integral part of G_{ACT}, are very different from the cold acoustics and are directly influenced by the flame temperature. Thus, the identification must take place in the presence of the thermoacoustic limit cycle.

The approach to identifying the open-loop plant relies on a probe signal consisting of low-amplitude sinusoids at frequencies near the limit-cycle frequency and within the passband of any bandpass filters used to filter the pressure signal before control. Using a Fourier transform of the output signal, the frequency response of the plant at a small number of frequencies can be determined. Using a least-squares approach, a low-order, discrete-time model can be fit to this data and is used as the model of the stable plant.

Since the open-loop plant is in a steady limit cycle, it is not immediately clear whether such an identification approach will produce a reasonable linear model or whether such a model will be stable or unstable. The experimental results have shown that very low-order linear models can account accurately for the frequency response data and that these models are always stable.

To understand this, consider the block diagram in Figure 3.6. From a describing function analysis, the gain of the limit cycle through the static nonlinearity is such that the total gain around the loop is unity. When a probe signal is injected into the system, we expect that the

frequency response at the probe frequency will be that of the linear system made up of the linear blocks in the diagram and with the nonlinear block replaced by a suitable linear gain.

To determine the value of this gain, consider an input to the nonlinearity of the form

$$x = A_1 \sin \omega_1 t + A_2 \sin(\omega_2 t + \theta) \qquad \textbf{[3.1]}$$

where ω_1 is the frequency of the limit cycle, ω_2 is the frequency of the probe and $A_1 >> A_2$. A first order approximation of the output of the nonlinearity, *f(x)*, is given by [3.2].

$$f(A_1 \sin \omega_1 t + A_2 \sin(\omega_2 t + \theta)) = f(A_1 \sin \omega_1 t) + f'(A_1 \sin \omega_1 t) A_2 \sin(\omega_2 t + \theta) \qquad \textbf{[3.2]}$$

and will be valid for A_2 sufficiently small. The gain of the nonlinearity at the limit cycle frequency is given by [3.3].

$$\frac{2}{A_1 T} \int_0^T \left[f(A_1 \sin \omega_1 t) + f'(A_1 \sin \omega_1 t) A_2 \sin(\omega_2 t + \theta) \right] \sin \omega_1 t dt \qquad \textbf{[3.3]}$$

where T is the length of a period of the overall waveform. If no period exists, then the limit as $T \to \infty$ can be taken. By arguing that the integral of incommensurate frequencies will vanish, the second term in the integral disappears and the linear gain associated with the limit cycle frequency, which is equal to the describing function of the nonlinearity, is

$$g_{LC} = \frac{2}{A_1 T} \int_0^T f(A_1 \sin \omega_1 t) \sin \omega_1 t dt \qquad \textbf{[3.4]}$$

The gain of the nonlinearity at the probe frequency is given by [3.5].

$$\frac{2}{A_2 T}\int_0^T \left[f(A_1 \sin\omega_1 t) + f'(A_1 \sin\omega_1 t) A_2 \sin(\omega_2 t + \theta)\right]\sin(\omega_2 t + \theta)dt \qquad \textbf{[3.5]}$$

Arguing as before, the first term in the integral will go to zero. In addition, the only part of the second term which will contribute to the integral is the constant component of $f'(A_1 \sin\omega_1 t)$ times the constant component of $A_2 \sin^2(\omega_2 t + \theta)$. Thus, the gain at the probe frequency is given by [3.6].

$$g_{\mathrm{Pr}} = \frac{1}{T}\int_0^T f'(A_1 \sin\omega_1 t)dt \qquad \textbf{[3.6]}$$

Note that the gain of the probe signal is independent of the amplitude and frequency of the probe signal, subject to the restriction that the amplitude of the probe is small.

For the tanh nonlinearity considered here, the limit-cycle and probe gains can be computed numerically and are shown in Figure 3.7. The gain of the probe signal is less than the gain of the limit cycle signal through the nonlinearity. Since the gain of the limit cycle frequency is just that value needed to make the closed-loop system marginally stable, the lower probe gain will cause the closed-loop system to appear stable. Since the probe gain is not a function of the probe frequency, the system identified by considering the frequency response at the probe frequency will appear linear and stable.

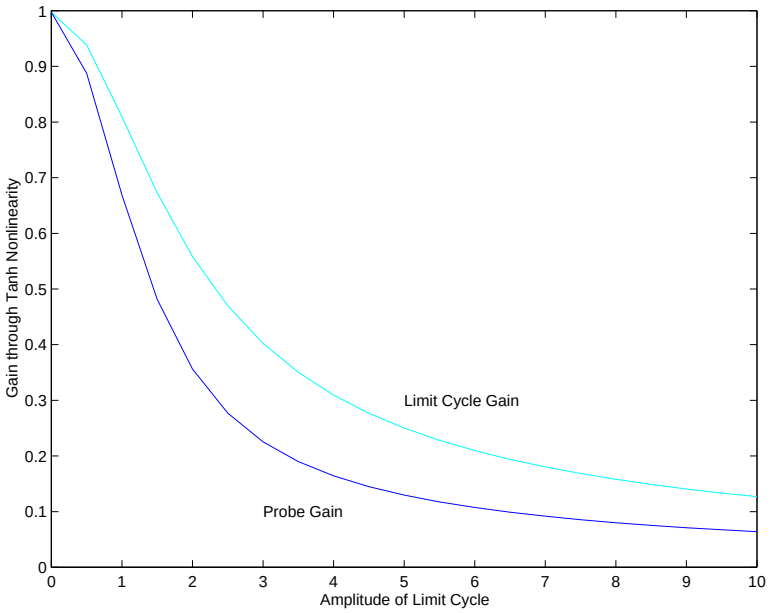

FIGURE 3.7 PROBE GAIN AND LIMIT CYCLE GAIN

Given the above analysis and in view of Figure 3.7, the identified transfer function of Figure 3.6 will be

$$\frac{P_T}{p} = \hat{G}_p = \frac{G_{ACT}}{1 - G_A G_F g_{\mathrm{Pr}}} \approx G_{ACT} \qquad \textbf{[3.7]}$$

The reason that this transfer function is approximately equal to G_{ACT} over the bandwidth of interest is because the denominator is very close to one at the probe frequencies. There are two reasons for this. First, the factor $G_A G_F g_{Pr}$ is always less than one at all frequencies in the bandwidth. Secondly, G_A contains lightly-damped acoustic poles that will have a high gain very near the instability frequency. The gain will be significantly lower a small distance from this frequency, where the probing is actually performed. Thus, at the probe frequencies, the factor $G_A G_F g_{Pr}$ will be significantly less than one, resulting in accurate measurements of G_{ACT}.

This plant estimate is stable at all probe frequencies, thereby avoiding the issue of attempting to use an unstable system identification, or a time-delay plant, as other investigations have discussed. In addition, it approximates G_{ACT}, which will be shown to be the desired transfer

function of the plant estimate. This system ID method also makes it possible to design a feedback controller *a priori* that will apply the correct phase to the system while avoiding secondary peaks induced from the controller feedback loop [16]. This process is described next.

3.5 FEEDBACK CONTROLLER DESIGN

The open-loop frequency response function that is the predictor for controller performance includes all components of the feedback loop. The example controller considered here has been designed as a bandpass filter with a lowpass component having a cutoff frequency of 178 Hz and a high pass component with a cutoff frequency of 200 Hz. With overlapping cutoff frequencies, the bandpass filter has a peak magnitude that is less than unity and a very narrow bandwidth. Because each of the filters have high rolloff rates of 160 dB per decade, the filter dominates the magnitude of the open-loop FRF. (This is evident by examining the shape of the frequency response data of Figure 3.8, which resembles a narrow bandpass filter). Changes in the plant will cause the magnitude and phase to shift left and right as well as up and down. However, the general bandpass shape of the controller provides enough gain to stabilize the plant without inducing spillover at the lower and higher frequency phase crossover points.

When the open-loop data was collected, the phase shifter had been adjusted to a value that seemed to work well in a variety of operating conditions, including the one shown in Figure 3.8. (This explains why the crossover points at 0° and 360° have high gain margins as desired). Changes in the plant, however, may cause the overall magnitude to decrease or shift, or cause the phase to shift or change shape slightly. If the controls engineer has the open-loop shape at his disposal, he can alter the gain and phase delay of the controller (and thus the open-loop plant) to regain the desired gain and phase margins. And since the general shape of the controller and plant does not change with widely varying operating conditions, the two spillover locations will be in the same vicinity of the FRF for most conditions (i.e. the controls engineer/search algorithm will know where to look to predict the feedback induced instabilities). In addition, it should be noted that the magnitude of the open-loop FRF decays rapidly below 150 Hz and above 200 Hz because of the bandpass filtering. The gain margins

at all other phase crossover points (both higher and lower in frequency) will be sufficiently high to ensure stability at those frequencies.

The high gain of the positive feedback controller at 180 Hz causes the unstable poles of the plant to travel into the stable left half plane. There are two complex conjugate poles (approx. 166 Hz and 194 Hz) from the control filter (or other plant dynamics) that will move into the right half plane as gain is increased. Consequently, there is a range of gain where the unstable plant poles move into the left half plane before the stable controller poles move into the right half plane. Depending on how far into the right half plane the unstable plant pole begins, it is certain that sufficient gain exists in the feedback loop for the small scale combustor to be stabilized (at nearly any operating condition) *without inducing the spillover at the adjacent frequencies*. (As the heat release increases, the unstable poles move further into the right half plane, requiring more gain to stabilize them. The gain at 180 Hz only needs to reach zero to stabilize the unstable poles, leaving sufficient gain margin at the adjacent phase crossover locations to ensure stability). However, the actuator (speaker) used in this example cannot provide the sound pressure level necessary to move the poles back into the left half plane for some high gain operating conditions. This limitation is not an important consideration for this study (since the condition examined is controllable), and can be remedied by a more powerful actuator. This discussion was intended to motivate the Bode gain/phase relationship from a root locus perspective. The added dynamics from the controller induced instabilities for high gain at two locations adjacent to the self excited instability. These locations are predicted from the open-loop transfer function.

Once the open-loop FRF is determined, a series of rules are examined that provide a deterministic measure of the predicted stability of the closed-loop system. These rules are summarized below using several illustrations of the open-loop transfer function to assist in the explanation.

1. First, the phase crossover frequency points for positive feedback (0° and -360°) are determined from the open-loop phase. In this example they are found to be 166 Hz and 194 Hz as shown by dotted vertical traces in the phase plot of Figure 3.8.

2. Next, the gain margin at these frequencies is determined by examining the open-loop gain value relative to 0 dB. Referring again to Figure 3.8, the gain margin at 166 Hz is approximately 20 dB and the gain margin at 194 Hz is 24 dB. This means that the gain can be raised by 20 dB before an instability occurs at 166 Hz. (Since the gain margin is less at 166 Hz, the gain margin at 194 Hz is ignored).

3. A specific gain margin must be established to meet the desired closed-loop design requirements. A gain margin of 10 dB ensures that peak values of feedback induced instabilities are limited to 3 dB. Therefore, the gain that can be applied to this system is limited to 10 dB to satisfy this design requirement.

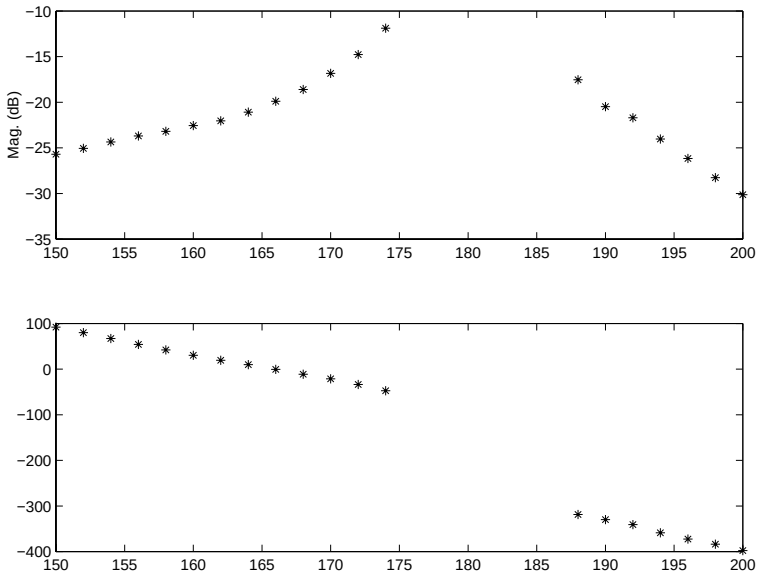

FIGURE 3.8 FEEDBACK CONTROLLER DESIGN - MAGNITUDE

4. The gain is then applied to the open-loop transfer function, shifting the magnitude up or down to satisfy the design criteria. Figure 3.9 illustrates this new FRF.

5. The phase margin determination requires a slight modification from the traditional definition due to the limited data set. Typically, the phase where the open-loop gain is zero is specified as the phase margin. In this case it should be obvious that the data does not afford the luxury of gain crossover points (which might occur at 175 Hz and

183 Hz through extrapolation). Therefore, instead of using 0 dB, the more conservative value of -10 dB (the gain margin) is chosen as the critical gain crossover point. The frequencies where this occurs are 166 Hz where the phase is 0° (as expected) and 190 Hz where the phase is -325°. These points correspond to phase margins of zero and 35 degrees respectively.

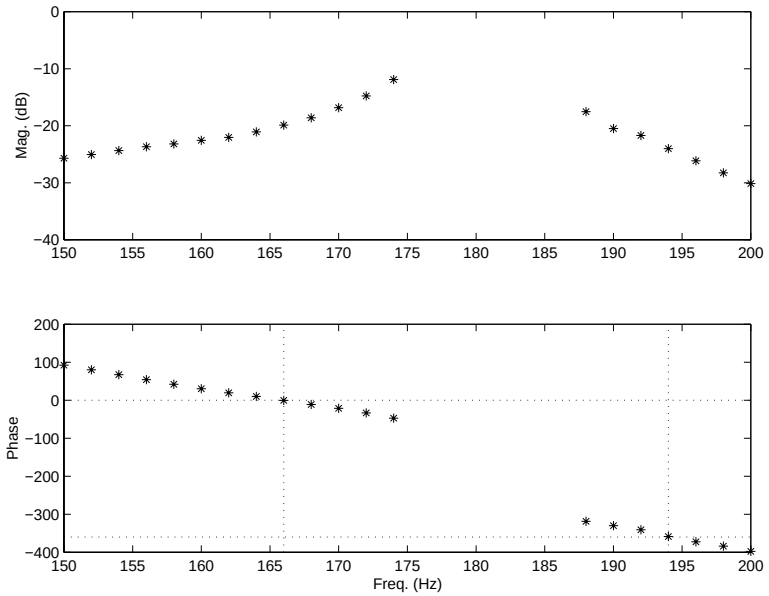

FIGURE 3.9 FEEDBACK CONTROLLER DESIGN - PHASE

6. Stability has been ensured by the gain margin calculation. Optimum performance in terms of the two spillover peaks can be created by adjusting the phase margins to be identical at the gain crossover points. A simple way to do this is to average the two calculated phase margins and apply the necessary digital delay. The number of digital delay samples needed depends on the sample rate and frequency of interest, and will increase with increasing frequency. Therefore the computed value will not exactly provide the correct delay for *both* phase margins, although the error will be quite small since the bandwidth is so narrow.

One final source of error in this computation will occur as a result of the discrete data points. Interpolation between the data points is quite time consuming for each gain margin and phase margin calculation, and is not necessary to ensure appropriate accuracy. For this data set, the

largest jump between magnitude values is 5 dB and the largest phase jump is 15°. The desired gain margins and phase margins can be easily adjusted to accommodate this uncertainty by recalculating the actual gain and phase margins after the gain and phase delay have been applied to the open-loop data.

The design procedure presented above can be used in conjunction with Figure 3.10 to create a feedback controller design that will be stable. In addition, the feedback induced instabilities can be limited to a preset value (determined from Figure 3.10), while ensuring that both instabilities will exhibit equal amplitude amplification. Figure 3.10 shows the predicted closed-loop magnitude (in dB) as a function of phase margin and gain margin *for positive feedback systems*. Note that at a phase margin of 0°, the gain margin must be greater than 10dB to ensure less than 3dB of closed-loop amplification. This plot can be used to establish the desired design criteria used in Step 3 of the design process described above.

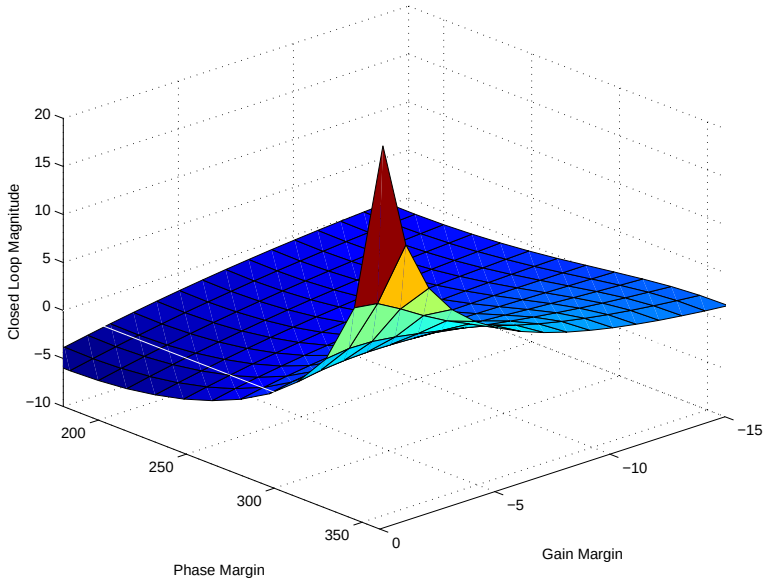

FIGURE 3.10 SPILLOVER AMPLITUDE PREDICTION

Given that these margins are equally spaced about the instability, maximum control can be ensured at the instability for a given value of gain since the phase at that frequency is optimal for positive feedback control (i.e. -180°). It should be noted that careful choice of the bandpass shape was made to ensure that the most control of the instability could be achieved.

This design approach will certainly work for any open-loop transfer function/fixed gain controller shape; however, other fixed-gain controller shapes (such as low pass or high pass) often have margins that cause the feedback induced instabilities to become high in amplitude before achieving appreciable control of the combustor instability. This frequency domain based design process will reveal to combustion/controls engineers that the frequency response *shape* of the phase shift controller and open-loop plant is critical to ensuring good performance.

Using the narrow bandpass filter controller shape (very simplistic, but high order filters) and the design procedure presented above with the open-loop FRF of Figure 3.8, the controller design shown in Figure 3.11 results. The unmodified open-loop FRF (plant and controller) is shown as circles in Figure 3.11. By first selecting the closest gain margin (164 Hz) from both phase crossover frequencies, the gain needed to just satisfy the desired gain margin of 10 dB was found to be 2.69. The trace shown as "+" signs illustrates the FRF after this amount of gain is applied. Next, the new phase margins are determined and the phase is adjusted through a digital delay so that both gain crossover points have the same phase margin. The "x" signs indicate the open-loop FRF after it has been modified by both the gain and the phase. With the same phase at both gain crossover points (at -10 dB) the amplitudes of the controller induced instabilities as these points will be the same. In addition, since the gain is less than -10 dB at the phase crossover points, no more than 3 dB of added amplitude will occur. This design results in stabilizing control of the thermoacoustic instability as will be shown in the following section. Furthermore, continual update of the controller gain and phase using the above procedure was shown to provide stabilizing control over a variety of operating conditions as discussed in the next chapter.

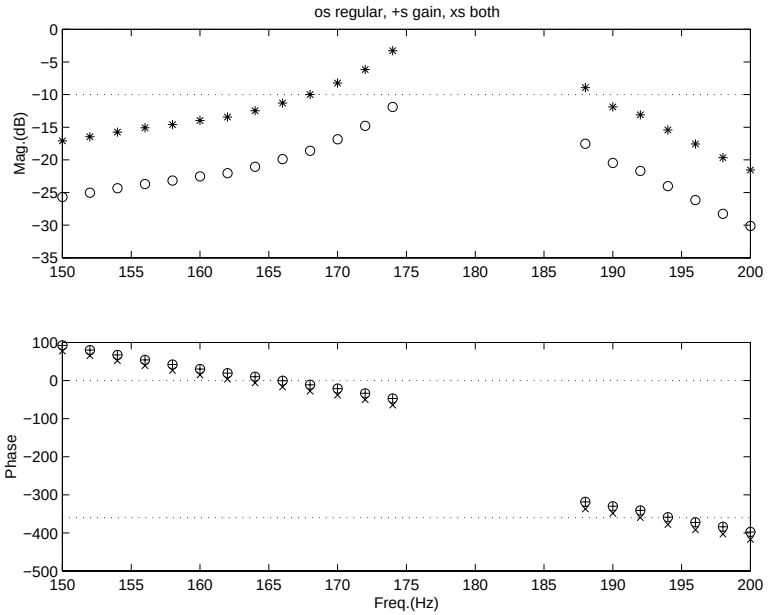

FIGURE 3.11 FEEDBACK CONTROLLER DESIGN RESULT

3.6 TYPICAL EXPERIMENTAL RESULTS

As motivated earlier, the inclusion of this material is intended to provide a baseline of performance for fixed gain feedback controllers from which other control methods can be referenced. The Rijke tube combustor rig described above was used most frequently for experimental testing of the algorithms developed herein. Although it is considered by many to be an impractical experiment (due primarily to the acoustic actuation method) it is effective for examining the performance characteristics for various control algorithms. In general, the performance of the control method itself should be independent of the actuator, and scalable to any self-excited system.

Power spectrum data was typically collected to establish the amount of attenuation achieved by a typical control design. In general, if a power spectrum is shown without an accompanying time trace, the system exhibited the illustrated behavior for all time. However, as will be shown for a variety of approaches, transient "searching" behavior was apparent in many control experiments. These data are typically represented with a time trace of appropriate duration to characterize the behavior.

Figure 3.12 illustrates typical behavior of the tuned feedback controller described in the previous section. The dotted trace shows the uncontrolled power spectrum of the limit cycling combustor described above. The solid trace shows a closed loop feedback controlled system where the gain has been manually optimized to prevent secondary peaks. The third trace illustrates the same feedback controller where too much gain and has been applied, generating two peaks at the phase crossovers on either side of the instability. It should be noted that using the design methodology described above (and ultimately automated by the neural network control design), the frequency and amplitude of these secondary peaks is predicted, and prevented.

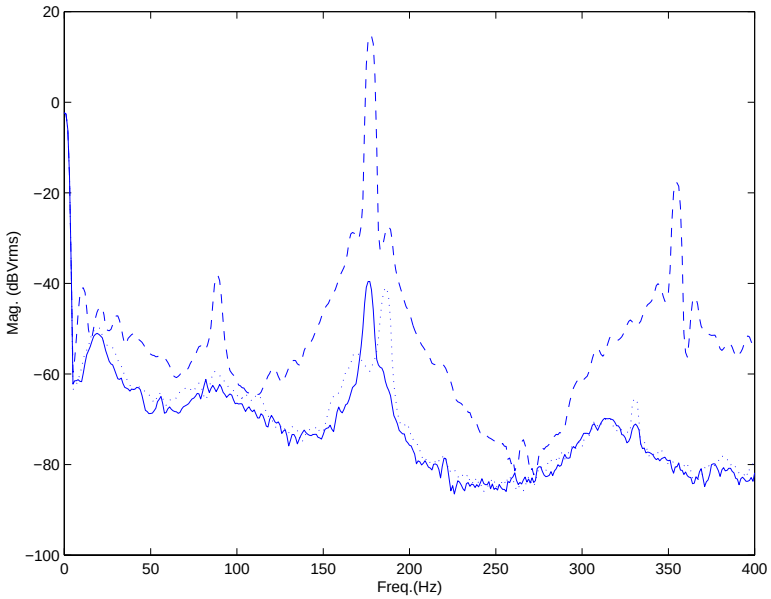

FIGURE 3.12 FEEDBACK CONTROLLER PERFORMANCE (DASHED-UNCONTROLLED, SOLID-CONTROLLED, DOTTED-EXCESS CONTROLLED GAIN)

For low heat release (low gain in the combustion instability loop) this is typical performance that does not vary over time. The question of stable versus unstable and linear versus nonlinear arises again when examining Figure 3.12. It is apparent that the control is being exercised on a nonlinear plant. Damping is only being added at a few Hertz surrounding the limit cycle frequency, but we see significant suppression over the entire bandwidth. The amount of gain applied by the controller may be used to determine if the suppression of that

instability is a linear function of the amount of damping being applied. While this is not the focus of this work, it is an interesting prospect for future contributions to this field.

For high heat release conditions (where the unstable pole is presumably further into the right half plane, thus requiring more control gain), stabilizing control is not so readily achieved. Figure 3.13 illustrates a time trace exhibiting a searching behavior after initiation of the fixed gain feedback controller.

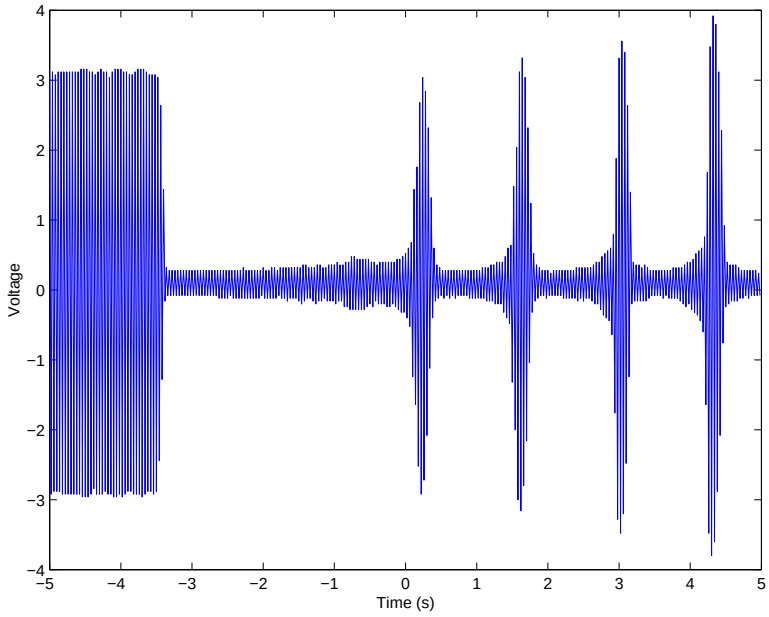

FIGURE 3.13 FEEDBACK CONTROLLER SEARCHING BEHAVIOR

This searching behavior at higher heat releases is a recurring theme present not only in this fixed gain controller, but also in the adaptive controllers, although in the TAG controller scheme to a lesser extent. The source of this behavior is analyzed and explained in detail in Chapter 5.

3.7 REVIEW

In this chapter fixed gain feedback control of combustion instabilities was presented. The significant contributions of this work focus on the system identification method and analytical techniques for designing fixed gain feedback controllers for the thermoacoustic instability.

These two concepts are carried throughout this work. The system identification method is an integral part of the neural network controller design as well as the key for developing an accurate plant estimate for use in Filtered-X based adaptive controllers. The fixed gain feedback controller is used as part of the neural network control method discussed next and is also used as a baseline for comparison to the adaptive control methods. Although similar fixed gain control approaches have been used in the past by many researchers, detailed discussion of the combustion system identification and feedback controller design has not been previously addressed.

Chapter 4

Artificial Neural Network Control

As with each of the adaptive control techniques presented in this work, the motivating factor behind using a neural network is to provide a suppressing or stabilizing control that automatically tracks changes in the plant. Changes in the plant frequency response resulting from changes in operating conditions or the inclusion of the controller itself, may render non-adaptive controller designs useless. A neural network has been designed to predict those changes and provide the predicted frequency response to a rule based loopshaping controller design algorithm.

During the course of designing the neural network and feedback controller algorithm, it became apparent that a secondary benefit would result from this approach. As discussed earlier, prior art has not successfully predicted the severity, location, or even existence of controller induced instabilities. However, the controller design algorithm implemented here as part of the neural network control approach, requires that limits are placed on the gain of the resulting controller design to prevent controller induced instabilities. Therefore the resulting design not only tracks changes in the plant and modifies the controller accordingly, but also prevents controller induced instabilities from forming by generating an optimal gain for given design constraints and controller shape.

This chapter describes how a neural network was trained to predict the frequency response of the thermoacoustics in the Rijke tube combustor and how that neural network output was used by the feedback controller design process to control combustion instabilities. The neural network training was performed using complex valued, open-loop frequency response function data as the desired signal with the operating conditions and sparse temperature profile as the

input signals[2]. Once the neural network was trained, it was used to predict the approximate phase and gain margins as a function of temperature and flow conditions. The margins were then used to automatically update and design a fixed shape feedback controller having the proper phase and magnitude to ensure stability and control in the presence of changing operating conditions.

4.1 NEURAL NETWORK TRAINING DATA

In order for the network to effectively interpolate, it was important to choose inputs that affect the desired output. In this case the desired output is the complex valued open-loop frequency response function (OLFRF) at frequencies surrounding the limit cycle frequency. It should be clear that one variable that will obviously affect the acoustic component of the thermoacoustic plant is the temperature in the tube (due to the dependence of acoustic pressure on temperature). Four temperatures in the tube were used to generate a profile for each operating condition tested. However, preliminary testing indicated that the variation in temperature was not enough to explain the limitations found in the feedback control performance at various operating conditions. For this reason, flow rate and equivalence ratio were added as inputs since they represent the only user controllable components of this combustion process.

A range of typical flow rates and equivalence ratios was chosen in an attempt to span a small space of combustor operating conditions. Eleven sets of operating conditions were chosen using three equivalence ratios from 0.47 to 0.82 and four total volume flow rates from 109 cc/sec to 145 cc/sec. All combinations of these conditions were tested (flow rates : 110, 120, 130, and 140 cc/sec and equivalence ratios: 0.47, 0.6, and 0.8) with one exception at 110 cc/sec and 0.47 where the flame could not be sustained. At each of these eleven conditions, four temperature measurements and 40 sine dwell frequency response values were recorded (complex values at 20 frequency points). Figure 4.1 illustrates the eleven frequency response magnitude data sets used in training the neural network.

---

[2] The open loop data was collected for a narrow frequency range surrounding the limit cycle instability by performing a sine dwell at discrete frequencies. The argument in favor of this approach to plant identification was presented in the previous chapter.

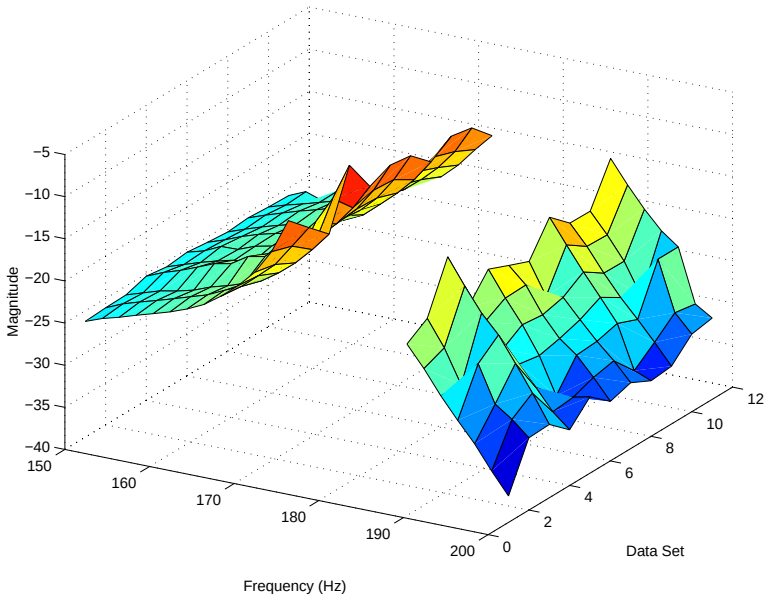

FIGURE 4.1 ALL TRAINING DATA SETS

The gap in the continuous FRF represents the locations where the limit cycle amplitude prevented accurate system identification. Nevertheless, mental interpolation indicates that a lightly damped complex pole exists at 180 Hz. This agrees with the expected stabilizing action of the controller when the gain is raised at this frequency. In addition, we see that the resulting identifications are stable systems, which is commensurate with the system identification discussion in the previous chapter.

One final note regarding the utility of this choice of inputs and the neural network should be made. Once the feedback control loop is closed, there is no efficient method for obtaining the open-loop frequency response. This is critical because the self-excited system dynamics have been known to change under the action of the controller. When this happens, a fixed-gain controller is not updated and may become unstable. Therefore the controller that was designed for a single operating condition, may not even work for that operating condition because its own presence influences the plant enough so that the design is no longer valid[3]. While the flow rate and equivalence ratio are not affected by the controller, the temperature profile inside the tube is. Therefore, by using temperature as an input to the neural network,

[3] This phenomenon is explained in further detail at the end of Chapter 5.

the estimate of the OLFRF can be updated even when the control loop is closed. Any affect that the controller itself may have on the open loop transfer function (and thus the temperature), can be represented and predicted by the neural net, which in turn allows the controller to be updated in real time. This is an important observation made by this work. Other on-line ID approaches cannot predict the open loop frequency response during control because the control loop is always closed during such procedures.

4.2 NEURAL NETWORK DESIGN AND TRAINING

Many iterations and modifications to the network were investigated before the final design was selected. These variations included: one and two hidden-layer networks, bipolar sigmoid and hyperbolic tangent squashing functions, static and adaptive update parameters, and complex-valued and real-valued backpropagation algorithms. Without examining the details of all design iterations, the final design is presented here with training results.

Once the eleven frequency response functions and input data vectors were collected, they were converted into MATLAB formatted arrays for use in designing and training the neural network. The frequency response data (desired network output) consisted of 20 complex values, each component having a value less than one. This is important to note because no scaling of the network output was required to avoid saturation of the squashing functions whose maximum values were set at unity. The network inputs, however, did require scaling. The thermocouple measurements of temperature ranged from 106° F to 604° F. These four inputs received a scaling of 1/610 before entering the network. In an effort to maximize the dynamic range of the squashing function (and ultimately the resolution of the DSP), the flow rate received a different scaling. The minimum value of the flow rate input was 109 cc/sec and the maximum value was 145 cc/sec. The scaling chosen for the flow rate variable was 1/150. The final input (the equivalence ratio) was not scaled, since its values ranged from 0.47 to 0.82.

The best solution for the converged neural network was obtained from a 6-20-20 network using a fixed update parameter of 0.95 for both layers, a complex-valued backpropagation algorithm, and the bipolar sigmoid squashing function that did not take into account any special handling for complex-valued numbers. The converged weights for this system were

determined from the training process conducted using original MATLAB. MATLAB facilitates the handling of a complex-valued number as a single array element, whereas C programming requires that the real and imaginary components be held as separate values. Realizing the potential difficulty for DSP implementation and the excessive computation required for complex multiplication's of four array elements, the network was redesigned to accommodate real and imaginary components simultaneously and completely independently. The resulting network can be thought of in three dimensions where the layers are represented from left to right, the nodes appear vertically in each layer, and one network sits on top of another into the page; one side is used for real components and one for imaginary components. This is shown graphically in Figure 4.2.

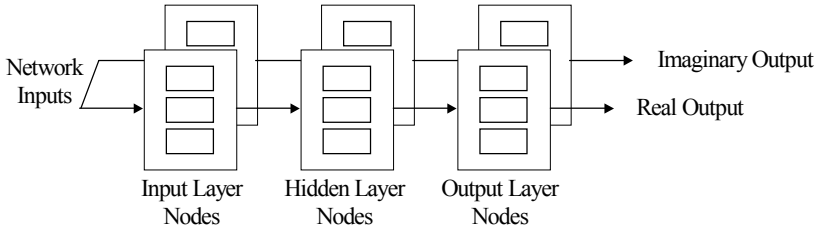

FIGURE 4.2 COMPLEX NETWORK

The convergence behavior for the complex backpropagation algorithm versus the real backpropagation used separately for real and imaginary values, provided almost identical results. Clearly, the synaptic weights converged to different values because the behavior of the squashing function changes drastically for real-valued versus complex-valued inputs. The network configuration shown in Figure 6 essentially doubles the number of weights used but simplifies the task of implementing the complex network in C code. The forty outputs of the network are then combined to form the twenty complex numbers representing the complex FRF. From that, magnitude and phase can be easily determined.

Figure 4.3 illustrates the epoch convergence of the network shown in Figure 4.2 for the *maximum error* over each epoch for 1,000 epochs. (i.e. the maximum error over all training data sets for each epoch). It is clear that by the 800^{th} epoch, there is little improvement in the error

and the network has converged. This plot represents the sum of the maximum error of real and imaginary components. The maximum error of every other training data set and point was, in fact, well below 0.1, approaching zero.

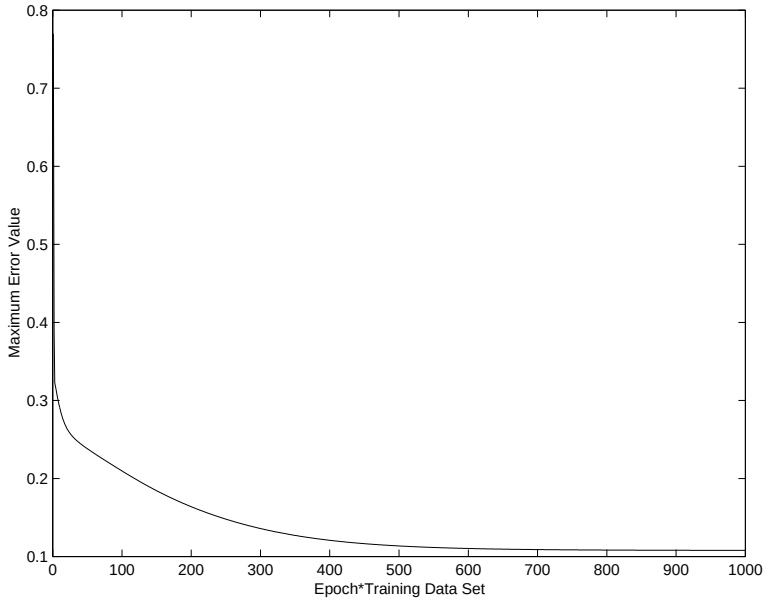

FIGURE 4.3 MAX ERROR OVER EPOCH

Once the network converged, the weights were saved and used to check the performance before implementing the network on the DSP. As mentioned earlier, a data set was collected that did not match any of the training data, and was used for checking the performance of the converged neural network. Figure 4.4 illustrates the actual value of the magnitude and phase of the open-loop transfer function data as compared to the neural network output. The actual data is shown as 'o' and the neural network output is shown as '+'. The errors are well within the tolerance needed to perform an accurate feedback controller design for these operating conditions.

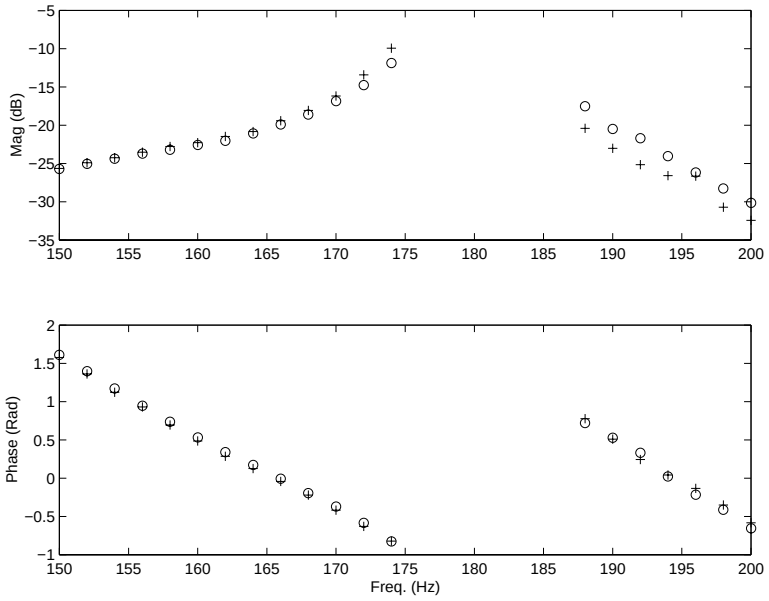

FIGURE 4.4 NEURAL NETWORK PERFORMANCE

After the network convergence was tested, the converged weights were saved into arrays. The first step in implementing the network in real time was to create a C code (included in the appendix) that simply did the necessary matrix multiplication and nonlinear squashing that constitutes the forward pass of the neural network. The inputs were designed to be collected either externally from the A/D or inputted manually from a graphical user interface. The only remaining task for implementing this in terms of an adaptable feedback controller is to now use the output of the neural network (the open loop frequency response function) and redesign the fixed-gain feedback controller using the feedback controller design process described earlier.

4.3 FEEDBACK CONTROLLER: ADAPTIVE UPDATE

The open-loop frequency response function that is the neural network output and the predictor for control includes all components of the feedback loop. The controller shape itself has been designed as a bandpass filter with a lowpass component having a cutoff frequency of 178 Hz and a high pass component with a cutoff frequency of 200 Hz. With overlapping cutoff frequencies, the bandpass filter has a peak magnitude that is less than unity with a very narrow bandwidth. Because each of the filters have high rolloff rates of 160 dB per decade,

the filter becomes the dominant magnitude component in the OLFRF. (This is evident by examining the shape of Figure 4.4 which resembles a narrow bandpass filter). Although, all of the dynamics of the combustion system are still represented by the frequency response data collected (the open loop FRF contains the plant and the controller). Changes in the plant will cause the magnitude and phase to shift left and right as well as up and down. However, the general shape of the controller provides enough gain to stabilize the plant without inducing spillover at the lower and higher frequency phase crossover points for many operating conditions. In addition, some amount of feedback gain has been included in the loop as was required by the system identification process. Therefore any changes predicted by the neural network/feedback controller design process will be included *in addition to* the phase and gain already present in combustion system. Finally, note that due to the steep rolloff of the bandpass controller design, no other crossover points in the system bandwidth can generate instabilities.

All of the components in the feedback control loop were included in creating the neural network training data. The FRF output of the neural network included all of the components shown in Figure 4.5.

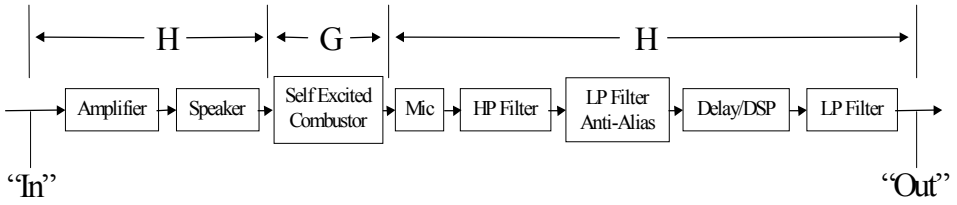

FIGURE 4.5 OPEN LOOP PLANT

The amplifier used to power the actuator was set at a gain of 0 dB and the delay in the DSP corresponded to approximately 274 degrees. This phase setting provided moderate control at a wide range of operating conditions and was determined by manual trial and error. This is not a necessary step in order for the neural network control to be effective. The feedback controller design algorithm will automatically determine the appropriate gain and phase for acceptable control at any condition.

Figure 4.6 illustrates the configuration of the neural network combined with the combustor feedback control loop. The unstable, self-excited combustor system (now represented by G) is controlled by the feedback controller H. Measurements of the combustor operating conditions and temperature profile are continually provided to the artificial neural network. The output of the network (the open-loop FRF) was used in the controller design procedure to automatically modify the gain and phase of the fixed shape controller, H. The digital feedback controller operated at a sample rate of 11 kHz on a TI C40 DSP, simultaneously with the neural network that updated once every second on the same DSP under separate timer interrupt subroutines. The C-code that performed this control operation is included in the Appendix.

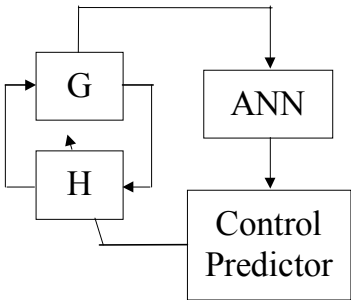

FIGURE 4.6 ANN CONTROL

Figure 4.7 illustrates three conditions of control for operating conditions of a total flow rate of 140 cc/sec and an equivalence ratio of 0.56.

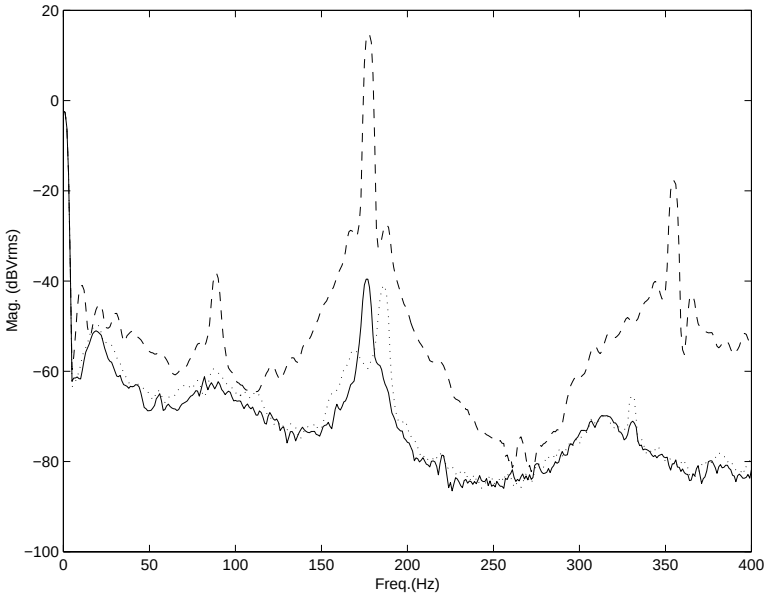

FIGURE 4.7 NARROWBAND ANN CONTROL PERFORMANCE

The higher magnitude (dashed) trace represents the RMS magnitude of the voltage for the pressure sensor at the bottom of the tube in the case where no acoustic feedback control is applied to the system. The lowest (solid) trace indicates the control provided by the neural network/feedback update algorithm. Although the free acoustic response of the combustor is not shown in Figure 4.7, the neural network clearly provides control that approaches the lightly damped modal shape of the tube. The parameters determined by the neural network for this controlled case were a phase of 256 degrees and a linear gain of 1.8. It should be clear that since all data points are less than the uncontrolled response, the neural network does not induce any new instabilities from excessive gain and poor phase margins. The dotted trace (shown just above the solid trace) in Figure 4.7 represents the control action that *could* happen as a result of a manual controller not governed by the neural network. The phase of the manual controller was chosen (based on subjective performance of the acoustic output) as 274 degrees while the gain was chosen to be 3.65. This excessive gain was more than enough to suppress the primary instability at 178 Hz but was too high to prevent controller induced instabilities at frequencies slightly higher and lower than 178 Hz.

The neural network is quite useful in predicting changes necessary to ensure a stable and effective feedback controller design in the face of changes in operating conditions. Figures 4.8

and 4.9 illustrate this effectiveness for a variety of operating conditions. Figure 4.8 shows the uncontrolled (dotted) and controlled overall acoustic **bandpowers** (0-800 Hz) for a flow rate of 130 cc/sec and steadily increasing equivalence ratio's from 0.48 to 0.6.

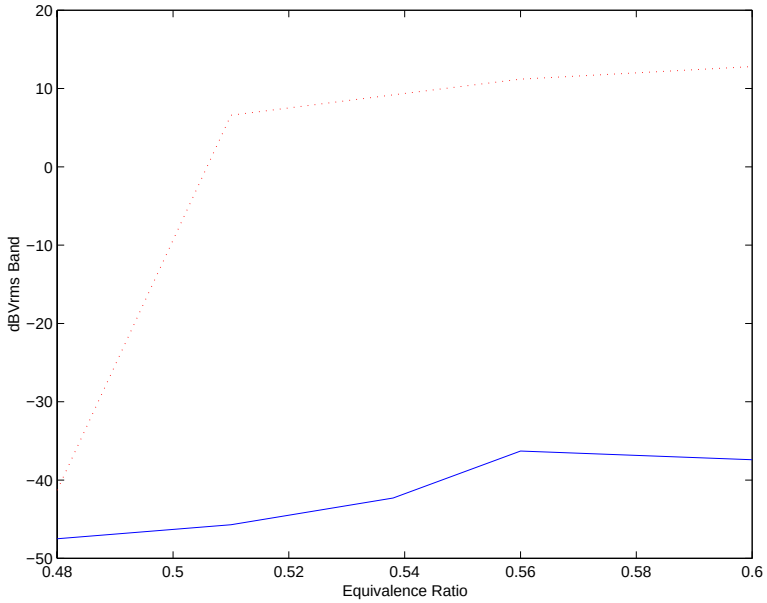

FIGURE 4.8 BANDPOWER AT 130 CC/SEC, INCREASING EQ. RATIO

Since the temperature changes will also affect the plant, the controller must update the feedback design to track these changes. With an average of 50 dB of control over the stated bandwidth, the controller is quite effective over all operating conditions. Figure 4.9 illustrates a similar data set with a flow rate of 140 cc/sec and a *decreasing* equivalence ratio from 0.56 to 0.47 similar performance is observed.

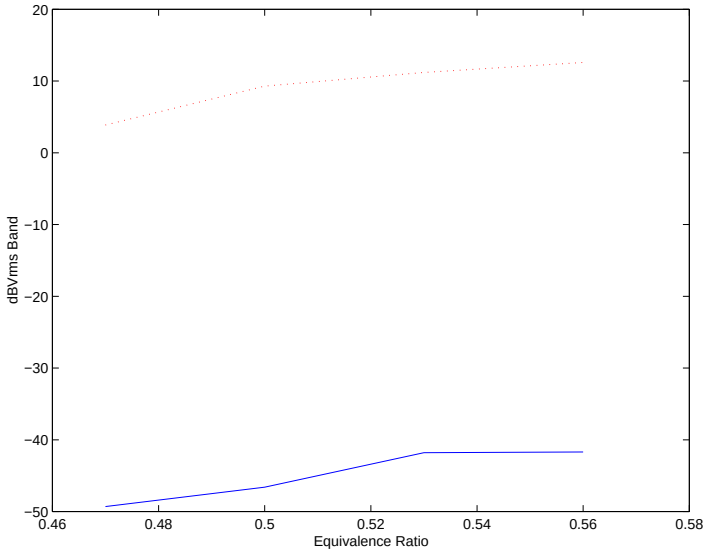

FIGURE 4.9 BANDPOWER AT 140 CC/SEC, DECREASING EQ. RATIO

The neural network feedback control strategy does not use the neural network directly in the actual control of the thermoacoustic instability. Instead it is used to predict the open loop frequency response of the plant to be controlled by a rule based feedback controller design routine. The result is a control system that predicts changes in the plant that occur either as a result of changing operating conditions or the control action itself.

4.4 NEURAL NETWORK CONCLUSIONS

This portion of the research illustrated that an artificial neural network can provide an effective system identification in the frequency domain. The output of the neural network was a function of system parameters that were measured in the open-loop, independent of the control actuation process. In the case examined here, the predicted frequency response function was used to update the gain and phase of a fixed shape feedback controller based on gain and phase crossover points that were deterministic. The same frequency response function could also be used to provide a control-to-error path estimate for an adaptive feedforward controller, although this was not explicitly examined by this work.

This approach holds many advantages over previous attempts at active noise control of thermoacoustic instabilities in combustors. Prior controllers have been predominantly manual,

requiring constant adjustment of the gain and phase of the controller to ensure stability for different operating conditions. Successes at using the phase shifting feedback controller have met with equal amounts of failure from controller induced instabilities (spillover). Without an accurate plant estimate, the controller is often poorly designed and insufficient gain or phase margins elsewhere in the spectrum prevent adequate control of the primary instability by causing a new feedback controller induced instability. By performing a careful system identification, a controller can be designed that satisfies the Bode gain/phase relationships and still provides adequate control. The ANN facilitates this by allowing real-time update of the open-loop frequency response in the face of changing combustor conditions as well as during closed-loop control. The example shown here illustrated how a neural network can provide as much as 50 dB of control over a range of operating conditions without manually updating the feedback controller.

While the network updated feedback controller is effective at controlling the instability over a wide range of conditions, an exhaustive system identification procedure is required to build a database of training data for the neural network. In real world applications this may be an impractical solution to the problem because of the difficulty in creating such a database.

Chapter 5

Adaptive Control

5.1 INTRODUCTION

During the past several years, there has been a trend away from mostly empirical or experimentally-based *active combustion control* (ACC) methods in favor of control systems that rely on more accurate understanding of the dynamic processes involved in the thermoacoustic limit cycling response. Early demonstrations of phase-shifting ACC designs relied only on a measurement of the acoustic pressure and actuation of the unsteady heat release rate after appropriate delay (i.e. phase shift) relative to the measured pressure signal. The phase-shifting controllers proved to be effective in many situations but were plagued by inadequate knowledge of how to predict the required phase, and gain, of the controller for varying operating conditions of the combustor. These problems naturally led to investigations of adaptive control methods.

A number of ACC researchers recognized that adaptive signal processing methods offered a possible alternative to the manually-tuned, phase-shifting controller. These adaptive filtering methods, such as the LMS algorithm proposed by Widrow and Stearns [49], had been highly successful in the active noise and vibration control community for narrowband disturbance rejection. The most relevant application of LMS control for noise or vibration control was the so-called Filtered-U algorithm [48] which required feedback compensation for the reference sensor. The ACC implementation is similar in its need for compensation because the reference sensor is often identical to the error sensor. A number of combustion researchers investigated the usefulness of these LMS algorithms for ACC [22,23,30,25,28]. However, most of the results from those experiments and numerical simulations indicated an uncertainty about the proper implementation with regard to employing a plant estimate. As a result, the literature

shows that the LMS controlled systems often diverged, sometimes minutes after the combustor's pressure signature seemed to have been reduced to acceptable levels.

This portion of this work investigates filtered-X LMS control applied to the self-excited thermoacoustic instability. Previous research has not carefully recognized that an appropriate system identification is required to ensure stable and predictable convergence. Together with the system identification procedure and argument presented in Chapter 3, this discussion explains why the stable control-to-error path is the appropriate (and only) choice for plant identification. Previous research has not identified this as an appropriate or even acceptable approach for system identification and control implementation.

The analysis of adaptive feedback control applied to a general system is presented in the following chapter. Those results show that adaptive feedback control is not a practical controller design because of inherent instability and algorithm divergence problems when the plant estimate does not exactly match the actual control-to-error path. This chapter assumes that a perfect identification is available. It is then shown that only one arguable choice for the system identification exists. It is also shown through simulation and experiment that stabilizing control is achievable when the appropriate system identification method is used.

An intermittent performance condition was also identified during experimental control of higher heat release operating conditions. A similar intermittency was seen in the simulation developed to model controller performance. The simulation illustrates an intermittency caused by feedback loop instabilities which could not be stabilized by the memoryless LMS algorithm. However when the RLS algorithm was employed on the same system, the system was stabilized. Ultimately, experimental results showed that feedback loop instabilities were not causing the intermittency witnessed when controlling higher heat release conditions. Instead, actuator authority was shown to limit the controllability as the plant changes under the influence of the controller.

The following section introduces the structure of adaptive feedback control for both exogenous disturbances and the self-excited system. The most appropriate choice for the plant

estimate is proposed and analyzed in the next section. Next, simulation and experimental results of the filtered-X forms of the LMS and RLS algorithm using the proposed system identification procedure of Chapter 3 are presented. The intermittent performance condition is then explained in detail. The final section provides concluding remarks.

5.2 ADAPTIVE FEEDBACK CONTROL

5.2.1 CLASSICAL DISTURBANCE SUPPRESSION

The adaptive feedback controller considered in this work can be viewed as a special case of Filtered-U control where the control-to-reference path and the control-to-error path are identical [48]. Figure 5.1 shows the adaptive feedback control block diagram for the case of an external disturbance and stable plant. It is instructive to briefly examine this system as a precursor to controlling the self-excited system.

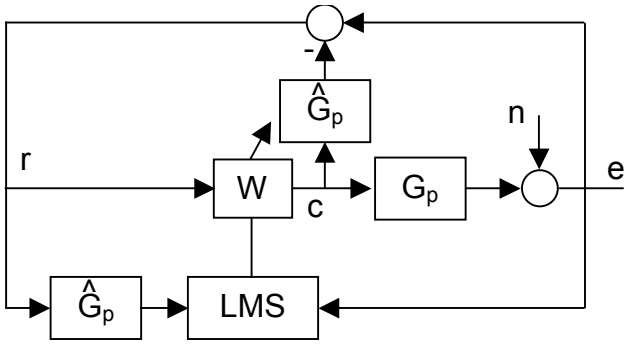

FIGURE 5.1 ADAPTIVE FEEDBACK EXTERNAL DISTURBANCE

In a purely feedforward control system, a separate reference signal that is correlated with the disturbance is used as the input to the adaptive filter. It is well-known that correct estimation of the dynamic phase, within ninety degrees, is sufficient to prevent divergence of the LMS gradient search [39]. In adaptive feedback control, the reference signal is derived directly from the error sensor by removing the component of the error signal that is due to the control signal, leaving only a measure of the disturbance. If we let the control signal be the output of the FIR adaptive filter (W), we note that it must go through the plant dynamics (G_p) before acting on the external disturbance (n). The dynamics represented by the plant include everything present in the control signal to error signal path, including the A/D and D/A.

Therefore, removing the control signal component from the error requires subtracting the output of the adaptive filter, filtered by an estimate of the plant, from the measured error signal. Hence, if the plant estimate is not perfect, a non-zero feedback path is introduced. The closed loop transfer function between the error and the disturbance can then be written as:

$$\frac{e}{n} = \frac{1 + \hat{G}_p W}{1 + \hat{G}_p W - G_p W} \qquad \textbf{[5.1]}$$

Unlike the self-excited system, if the plant estimate is exact ($\hat{G}_p = G_p$), there is no feedback loop since the denominator of the above transfer function vanishes and the system behaves as a strictly feedforward system where $\hat{G}_p$ and W are both stable systems. For the case where $\hat{G}_p \neq G_p$, it is clear that the poles of [5.1] will change with the adaptation of the filter W and represent a potential source of controller instability.

5.1.2 SELF-EXCITED SYSTEMS

Figure 5.2 illustrates a simplified block diagram of an adaptive feedback controller applied to a self-excited system. Although the physical self-excited system is extremely complex and a subject of ongoing research, a simplified model consisting of linear acoustics, G_A, linear flame dynamics, G_F, and a nonlinear coupling is used in the Figure. In the analysis and simulation, the nonlinearity is treated as a static, saturating-type nonlinearity. Though crude from a broadband modeling point of view, the extremely tonal nature of the system makes this a useful approximation.

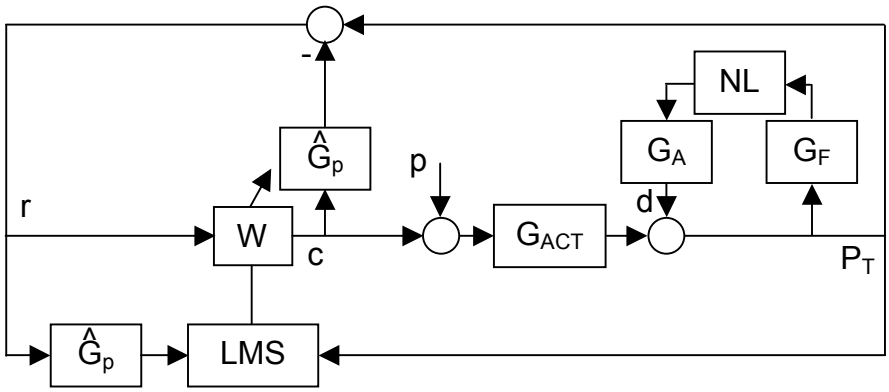

FIGURE 5.2 ADAPTIVE FEEDBACK SELF-EXCITED

The actuation signal passes through a linear system, G_{ACT}, that incorporates both the actuator dynamics and the acoustic dynamics. Since the outputs of G_A and G_{ACT} are both acoustic pressures, they can be superposed to produce the total combustor pressure variation, P_T. In the controller, the output of the adaptive filter is filtered by the plant estimate and is used to generate the reference signal from the error signal as before, although the appropriate plant estimate is less obvious now as a result of the inclusion of the self-excited system.

The controlled system consists of two main loops, the physical feedback loop and the control loop, as shown in Figure 5.3.

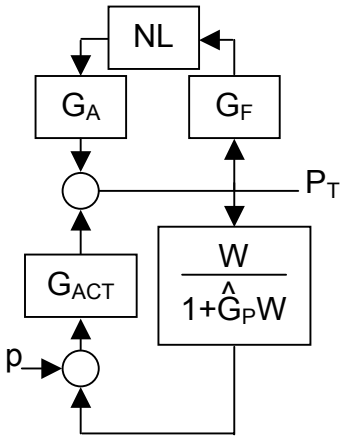

FIGURE 5.3 REDRAWN CONTROLLED SYSTEM

The optimal controller is defined to be that which completely nullifies the physical feedback loop. Equating the top loop to the bottom loop (with a minus sign) and solving for the optimal adaptive filter (W_{OPT}), results in

$$W_{opt} = \frac{-G_A G_F}{G_{ACT} + G_A G_F \hat{G}_p} \qquad \textbf{[5.2]}$$

By substituting [5.2] into the block diagram of Figure 5.3 as the adaptive filter W, it is obvious that the lower loop (feedback controller) exactly cancels the upper loop $G_A G_F$ resulting in a completely stabilized closed loop system. Equation 5.3 illustrates this result for the probe input shown in Figure 5.3:

$$\frac{P_T}{p} = \left. \frac{G_{ACT}(1+\hat{G}_p W)}{(1-G_A G_F)(1+\hat{G}_p W) - G_{ACT} W} \right|_{W=W_{opt}} = G_{ACT} \qquad \textbf{[5.3]}$$

Discussion of the optimal adaptive filter weights is more interesting for this self-excited plant application because of the quiescent state that the combustor will reach as soon as the poles have crossed back into the left-half Laplace plane under the action of the controller. Because the open-loop self-excited system of [5.3] does not contain dynamics that are on the imaginary

axis (i.e. marginally stable), there is a set of gains (between the imaginary axis and the optimal solution) that will stabilize the system without requiring the adaptive filter to reach its optimal solution. This system will be more lightly damped than the open-loop system but still stabilized. If the adaptation causes the system to stabilize, the error signal will go to zero and the adaptation will stop, never reaching the optimal gain.

5.3 THE CORRECT PLANT ESTIMATE

Initially, the system will be examined in the linear range so that the nonlinearity reduces to a simple gain that can be lumped with the flame dynamics, G_F. The total pressure (P_T) serves as the error signal to be reduced and is used by the adaptive feedback structure to update the weights and create the reference signal. The expression for the transfer function between the probe input of Figure 5.3 and P_T results in:

$$\frac{P_T}{p} = \frac{G_{ACT}(1+\hat{G}_p W)}{1 - G_A G_F - G_A G_F \hat{G}_p W + \hat{G}_p W - G_{ACT} W} \qquad \textbf{[5.4]}$$

In a purely feedforward situation, the dynamics from the control-to-error path are clear, and can be identified directly, often in the absence of the disturbance, and a model can be generated. The appropriate choice for the control-to-error path estimate is not as clear when the self-excited system is addressed. The self-excited system of Figure 5.3 offers two logical choices for the plant estimate. Following the standard procedure for feedforward problems, one choice for the plant estimate is the open loop dynamics of the control-to-error path, which yields

$$\frac{P_T}{p} = \hat{G}_p = \frac{G_{ACT}}{1 - G_A G_F} \qquad \textbf{[5.5]}$$

The acoustic dynamics have been moved from the *forward* path of the self excited loop and appear separately as part of the actuator dynamics and the self-excited *feedback* loop. (The same

acoustics influence the self-excited loop and the actuator path). Substituting this choice for the plant estimate, [5.5], into the denominator of [5.4] yields

$$1 - G_A G_F - G_A G_F \hat{G}_p W + \hat{G}_p W - G_{ACT} W \Big|_{\hat{G}_p = \frac{G_{ACT}}{1 - G_A G_F}} = 1 - G_A G_F \qquad \textbf{[5.6]}$$

This result guarantees that the adaptive filter cannot influence the poles of the closed loop system, and they will remain in the unstable right half plane. Therefore, this choice of the plant estimate [5.5] is not considered to be a valid solution and can never robustly stabilize the self-excited system.

An alternative proposal is to use the actuator path alone as the plant estimate such that $\hat{G}_p = G_{ACT}$. Assume the output of the acoustic portion of the self-excited loop is the external disturbance to be canceled at the error sensor. In this case, the dynamics between the control output and the error sensor represent the actual control-to-error path. In addition, the artificial reference signal now becomes an estimate of the exact disturbance signal at the error sensor. This can be seen by recognizing that:

$$\begin{aligned} P_T &= d + G_{act} c \\ r &= P_T - \hat{G}_p c = d + G_{act} c - \hat{G}_p c \end{aligned} \qquad \textbf{[5.7]}$$

in view of Figure 5.2 where d is the output of the acoustic plant, c is the output of the controller, P_T is the measured error signal and r is the derived reference signal. Not only is the reference signal accurately representing the disturbance to be cancelled (when the plant estimate is G_{ACT}), but the required plant estimate is of a strictly stable system. Using G_{ACT} as the control-to-error path estimate, we can again examine the closed loop system of [5.4].

$$\frac{P_T}{p} = \frac{G_{ACT}(1+\hat{G}_p W)}{1 - G_A G_F - G_A G_F \hat{G}_p W + \hat{G}_p W - G_{ACT} W}\bigg|_{\hat{G}_p = G_{act}} = \frac{G_{ACT}(1+G_{ACT} W)}{1 - G_A G_F - G_A G_F G_{ACT} W} \quad \textbf{[5.8]}$$

It is clear from [5.8] that the adaptive filter can now influence both the zeros and the poles of the closed loop control system, allowing for the possibility of stabilizing the self-excited system.

If we assume that the plant estimation error is zero and $\hat{G}_p$ is exactly equal to G_{ACT}, the block diagram of Figure 5.2 can be redrawn as shown in Figure 5.4.

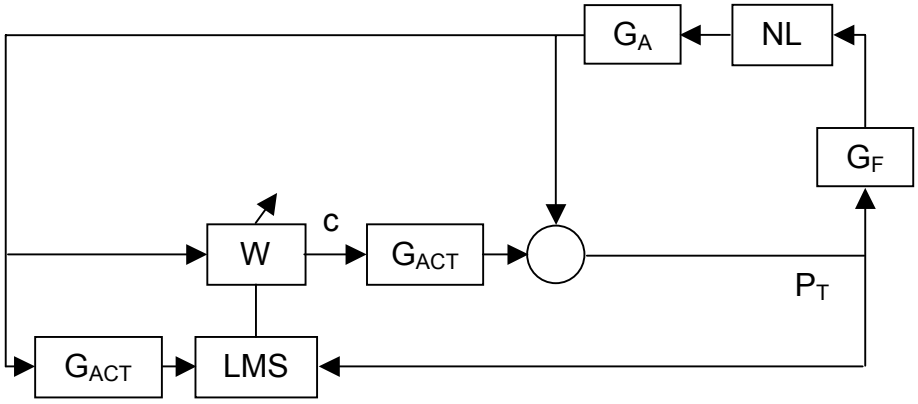

FIGURE 5.4 PERFECT IDENTIFICATION DIAGRAM REDRAWN

It is clear that when using the appropriate plant estimate (assuming perfect identification), the system is identical to the feedforward filtered-X structure and can theoretically behave as a feedforward system. In view of Figure 5.3, it is easy to see how the adaptive filter imparts the needed gain and phase to control the limit cycling system through the feedback loop. The significance of the control-to-error path estimate ($\hat{G}_P$) in the controller transfer function is also evident from Figure 5.3.

In practice, achieving a perfect system identification is not always practical. Here it is shown that if such a perfect identification was achievable, the appropriate plant estimate is the actuator dynamics. (The following chapter addresses the effects of errors in the plant estimate on controller stability). It is not a trivial task to obtain the actuator dynamics since they are influenced by the limit cycling system. However, the system identification procedure presented

in Chapter 3 illustrates how the actuator dynamics can be closely approximated by low level probing near the limit cycle frequency followed by a least squares model fit. In the following simulations and experiments, this system identification approach was employed and shown to generate models accurate enough to achieve stabilizing control.

5.4 SIMULATION

5.4.1 GENERAL

A simulation has been designed to permit rapid and easy investigation of the performance of the adaptive feedback controller in conjunction with the self-excited, limit cycling system. Results from the simulation agree closely with the behavior of the actual experiment. This is undoubtedly due to the fact that the dynamics which dominate the system are a single pair of lightly-damped acoustic poles. The two-part simulation described below is included in the Appendix.

Figure 5.2 represents the general form of the adaptively controlled self-excited system that was simulated. In the simulation, the self-excited loop consisted of a low pass filter to represent a model of the flame dynamics (G_F), a static nonlinearity represented by a hyperbolic tangent function, and a single-mode lightly-damped (2%) acoustical model (G_A) at approximately 175 Hz. The loop gain and nonlinearity gain were adjusted to yield a steady limit cycle after approximately 2 seconds at a sampling rate of 1600 Hz. The actuator path consisted of the same acoustical model plus some amount of phase delay. For the experiment, this delay represents all components in the control-to-error path. Equation 5.9 illustrates the actual transfer functions used in the simulation.

$$G_A = \frac{\text{-300000}}{s^2 + 43.98s + 1.21e6} \quad G_f = \frac{1500}{s + 1257} \quad G_{act} = \frac{\text{-.05581}z\text{-.0553}}{z^4 - 1.525z^3 + .9728z^2} \qquad \textbf{[5.9]}$$

The simulation runs in two separate modes, as does the experimental setup. After the limit cycle is established, a multi-tone probe signal is applied to the open loop plant as shown in Figure 5.5.

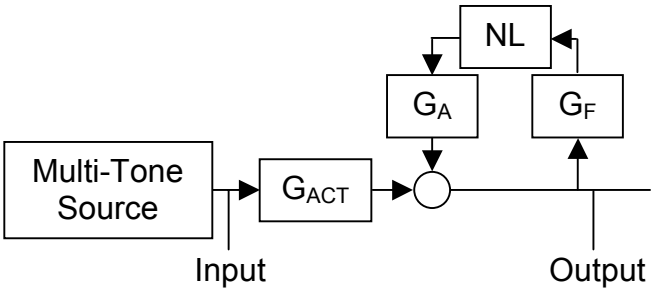

FIGURE 5.5 SYSTEM IDENTIFICATION – OPEN LOOP

The input to output relationship at the probe frequencies establishes the magnitude and phase of the linear plant as described in the system identification section from Chapter 3. In the simulation, the limit cycle is established prior to executing the identification with the multi-tone source input. As shown in Chapter 3, the resulting identification closely approximates G_{ACT} for the case where the input sinusoids are sufficiently lower than the limit cycle amplitude. The discrete frequency response data representing G_{ACT} is then used to generate a least squares infinite impulse response (IIR) transfer function fit in the z-domain, typically of order less than 6, with a pole very near the unit circle representing the "hot" acoustic mode. This fit is then used as the plant estimate, $\hat{G}_p$, during the second mode of the simulation. Figure 5.6 illustrates the results of the system identification portion of the simulation. The blue asterisks indicate the frequency response data collected with the multi-tone source in the presence of the limit cycle. The solid line illustrates the IIR transfer function fit to that data while the dotted line indicates the actual frequency response of the actuator dynamics. As predicted by [3.7] the actuator dynamics are closely approximated by the system identification procedure described in Chapter 3.

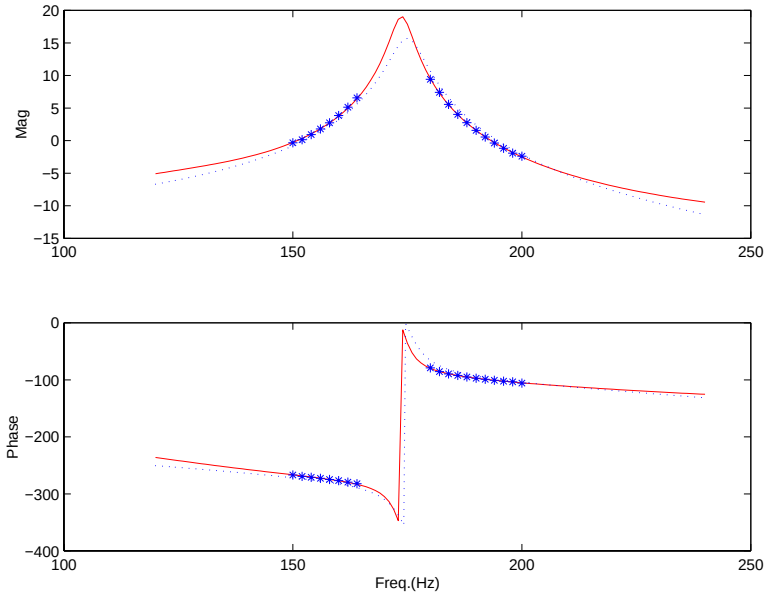

FIGURE 5.6 SIMULATION IDENTIFICATION RESULTS

After the limit cycle has reached a steady state, and the probe frequencies have been turned off, the plant model shown in Figure 5.6 is used in the adaptive feedback control loop shown in Figure 5.2; both as the Filtered-X part of the LMS and RLS algorithms and the plant estimate used to derive the reference signal.

5.4.2 LEAST MEAN SQUARES ALGORITHM

Implemented as shown in Figure 5.2, the Filtered-X LMS algorithm was used to control the self-excited system after it had sufficiently reached a stable limit cycle. To first simulate a low heat release operating condition, the plant dynamics shown in [5.9] were slightly altered to result in a lower loop gain. This was accomplished by reducing the gain of the flame dynamics from 1500 to 500. The plant estimate obtained from the system identification procedure (and shown in Figure 5.6) was used for both the feedback compensation and gradient adjustment of the Filtered-X algorithm. The FIR adaptive filter was chosen to have 2 weights for controlling the limit cycle frequency. This was determined to be adequate for the low heat release condition examined here. The adaptation stabilized the system within approximately 1 second using a convergence parameter of 1e-5. Figure 5.7 illustrates the power spectra of the uncontrolled and controlled systems.

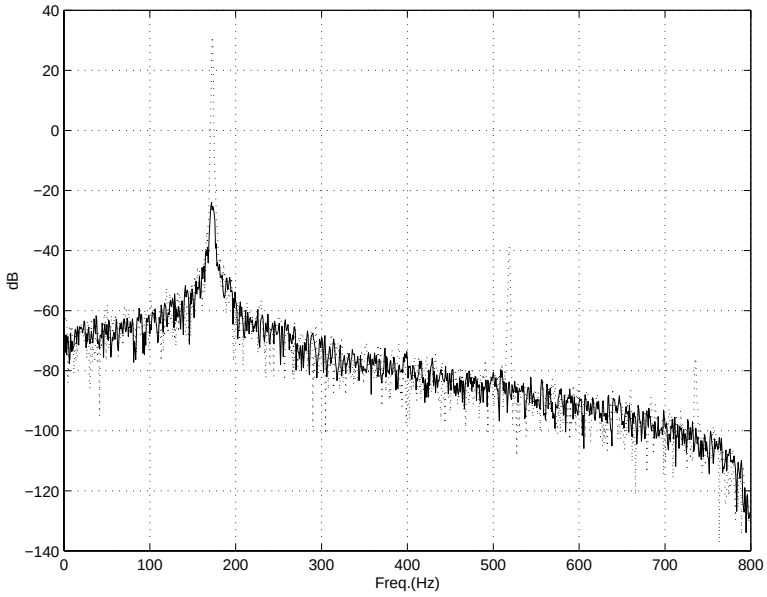

FIGURE 5.7 LOW HEAT RELEASE LMS SIMULATION

As mentioned earlier, it is not required that the adaptive filter achieve the optimal gain in order to drive the error signal to zero. Figure 5.8 clearly illustrates this by showing the path of the magnitude and phase of the actual adaptive filter during adaptation, as compared to the optimal magnitude and phase as computed from [5.2], at the limit cycle frequency.

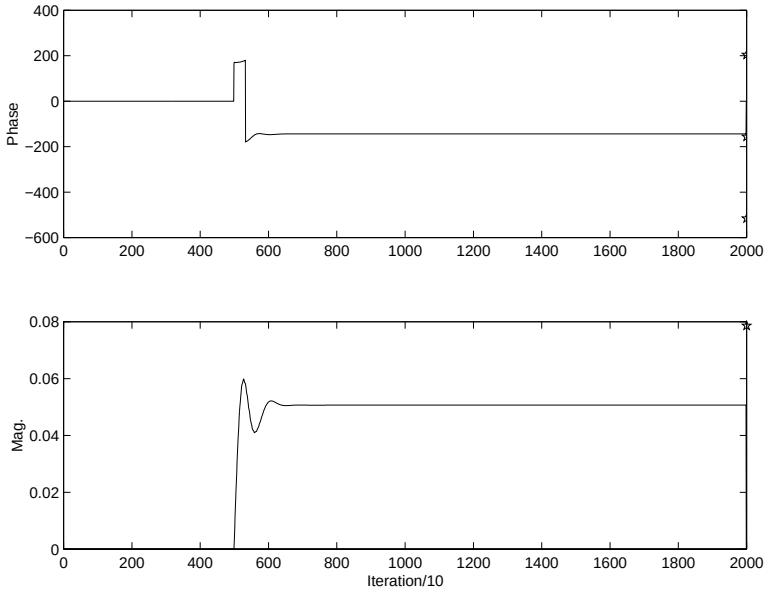

FIGURE 5.8 LOW HEAT RELEASE LMS PATH TO OPTIMAL

A second simulation was investigated in an effort to mimic the intermittent control witnessed in experiments at higher heat release conditions. The primary difference in the simulation and experiment was a bandpass filter that was used to filter out-of-band frequency components. This filter adds significant dynamics which ultimately affect adaptation and require additional adaptive filter weights to avoid instability. Using the dynamics of [5.9] to represent the higher heat release operating conditions, adding a bandpass filter, and increasing the adaptive filter size from 2 to 10 resulted in an intermittent searching condition not unlike the conditions seen in the experiment. In the controlled environment of a simulation, it is easier to identify the culprit of the intermittent behavior because every system parameter is available.

By investigating the feedback loops generated during adaptation, it was determined that the intermittency in the simulation resulted from the generation of unstable poles near the limit cycle frequency. Essentially, the added dynamics from the bandpass filter and the adaptive filter in the feedback loop, created unstable feedback loops within the structure of Figure 5.2. This is most easily explained by considering the Nyquist diagram at various points in the adaptation. First consider Figure 5.3. The open (control) loop with respect to the probe input and pressure output is expressed as

$$OLTF = \frac{G_{ACT}}{1 - G_A G_F}\left(\frac{-W}{1 + \hat{G}_P W}\right) \qquad \textbf{[5.10]}$$

where the bandpass filter is absorbed into the adaptive filter and the minus sign permits Nyquist analysis of a negative feedback system.

It is important to note here that the Nyquist plot can only be evaluated at a specific point in time, since the adaptive filter is continually changing. Therefore, the number of encirclements required to achieve stabilizing control may vary since the number of open loop unstable poles is a function of the adaptive filter. Figure 5.9 illustrates the intermittent time response of the LMS control of the high heat release condition. In addition, the Nyquist diagrams for various moments in time are also presented with associated stability criteria in the titles. Inherent in the evaluation of the Nyquist (and Bode) criteria is the assumption of system linearity as well as time invariance. The gain of the nonlinearity within it's clipping region can be accounted for in order to evaluate 5.10. While examining instantaneous Nyquist plots in this time varying system is not strictly acceptable, it can provided insight into the stability of the system at a specific point in time. If W is assumed to be held fixed at the moment of examination of the Nyquist criteria, we can establish the stability of the system at that specific moment in time. At the very least, this provides a tool for examining the movement of the poles over time and permits instantaneous stability information. No assumption is made for any of the Nyquist or Bode analyses, that stability will be guaranteed for all time, as long as W continues to adapt. Therefore, the Nyquist plots in the following figure do not represent controller stability *predictions* but instead provide instantaneous stability information during adaptation.

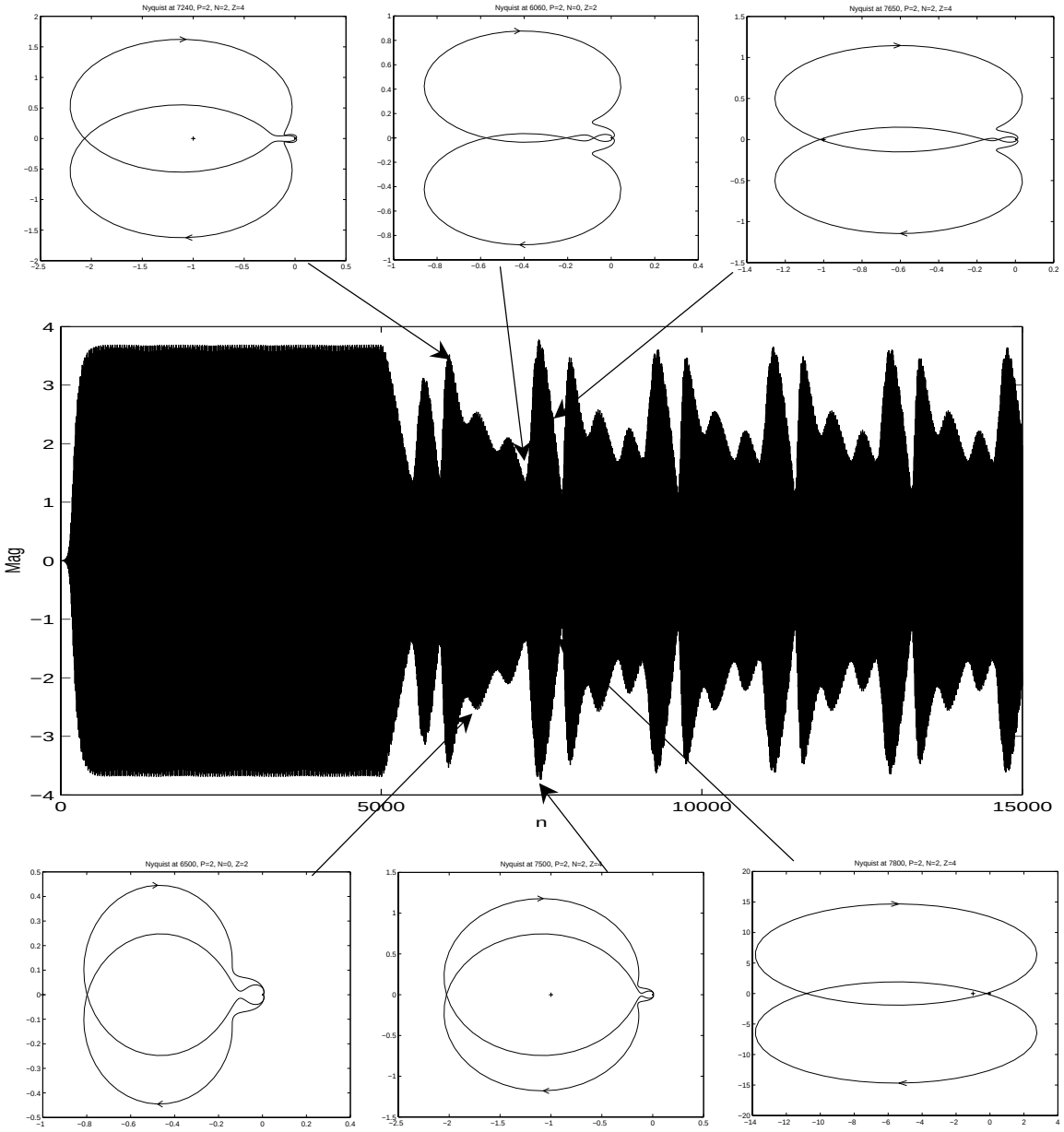

FIGURE 5.9 LMS INTERMITTENT STABILITY SIMULATION

The Nyquist plots shown above illustrate the stability of the closed loop system for different moments in time. In this case, the number of open loop unstable poles remains at 2 for the entire duration of the intermittency. The first two plots at 6060 and 6500 do not generate any encirclements of the –1 point and therefore the closed loop system has 2 unstable poles. At iteration 7240 two clockwise encirclements are generated during the adaptation. Unfortunately two *counterclockwise* encirclements are required to stabilize the system, and the result is 4 unstable

closed loop poles. The same result is seen at iterations 7500, 7650 and 7800 where the adaptive filter is unable to effectively generate the required encirclements. The process repeats starting at iteration 8000. It is interesting to examine the path of the frequency response of the controller as compared to the optimal solution at the limit cycle frequency as shown in Figure 5.10.

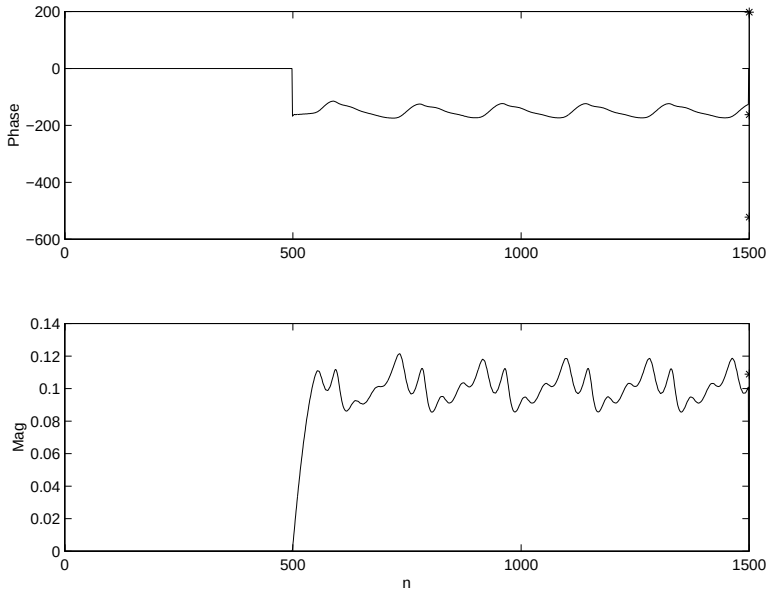

FIGURE 5.10 LMS INTERMITTENT PATH TO OPTIMAL

It is clear that the optimal magnitude and phase at the limit cycle frequency is reached by the adaptive filter and it cycles within the surrounding areas in conjunction with the intermittency. The difficulty arises due to the inability of the LMS algorithm to control frequencies that are not persistently excited. The unstable loops generated during adaptation create controller induced instabilities at frequencies other than the limit cycle frequency. Once these tones become predominant in the mean squared error, the LMS algorithm attempts to control these frequencies, while "forgetting" about the limit cycle frequency. This lack of memory inherent in the LMS algorithm is the cause of the inability to maintain stabilizing control in this particular simulation.

5.4.3 RECURSIVE LEAST SQUARES ALGORITHM

The memoryless LMS algorithm can be replaced by the more computationally intensive Recursive Least Squares (RLS) algorithm that retains knowledge of prior disturbances [47]. Employing the RLS algorithm in the same controller structure of Figure 5.2, the system is stabilized within one second of initiating control. Figure 5.11 is a similar representation to that of Figure 5.9, of the changing stability of the RLS controlled system.

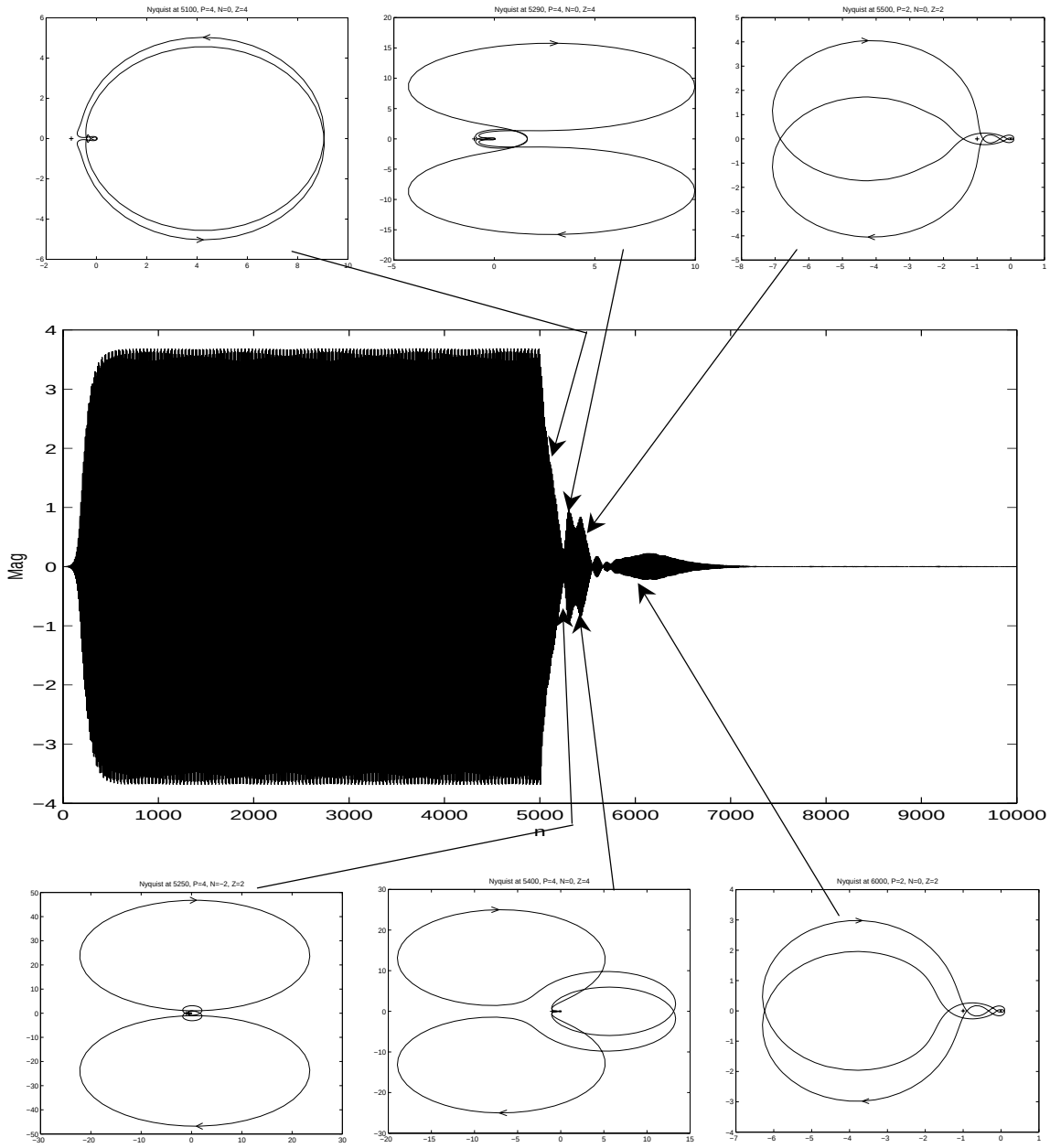

FIGURE 5.11 RLS INTERMITTENT STABILITY SIMULATION

As the RLS algorithm begins to converge at iteration 5100, there are 4 unstable open loop poles requiring 4 counter clockwise encirclements to ensure stability. As the algorithm adapts through iteration 5250 two counterclockwise encirclements are made but the system is still not stabilized. Through iteration 5290 and 5400 the frequency response begins to change and by iteration 5500 we see that only two open loop poles are unstable, requiring two

counterclockwise encirclements for stability. By iteration 6800 shown in Figure 5.12, the system has been stabilized[4].

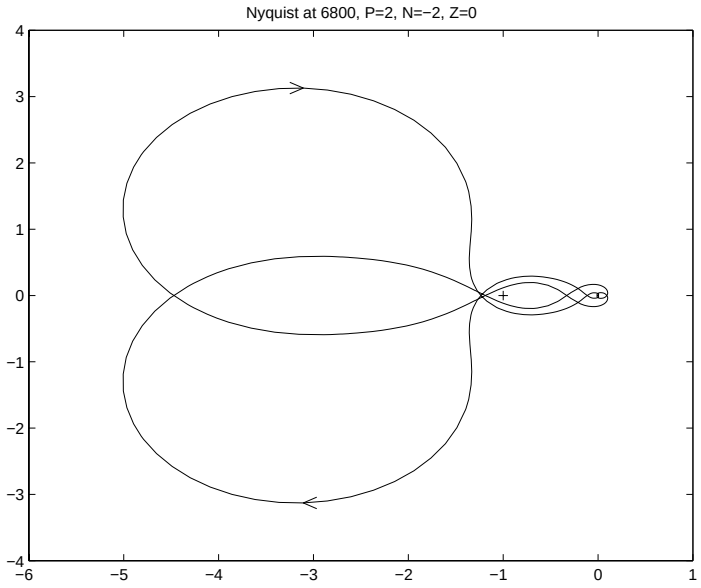

FIGURE 5.12 CONVERGED RLS CONTROLLER NYQUIST DIAGRAM

This set of simulations illustrates one possible mechanism for instability that may occur when employing an adaptive controller as shown in Figure 5.2. More detailed analysis of this and other instability problems is presented in the following chapter. While the RLS algorithm clearly offers significant benefits in avoiding controller induced instabilities, the intermittent behavior controlled in this simulation was not remedied in the experiment by the RLS algorithm.

5.5 EXPERIMENTAL RESULTS

The experimental process was identical to that described in the simulation section above. A multi-tone FRF was performed on the self-excited plant and a least squares fit was applied to

[4] For the benefit of recreating this simulation, it should be noted that the hyperbolic tangent function generated a less than unity gain in its linear region in the plant feedback loop. This gain must be taken into account when displaying the open loop frequency response data.

the data to generate an IIR filter model that represented the control-to-error path. This model was then used in the structure shown in Figure 5.2.

With the heat release at a relatively low gain (controlled by adjusting the equivalence ratio to a value of 0.51 and a total flow rate of 120 cc/sec), the Rijke tube combustor instability at 175 Hz was stabilized indefinitely with a two weight adaptive filter employing the LMS adaptation algorithm. Figure 5.13 shows (in asterisks) the actual magnitude and phase data collected from the tube along with the 6th order model frequency response shown as the solid line.

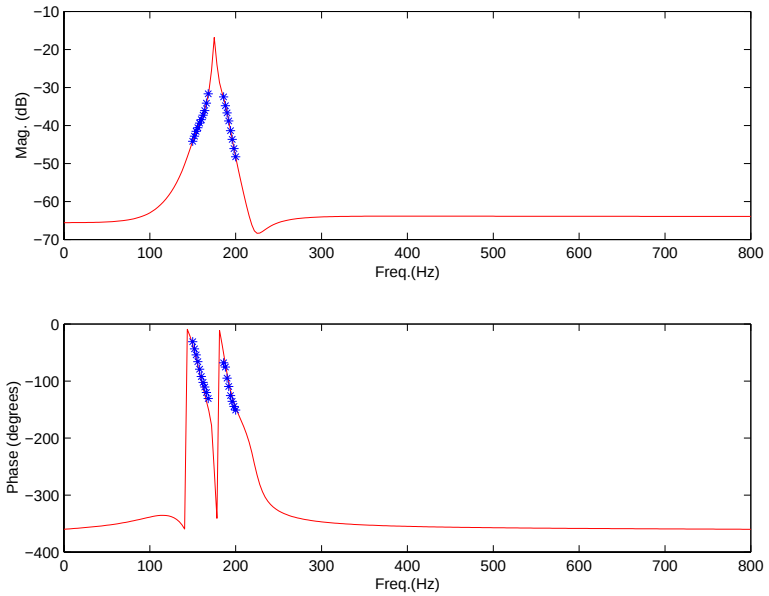

FIGURE 5.13 EXPERIMENTAL MODEL DATA AND FIT

Figure 5.14 shows the uncontrolled (dotted) and controlled power spectra of the total pressure in the tube (converted from voltage units). The second harmonic at 350 Hz disappears under control, revealing the shape of the third acoustic mode of the tube. The natural damping of the second acoustic mode is greater than that which is shown in Figure 5.14, but as discussed earlier, the system can be stabilized by having a pole in the left half plane that is more lightly damped than the natural acoustic mode.

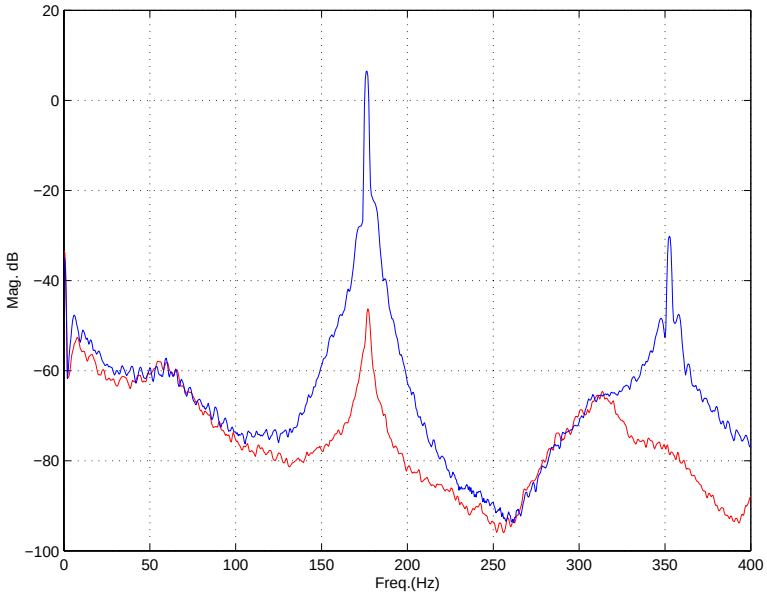

FIGURE 5.14 LOW HEAT RELEASE EXPERIMENTAL LMS CONTROL

A manually adjustable gain and phase shift controller was also applied to the same limit cycling system. Referring to Figure 5.3, it is apparent that the fixed gain controller replaces the transfer function:

$$\frac{W}{1+\hat{G}_p W} \qquad \textbf{[5.11]}$$

Examining the magnitude and phase of the converged equation 5.11 at 175 Hz as compared to the magnitude and phase of the fixed feedback controller, it is seen in Figure 5.15 that the phase of both controllers is nearly the same at 175 Hz. The magnitude, however, is significantly lower for the adaptive system and will not increase with time because the error signal has been driven below the 1-bit noise floor of the A/D. It is known that excessive gain can produce controller-induced instabilities[16]. The adaptive controller can prevent controller induced instabilities by changing its shape and adjusting its magnitude to minimize the mean squared error.

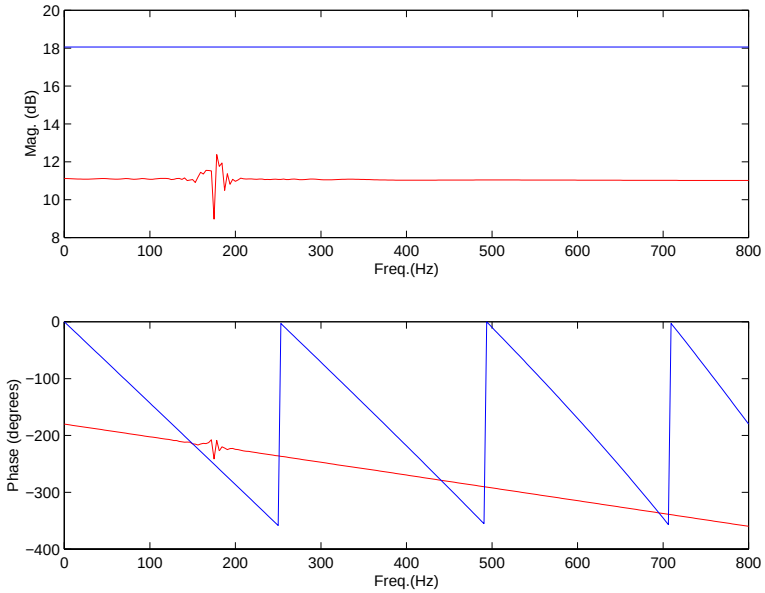

FIGURE 5.15 FIXED GAIN AND ADAPTIVE CONTROLLER COMPARISON

The results discussed above are indicative of the results obtained at a number of operating conditions at low equivalence ratios. As the equivalence ratio, and hence heat release, was increased, a point was reached where intermittent behavior was observed. Figure 5.16 compares the convergence behavior in the time domain of the adaptive feedback LMS algorithm for low and high heat release conditions. The upper time trace represents the convergence corresponding to the control performance in Figure 5.14 whereas the lower trace exhibits the intermittent searching behavior present at the higher heat release operating conditions.

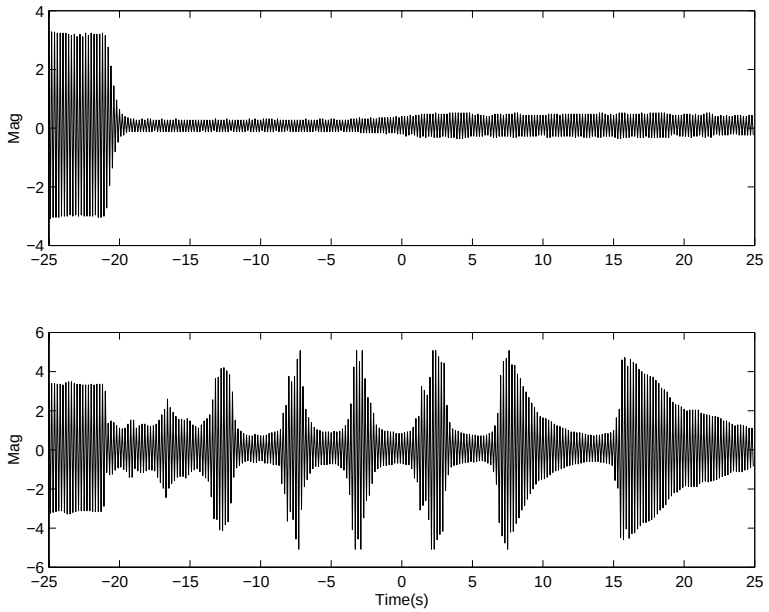

FIGURE 5.16 LOW AND HIGH HEAT RELEASE LMS CONTROL

As discussed above, the simulation predicted that the intermittency could be caused by the inability of the LMS controller to effectively control multiple disturbances occurring over different time periods. Also shown in simulation was the successful implementation of an RLS control algorithm that retained memory of previous disturbances and was therefore able to stabilize the high heat release system. The RLS controller was experimentally applied to the higher heat release operating conditions (equivalence ratio = 0.6 and total flow = 135 cc/sec) in the Rijke tube combustor. Figure 5.17 illustrates the corresponding time trace of that experiment.

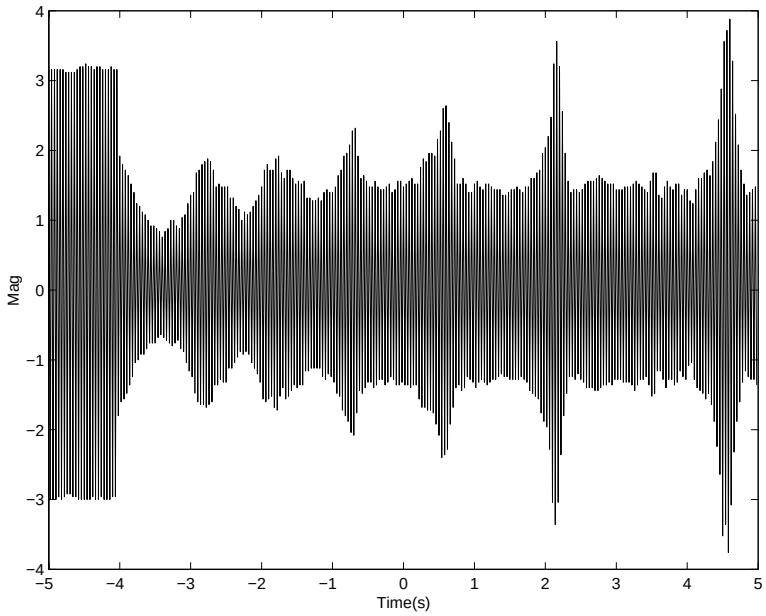

FIGURE 5.17 RLS CONTROL – HIGH HEAT RELEASE

It is clear that the RLS algorithm does not solve the intermittency problem at the higher heat release conditions. This provides convincing evidence that the intermittency is caused by a source other than feedback loop instabilities.

To better understand the intermittency phenomenon, a fixed gain feedback controller was applied to the combustor at the same operating conditions. This removed the variability inherent in the time varying (adaptive) controllers (both RLS and LMS). As shown in Figure 5.18, the fixed gain, controlled system exhibited the same cyclic intermittency.

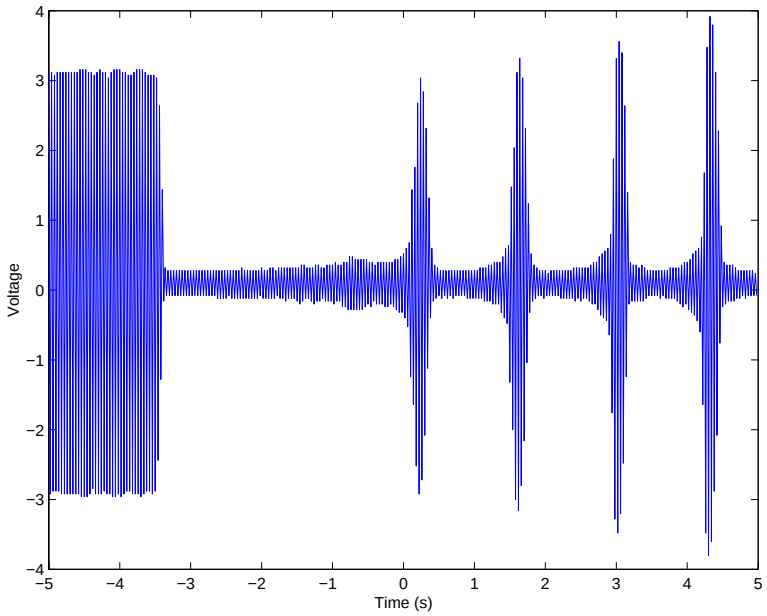

FIGURE 5.18 FIXED GAIN FEEDBACK CONTROL – HIGH HEAT RELEASE

Since the fixed gain feedback controller has no time varying components, it was determined that the flame dynamics must be changing in a periodic manner to cause the intermittent behavior. The following section provides ample experimental evidence to support this intermittency hypothesis.

5.6 ACTUATOR AUTHORITY AS A SOURCE OF INTERMITTENCY

Researchers have frequently witnessed intermittent behavior of self-excited systems when controlled by adaptive approaches. Quite often this behavior is attributed to algorithmic anomalies or controller induced instabilities. While each of these problems can contribute to searching or marginally stable behavior (as discussed in the following chapter), a third reason for intermittent behavior is presented here which is not related to time varying control. It is important to distinguish this form of intermittency from other instability mechanisms because the controller design itself is not at fault.

The self-excited combustion system is unique in that the plant dynamics change under the action of the controller. For a given set of limit cycling *operating conditions* described by a fixed equivalence ratio and flow rate, the combustor *operating point* can be described by the dynamic

gain of the flame dynamics, unsteady heat release rate that is a function of temperature, heat transfer rates to the combustor walls, and other unmodeled, low frequency dynamics. The pressure fluctuations from the limit cycle influence these low frequency dynamics. Consequently, when the pressure fluctuations are reduced by the feedback control, the operating point changes. This new, controlled, operating point can have enough increased gain and altered dynamics so that the actual control effectiveness may be limited by the original controller gain, controller phase, or actuator power. This effect can also be more detrimental at higher heat release conditions where actuator authority limitations become more relevant, required controller gain in the closed loop is higher, and the phase required for optimal application of controller gain has changed significantly. After experimentally describing the source of intermittency as a function of changing plant dynamics, a controller design solution is presented here where both controller phase and magnitude changes favorably correct the intermittency problem.

The physical behaviors causing the increased transfer function gain due to the lack of flame oscillation are described in some detail in [60]. Although the reasons for this changing gain as a function of flame oscillation are not clearly proven in terms of physical dynamics, there are several hypotheses. When the flame is disturbed by acoustic oscillations, fewer reactants can be effectively burned, thus reducing the amount of unsteady heat release that can occur. Another possible reason is that when the flame is not oscillating, it is "sitting down" on the flame holder and is distributed over a much smaller dimension in the direction of the flow. With the majority of the heat release concentrated in a more localized area, more gain can couple into the acoustic mode at a specific location. Depending on the combustor geometry, this may be a stabilizing or destabilizing effect. A third physical explanation of reduced flame transfer function gain is that dynamic oscillation of the flame (by the acoustic pressure fluctuations) causes more heat to be effectively transferred to the flame holder and surrounding walls rather than into the acoustic self excited loop. Whatever the reason for the altered gain, the following experimental evidence shows that the effect is real and repeatable. This effect can adversely affect the control performance and will be considered when redesigning the controller.

Based on the above observation, a hypothesis was developed and proven experimentally to define the searching phenomenon seen for fixed gain feedback control. The hypothesis can be explained most effectively in a multi-step process representing the transient characteristics seen in Figure 5.18. It is helpful to first recognize that the linear representation of the unstable pole in the s-plane moves further into the right half plane as the heat release is increased; this corresponds to an increase in self-excited loop gain. This indicates that more control authority/gain is required at higher heat release conditions to stabilize the system. **The core of the hypothesis is that the operating point changes, causing the self-excited loop gain to increase, when the flame is not being excited by oscillating pressure**. If we begin with the uncontrolled system at a high heat release operating condition and refer to Figure 5.19, the following physical phenomena occur:

- Without control, the self-excited linear system pole resides in the right half plane at operating point T1. Recognize that the *operating point* may change while the *operating conditions* remain constant.
- When the feedback controller stabilizes the system, the controlled system pole moves to location 2, still at the T1 operating point. Because the flame is no longer oscillating, the operating point begins to change causing gain in the self excited loop to increase. The controlled system pole gradually moves to location 3.
- When the self excited loop gain reaches operating point T2, the gain applied by the feedback controller is no longer sufficient to stabilize the system, and the flame begins to oscillate as the limit cycle grows.
- After sufficient oscillation occurs, the operating point moves back to T1, the self-excited loop gain is reduced, and the feedback control gain can again stabilize the system. The process repeats indefinitely.

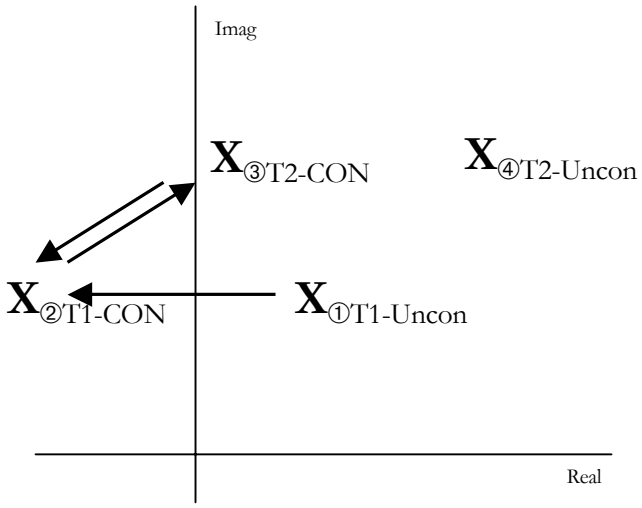

FIGURE 5.19 CONTROLLED SYSTEM POLE LOCATIONS

It is clear that this occurs because there is insufficient gain in the feedback controller to keep the system stable after initial control raises the self-excited loop gain. Indefinite stabilization only occurs when the controller has enough gain to stabilize the self-excited loop when the flame is not oscillating. Position 4 represents the *uncontrolled* self-excited dynamics if the flame were not oscillating, at the original operating condition and the new operating point. Because a stable flame increases the loop gain of the self-excited system, the controller must be capable of stabilizing the pole as it exists in location 4. For the experimental Rijke tube examined here, this only occurs in the range of lower equivalence ratios, based solely on the power of the acoustic actuator.

A series of experimental tests was devised to illustrate the above hypothesis. As a corollary to the hypothesis, it is assumed that **oscillation of the flame induced by acoustic pressure fluctuations reduces the gain in the self-excited loop**. To illustrate this effect, the Rijke tube operating conditions were set so that the fixed gain feedback control generated the undesirable intermittency behavior similar to Figure 5.18. After the intermittency was established, an external acoustic probe signal was injected into the combustion chamber at a high enough amplitude to oscillate the laminar flame. The time response is shown in Figure 5.20.

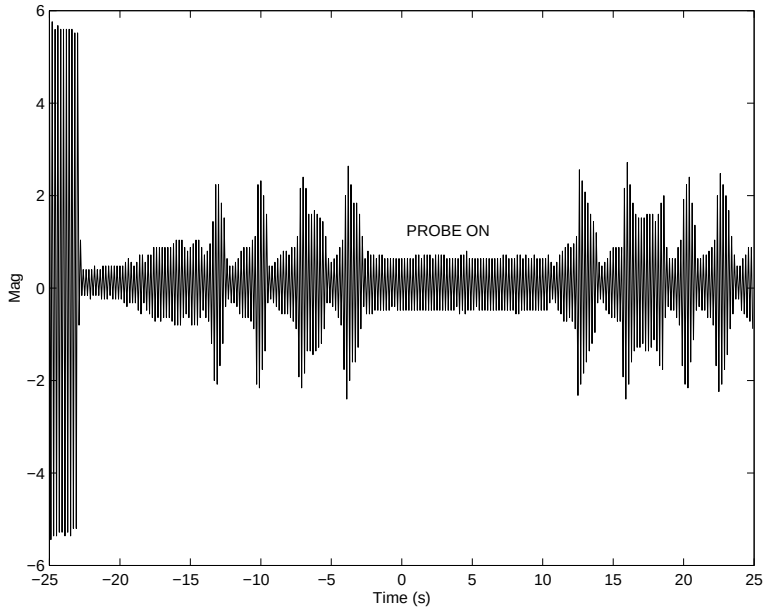

FIGURE 5.20 PROBE WITH INTERMITTENCY

Under the conditions of the hypothesis, the probe oscillates the flame and subsequently reduces the gain in the self-excited plant. As a result, the feedback controller should have enough gain to exercise control over the new plant whose gain has been reduced by the external probe. Beginning at approximately –3 seconds, the probe is turned on and the intermittency stops. This is due to the fact that the controller has placed the pole in a new stable limit cycle commensurate with the available actuator power. This will fall somewhere between positions 2 and 3 in Figure 5.19. When the probe signal is turned off at approximately 10 seconds, the intermittency behavior resumes as expected.

Figure 5.21 illustrates the power spectra of a single average for three locations on Figure 5.20. The dotted trace depicts the peak spectrum during a high intermittency cycle whereas the solid spectrum shows the minimum spectrum during a low intermittency cycle. The dashed trace represents the point in time when the probe frequency (at 130 Hz) was on.

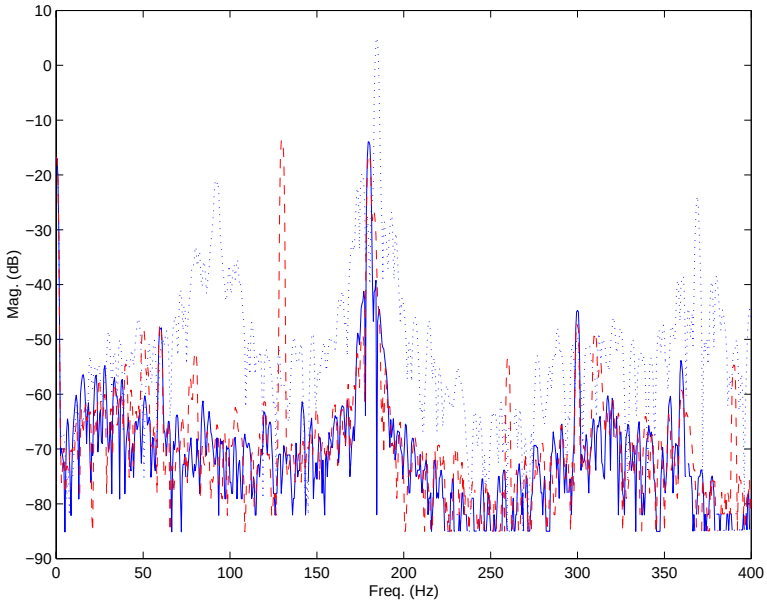

FIGURE 5.21 PROBE INTERMITTENCY SPECTRA

By injecting the probe at an amplitude equal to the minimum oscillating pressure seen during the intermittency cycle, the overall RMS pressure was limited to that of the minimum oscillation pressure. This may be viewed as a form of controller design where the intermittency is eliminated and the RMS pressure is reduced by 20 dB. But more importantly, this experiment illustrates that the loop gain is reduced by oscillating pressure, and conversely it is increased by the lack of oscillation.

A second experiment was conducted to analyze the effect of the amplitude of the probe signal on the self-excited loop gain. During intermittency, the control actuator is exercising it's maximum authority and it is still unable to maintain stabilizing control. As shown in Figure 5.20, the oscillation of the external probe reduced the gain of the self excited loop enough to allow the maximum available control authority to be sufficient to maintain a stable limit cycle. This implies that the oscillation has moved the pole positions of Figure 5.19 further into the left half plane by reducing the gain in the self excited loop. Consequently, higher amplitude oscillations should result in higher reductions in self excited loop gain. This effect is illustrated in Figure 5.22.

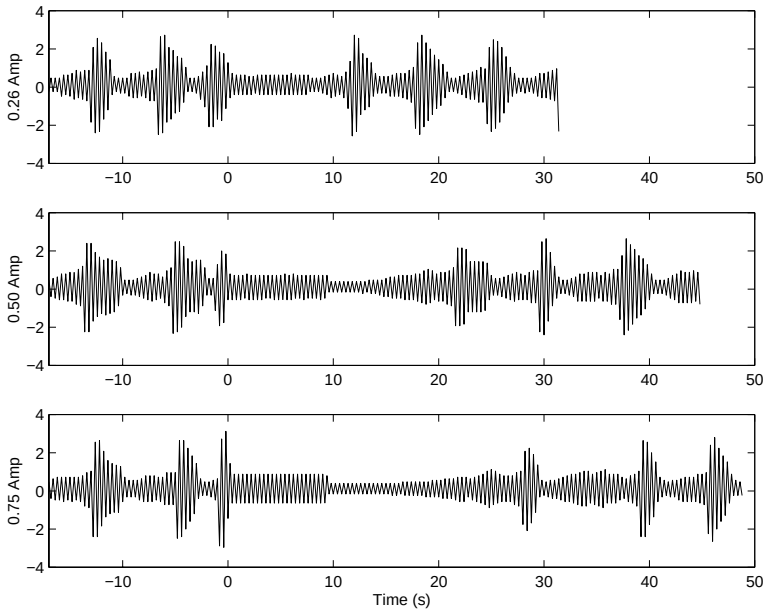

FIGURE 5.22 PROBE AMPLITUDE EFFECTS ON INTERMITTENCY RECOVERY TIME

Each of three probe amplitudes (0.26V, 0.5V and 0.75V) was initiated at time 0 and kept on for approximately 10 seconds. Upon release of the external probe at 10 seconds, the intermittency returned after increasingly long durations. This implies that the controlled pole location of position 2 in Figure 5.19 experienced a longer transient before returning to the familiar cycle between position 2 and position 3. The higher amplitude probe signals reduced the self-excited loop gain thereby causing the existing control authority to be more stabilizing. Restated, the time required to return to the intermittent behavior increased with probe gain because the controlled system pole was further into the left half plane after the probe was released.

The *period* of the intermittency also holds some information regarding the location of the poles on Figure 5.19. A transient response occurs each time the pole shifts from position 2 to position 3 and back, which is a function of the distance between the two pole locations. We have some control over the pole locations by imparting more or less gain to the feedback controller within a small window surrounding the limitations of the actuator. Figure 5.23 illustrates the effects of increasing the controller gain on the intermittency period for a given operating condition.

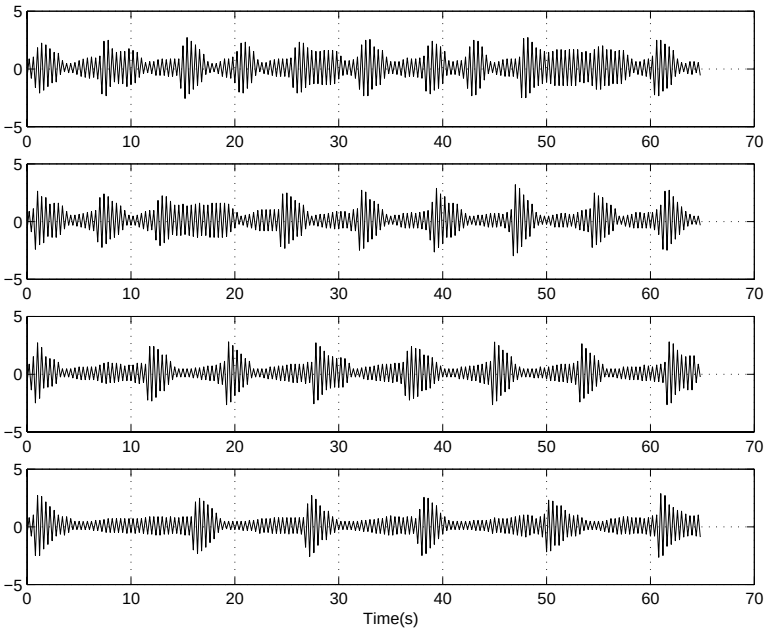

FIGURE 5.23 CONTROLLER GAIN INTERMITTENCY PERIOD

With each increase in controller feedback gain, the intermittency period increased. Two distinct behaviors occur when increasing controller gain that contribute to this increased period. First, higher control gain moves the stabilized position 2 of Figure 5.19 further into the left half plane, as much as can be tolerated by the given actuator power. Second, increased stabilized time (lower amplitude acoustic oscillations) contributes to greater gain in the self excited loop, moving the unstable position 3 (of Figure 5.19) further into the right half plane. Therefore as the control gain is increased, the "distance" between the two operating points grows and the transient response between conditions increases[5].

Evidence of the existence of the "virtual" pole location of position 4 in Figure 5.19 is also readily available. When the feedback control is immediately released after intermittent oscillation, the operating point is briefly at position 4 and ultimately decays to position 1. This is seen in the transient time response of Figure 5.24 where the feedback control is abruptly released.

[5] Heat transfer rates do not change in the system and therefore do not contribute to changing transients.

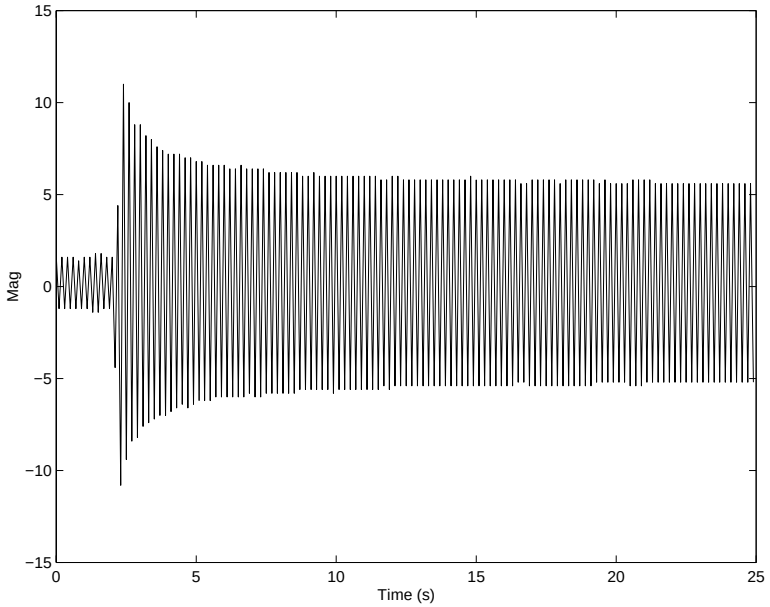

FIGURE 5.24 VIRTUAL POLE TRANSIENT RESPONSE

While these experimental studies provide supporting evidence toward the hypothesis, they do not prove that it is correct. The difficulty in directly illustrating the effects of oscillations on the flame dynamics transfer function lies in the fact that the nonlinearity in the self-excited loop is unknown. Therefore, the flame dynamics transfer function cannot be directly analyzed in the absence of the acoustics.

However, a separate test rig was constructed that presented a burner stabilized flame similar to that in the Rijke tube, without the acoustic chamber. Lacking the acoustic interaction, the system is not unstable and therefore does not contain a nonlinearity. To prove the dependence of loop gain on flame oscillation, this burner stabilized flame was excited at various probe amplitudes while the gain of the flame transfer function (acoustic velocity to OH*) was recorded. The following table shows the results.

TABLE 5.1 FRF AMPLITUDE AS A FUNCTION OF PROBE GAIN

Probe Gain (V) @ 130 Hz	FRF Amplitude (dB) @ 170 Hz
0.0	0.86
0.05	0.82
0.1	0.58
0.2	-1.32
0.3	-3.00

The FRF amplitude of the flame dynamics transfer function translates directly into self excited loop gain once the acoustic dynamics are present. It is therefore clear that changes in acoustic pressure oscillations affect the gain of the self excited loop. It should be noted that this effect can also be observed in the low equivalence ratio cases that were stabilized. For example, in the upper trace of Figure 5.16, near the zero second point, a change in the level of the controlled oscillation is observed. This is undoubtedly due to the changing of the flame dynamics following the dramatic change in oscillation amplitude after control is first applied.

The previous discussions illustrate that the intermittency behavior is caused by changing plant dynamics. It should also be clear that the dynamics represented by Figure 5.19 are an accurate representation of the actual behavior of the controlled system. *Actuator authority* has been stated to be the reason for the inability of the control system to impart enough gain to control the higher heat release operating condition. This is confirmed by examining Figure 5.25.

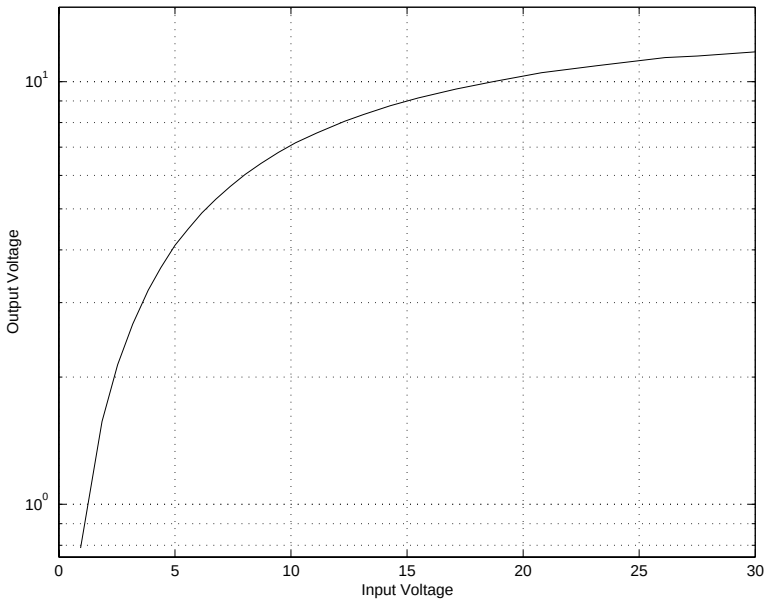

FIGURE 5.25 ACTUATOR AMPLITUDE RESPONSE

Figure 5.25 illustrates the pressure output (expressed in voltage) as a function of the input voltage to the speaker. The pressure voltage (y-axis data) is presented on a log scale because the ability to control sound pressure is most commonly expressed in dB (log units). Appreciable increases in output pressure for similar increases in input voltage continue until between 15 and 20 V of input voltage. At this point, increases in the pressure output of the speaker are significantly reduced, and no further appreciable actuation authority can be provided.

For the high heat release operating condition considered above, when the flow rate is 135 cc/sec and the equivalence ratio of 0.6, the actuator did not have enough power to achieve effective (stabilizing) control (Figure 5.18). Figure 5.26 illustrates the early transient voltage applied to the actuator over a 2.5 second period at the inception of control for an even higher equivalence ratio of 0.64 corresponding to higher unsteady heat release rate and self-excited loop gain.

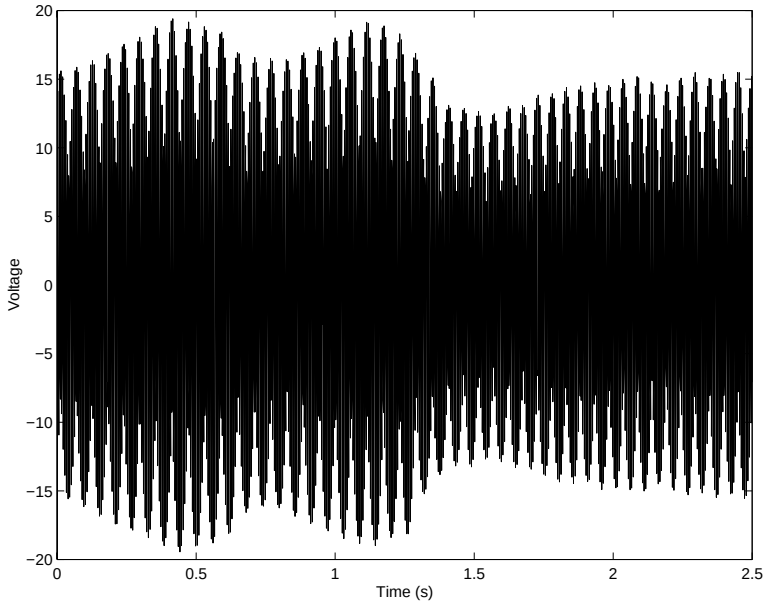

FIGURE 5.26 ACTUATOR VOLTAGE FOR HIGH HEAT RELEASE

During the first second of control, the actuator is driven with nearly 20 volts (peak). Referring to Figure 5.25, this is clearly in the nonlinear range and the actuator has difficulty providing the SPL required to achieve control. The feedback control system began intermittency after the first 2.5 seconds. Acoustic actuators capable of delivering higher amplitude SPL's in a more linear fashion than that illustrated in Figure 5.25, will facilitate control at a broader range of operating conditions, eliminating the intermittency for higher heat release conditions.

In this particular case the actuator does not have the power to stabilize the system indefinitely, therefore no controller design can provide stabilizing control. However, it is possible to redesign the feedback controller such that a lower amplitude limit cycle is created, without generating an intermittency. A new, lower amplitude, stable limit cycle is clearly more desirable than high amplitude intermittencies, although the actuator may be operating near its power limitations. Figure 5.27 illustrates the application of a controller with a certain magnitude and phase setting designed to stabilize "T1" flame condition discussed above.

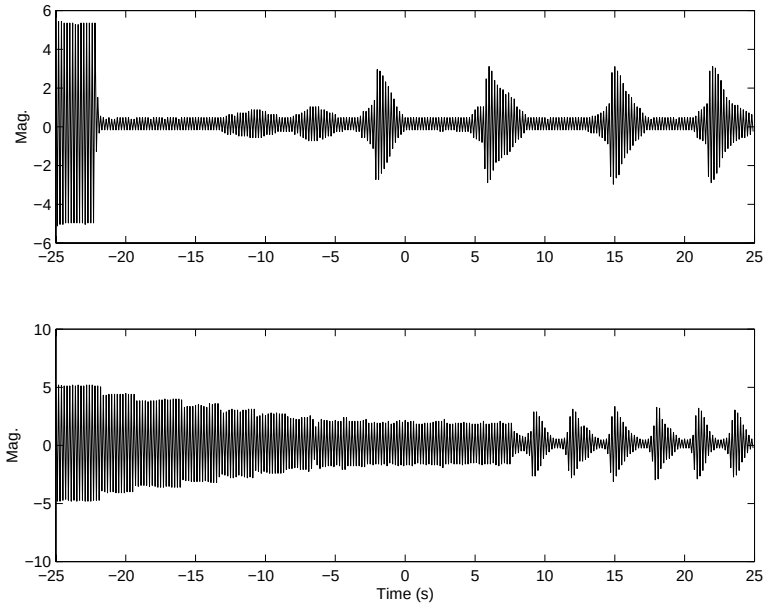

FIGURE 5.27 SUB-OPTIMAL CONTROL

The upper plot of Figure 5.27 illustrates the fast application (turning on) of the feedback controller designed for this flame condition. After approximately 10-15 seconds the intermittency begins. Applying the same gain gradually to the self-excited system, we see that the intermittency occurs regardless of the speed of application of the gain. Although it is (experimentally) clear from the above discussions that actuator authority limits controllability of the system and helps cause the intermittency, the controller can be redesigned to prevent the intermittency if it is designed to exercise the maximum amount of control for the "T2" flame condition.

In order to design a controller (magnitude AND phase) for a specific condition, we must first generate that condition. Since the controller itself affects the plant and generates the condition requiring control, we mush slowly approach that condition while continually searching for a better controller design. First assume that the controller designed for condition "T1" is acceptable for controlling the T2 condition. We slowly increase the feedback gain on the controller while examining different phase settings to achieve the minimum error for a given gain setting. This process repeats until either 1) further increases in gain and subsequent phase adjustment do not result in detectable decreases in the error signal (indicates actuator is

saturated) or 2) the system is stabilized. The upper plot of figure 5.28 illustrates this iterative manual control design process.

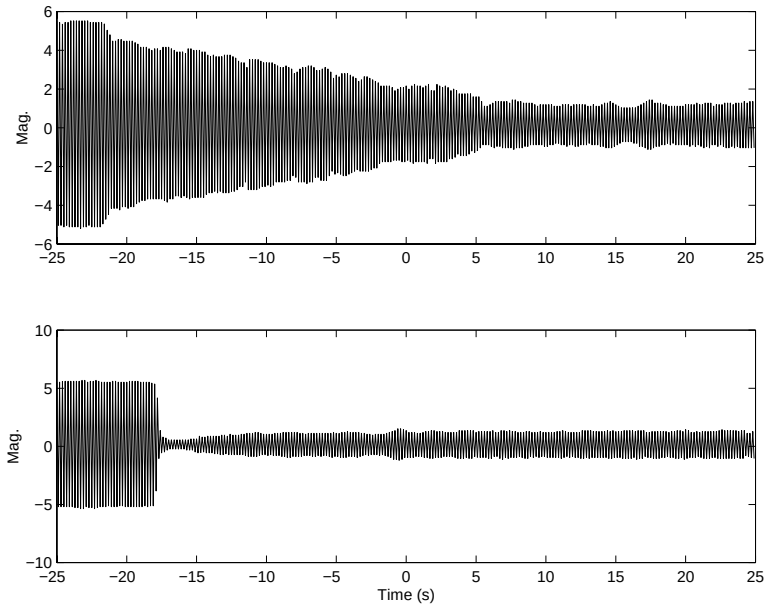

FIGURE 5.28 GAIN SCHEDULED CONTROL

This new controller magnitude and phase has now been designed for the flame condition that it will be controlling because that condition was created by the existence of the controller in the loop. Now, when the controller is turned on instantaneously as shown in the lower plot of Figure 5.28, the system doe not oscillate intermittently. Instead, a lower amplitude stable limit cycle is created at the limits of the actuator authority at a different phase and gain setting that might be selected to control the "T1" flame condition.

For adaptive controllers, this can be implemented using an appropriately large and scheduled leakage parameter so that the adaptive weights cannot reach their optimal solution immediately. The adaptive filter would then gradually adapt to an optimal solution, allowing the controlled flame condition to be taken into account during slow adaptation. Another possible solution is to add a secondary probe signal to the control signal to eliminate the searching behavior as seen in Figure 5.21. This intentionally oscillates the flame so that the self excited loop gain is low enough that the controller can maintain stabilizing control at the limit

cycle frequency. Each of these techniques strives to reduce the limit cycle amplitude as much as possible using all of the available actuator authority, without allowing intermittency.

5.7 CONCLUSIONS

Previous research aimed at applying filtered-X LMS techniques to control combustion instabilities has met with limited success. One reason for this limited success is that the self-excited problem is fundamentally different from the stable, exogenous-disturbance problem. This chapter shows that the most appropriate choice for the plant dynamics in a filtered-X LMS structure is the control-to-error dynamics, which include the hot acoustics but not the physical feedback loop of the self-excited system. Furthermore, it is shown that this stable transfer function can be accurately estimated when the self-excited loop is closed.

Experimental results on a Rijke tube combustor with acoustic actuation have shown that an LMS-based adaptive controller, using the identification technique discussed in Chapter 3, can stabilize the combustor indefinitely. For operating conditions that did not achieve stability, a searching behavior was observed. Although simulations indicated that unstable feedback loops can generate such behavior, the intermittency was ultimately shown to be due to limitations in actuator authority and not the adaptive nature of the controller. Experiments showed that the gain of the physical feedback loop was related to the RMS velocity fluctuations in the combustor and this gain increased as control reduced the fluctuations. At the higher heat release conditions, the actuator was not powerful enough to stabilize the system after the loop gain increased following an initial reduction in oscillations.

Although the adaptive structure proposed in here performed reliably in experiments, this structure introduces additional feedback loops and differs fundamentally from feedforward LMS implementations, which have strong stability guarantees. The following chapter provides a detailed analysis of the stability and convergence of the adaptive feedback structure.

Chapter 6

Adaptive Feedback Control Analysis

Adaptive feedforward control is inherently stable and can effectively attenuate and often cancel disturbances. However, the requirement for a coherent reference signal that is unaffected by the control signal prevents practical implementation for many applications. The primary reason for this limitation is that contamination of the reference by the control signal invariably creates a feedback loop, thus rendering the stability advantage of feedforward control nonexistent.

When the required reference signal is contaminated by the control signal, the problem can be converted to a feedforward form by adding an additional signal path that cancels the effect of the control signal on the reference. When the reference signal is identical to the error signal, it is termed "filtered-E" control. Filtered-U control is a more general version where the reference and error signals are physically different, but are both influenced by the control actuator. Adaptive IIR filtering can be used to try to *adaptively* cancel the feedback path created by the control signal's influence on the reference signal. "Adaptive IIR" and "filtered-U" are often used interchangeably because fixed gain compensation of the feedback path is less common in practice. The majority of the discussion in this chapter focuses on filtered-E control but the conclusions are extended to filtered-U forms. The filtered-E approach was used exclusively throughout Chapter 5.

Adaptive LMS-based feedback controllers have been implemented in a variety of forms on a variety of systems including thermoacoustic instabilities. While some success has been realized in specific applications, sporadic behavior has plagued broad acceptance. This chapter examines two distinct mechanisms that may explain these unstable behaviors: feedback loop instabilities and algorithm divergence. Unlike feedforward adaptive control, feedback loop instabilities can be created when adaptive controllers are used in structures containing feedback

loops. This mechanism is examined as a function of plant estimation error for both stable and unstable systems. A second mode of instability can occur when the plant estimate is inaccurate, causing the filtered-X LMS algorithm to diverge. This discussion shows why the conventional interpretation of acceptable plant estimation errors is incorrect in a feedback setting and presents a method for computing the correct gradient filter.

The chapter is organized as follows. A brief introduction to filtered-E control is provided in the context of filtered-X LMS control. Feedback loop instabilities and algorithm divergence are examined analytically in terms of the plant estimate for stable systems. This explanation of instabilities experienced during adaptation presents some expected causes for sporadic behavior in experimental applications. Next, the results are extended to filtered-U control structures as well as the control of unstable, self-excited plants. In addition, the dependence of the instabilities on each other, and the use of online system identification techniques are examined for both adaptive feedback and filtered-U control. Finally, two simulations are presented. The first illustrates a feedback loop instability independent of algorithm divergence. The second simulation shows how a conventionally accurate plant estimate can yield an algorithm divergence independent of a loop instability. This is shown to agree with the analytical results.

6.1 FILTERED-E CONTROL

6.1.1 OVERVIEW

Adaptive feedforward control has received considerable attention over the last few decades, particularly with application to active noise control [46]. The popular filtered-X variant shown in Figure 6.1 has clear advantages over comparable feedback structures.

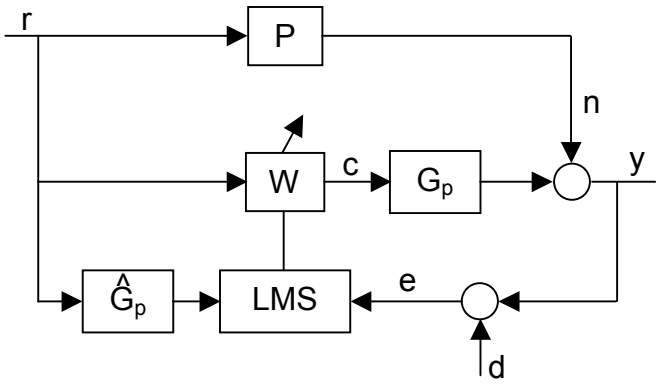

FIGURE 6.1 ADAPTIVE FEEDFORWARD CONTROL

Due to its feedforward architecture, the control system is inherently stable when W is an FIR filter and the adaptation is sufficiently slow. In addition, the filtered-X LMS algorithm ensures convergence for physical systems whose adaptive filter output encounters a dynamic system before being sensed by the error signal.

The LMS algorithm updates the future weights of the adaptive filter in response to a scaled, instantaneous measurement of the local gradient (derivative of the squared error) as

$$W_{k+1} = W_k - \mu \nabla_k \qquad \textbf{[6.1]}$$

The "filtered-X" moniker indicates that the reference signal must be filtered by an estimate of the control-to-error dynamics in order to accurately estimate the correct gradient at the error signal. This can be seen by computing the gradient directly as the derivative of the squared error with respect to the weight vector as shown below.

$$
\begin{aligned}
E(z) &= -N(z) - G_p(z)W(z)R(z) \\
\nabla E(z) &= \frac{dE(z)}{dW(z)} = -G_p(z)R(z) \\
\nabla e_k &= -G_p * \vec{r}_k \\
\nabla_k &= \nabla e_k{}^2 = 2[\nabla e_k]e_k = -2(G_p * \vec{r}_k)e_k
\end{aligned}
\qquad \textbf{[6.2]}
$$

where * denotes the convolution operation in the sample domain.

It is clear that the reference input (r) must be filtered by the plant before being multiplied by the error to compute the instantaneous gradient. Since the plant itself is not available in physical applications, an estimate of that plant transfer function is typically used. It is well known [39, 48, 40] that this estimate must be accurate to within 90° of phase when compared with the actual plant to ensure convergence of the algorithm. If the estimate is incorrect by more than 90°, the algorithm will search in the wrong direction and eventually diverge[6].

One of the primary limitations of practical implementation of the adaptive feedforward controller of Figure 6.1 is the requirement for an uncontrollable, coherent reference signal. The LMS algorithm assumes that r is highly correlated with n (the disturbance to be canceled) and that the output of the adaptive filter (c) does not influence r. If the former is violated the control performance suffers; if the latter is not satisfied, a feedback loop is introduced that might become unstable during adaptation. In active noise control applications, it is often difficult to obtain a reference signal that is both coherent with the disturbance and not influenced by the controller. Adaptive feedback control attempts to remedy this problem.

Figure 6.2 illustrates a typical filtered-E controller arrangement [56, 48].

---

[6] This result has been proven using a variety of tehcniques [39,48,40]. However, the literature only contians proofs for single sinusoids and/or special sampling conditions. Although no broadband proof of the 90° rule exists, all experiments and simulations confirm the criteria in a broadband sense. Proving this criteria for generalized systems may be a source of future work.

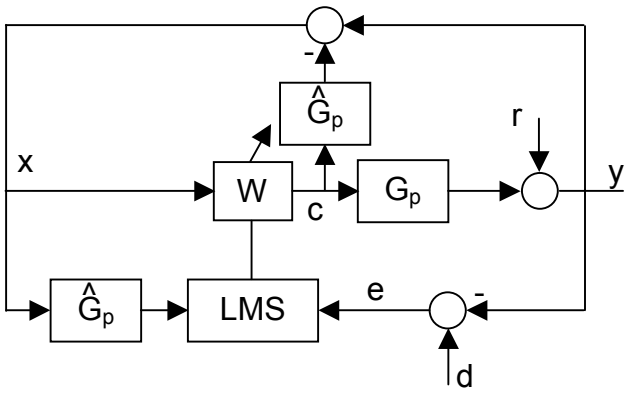

FIGURE 6.2 FILTERED-E CONTROL

This arrangement employs the filtered-X LMS algorithm with an estimate of the actual control-to-error path, $\hat{G}_p$. The external disturbance (r) enters at the error sensor along with the filtered control output as in Figure 6.1. Since there is not another reference signal available, the error is used to estimate the reference signal (x) by subtracting the influence of the controller from the error signal sensor.

$$x = (r + G_p c) - \hat{G}_p c \qquad \textbf{[6.3]}$$

In view of [6.3], if $\hat{G}_p = G_p$ the reference signal is exactly equal to the disturbance to be canceled and is therefore coherent and uncontrollable. Significant difficulties can arise when $\hat{G}_p$ deviates from G_p.

Before continuing, it should be noted that Figure 6.3 illustrates the same system of Figure 6.2, only redrawn.

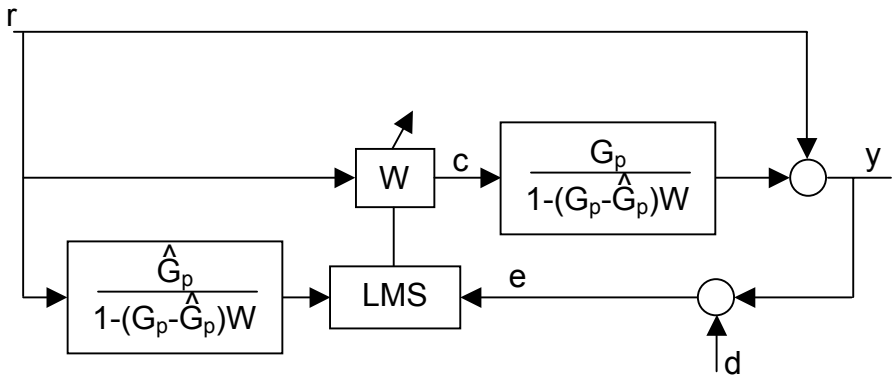

FIGURE 6.3 FILTERED-E CONTROL REDRAWN

This reformulation of the filtered-E block diagram into a feedforward, filtered-X style system, clearly shows the inherent dependencies that the system has on the adaptive filter. Here we see that the adaptive filter is a part of the control-to-error path and can also adapt poles. The effects of these dependencies on the stability of filtered-E controllers are the focus of this chapter.

6.1.2 FEEDBACK LOOP INSTABILITIES

Simply using an adaptive filter in a control system does not imply global stability. In fact, if it is employed in an arrangement as in Figure 6.2, stability can not be guaranteed during adaptation. Consider the system of Figure 6.2 at a moment in time when the adaptation is slow, or has stopped. A transfer function expressing the system input to output relationship is

$$\frac{y}{r} = \frac{1+\hat{G}_p W}{1+\hat{G}_p W - G_p W} \qquad \textbf{[6.4]}$$

If $\hat{G}_p$ is exactly equal to G_p the denominator vanishes, leaving a strictly feedforward system. Assuming W is an FIR filter and the control-to-error path is a stable system, the system dynamics are guaranteed to be stable regardless of W. If however, $\hat{G}_p$ is not equal to G_p at any frequency, the system poles can become unstable and are defined by the denominator of [6.4].

There are many classical control techniques that can be used to analyze the stability of linear systems including root locus, Routh Hurwitz, Nyquist plots, and Bode plots [50]. For experimental systems where dynamics are not explicitly known, the most convenient and intuitive of these is the Bode analysis. The Bode stability criteria uses the open loop frequency response function to predict closed loop performance. The open loop transfer function of Figure 6.2 can be expressed as

$$\frac{G_p W}{1+\hat{G}_p W} \qquad \textbf{[6.5]}$$

At frequencies where the magnitude of [6.5] is greater than unity for phase values equal to 360 degree multiples (for positive feedback), the loop will be unstable. It should be noted that the Bode analysis assumes that the open loop transfer function is stable, i.e. that the roots of (1+ $\hat{G}_p W$) are in the left half plane. If they are not (determined by examining the open loop frequency response of $\hat{G}_p W$), the Nyquist criteria provides a similar stability analysis for the closed loop system assuming the number of unstable roots is known explicitly.[7]

It should be clear from [6.4] and [6.5] that any loop instability resulting from unstable poles of [6.4] is a function of both the adaptive filter and the error between the plant and its estimate. This is a system dependent phenomenon which cannot be predicted by assuming W only reaches a fraction of the optimal solution as suggested by [53]. The optimal adaptive filter (found when the error is set to zero) is

[7] Inherent in the use of Bode and Nyquist stability criteria is the assumption of linearity and time invariance. While the systems considered here are typically linear, or operating within the bounds of any present non-linearities, they are not strictly time invariant because of the presence of the adaptive filter W in the open loop plant. Nevertheless, these stability tools can be applied assuming that the adaptive filter is held fixed at the point in time at which they are examined. This gives no guarantees concerning future stability, but provides an indication of the instantaneous stability assuming adaptation has stopped.

$$W_{opt} = -\frac{1}{\hat{G}_p} \qquad \textbf{[6.6]}$$

Assuming a plant estimate error exists, and the adaptive filter has reached the optimal, [6.4] can still become unstable at a specific frequency even though the numerator is zero. Likewise, it is possible that the denominator of [6.4] is stable, and the system has driven the error to zero with no unstable roots. The stability of the system must be examined on a case by case basis. It will be a function of the frequency dependent error between the plant and plant estimate as well as the size and shape of the adaptive filter, regardless of whether it has reached the optimal solution.

Equation [6.6] illustrates that the optimal solution is only a function of the plant estimate, which we have obtained *a priori*. This raises important questions about the purpose of adapting if the optimal solution is already pre-determined. For broadband disturbance suppression, [6.6] must be satisfied at every frequency. Typically this is an impractical modeling task for non-minimum phase systems or finite duration FIR filters. Adaptation of W will result in the best compromise for control by inverting at the specific frequencies contributing most to the mean squared error. Tracking changes in those disturbance frequencies also presents a good argument in favor of adapting W which will ensure the optimal is maintained.

6.1.3 ALGORITHM DIVERGENCE

Conventional interpretation of the plant estimation error for the filtered-X LMS algorithm indicates a 90° error between the control-to-error path and it's estimate is tolerable. This discussion illustrates that this interpretation is not valid for the filtered-E system of Figure 6.2. First consider that

$$x = y - \hat{G}_p c = r + (G_p - \hat{G}_p)c \qquad \textbf{[6.7]}$$

follows from Figure 6.2 and [6.3].

Assuming slow adaptation, it is possible to rearrange Figure 6.2 such that the disturbance (r) is the system input as well as the exogenous disturbance; Figure 6.3 results. The feedforward structure of Figure 6.3 facilitates the understanding of the *actual* plant error analysis as compared to the *conventional* plant error.

The *conventional* plant estimate error of this system is the difference in the control-to-error path and the estimate of the control-to-error path used for the "filtered-X" portion of the algorithm. From Figure 6.3, this can be seen to be

$$\angle\left(\frac{G_p}{1-(G_p-\hat{G}_p)W}\right)-\angle\left(\frac{\hat{G}_p}{1-(G_p-\hat{G}_p)W}\right)<90^\circ \qquad \textbf{[6.8]}$$

This is expressed equivalently as

$$\angle G_p-\angle\hat{G}_p<90^\circ \qquad \textbf{[6.9]}$$

and is hereafter defined as the *conventional plant estimation error* (which is equivalent to the plant estimation error in view of [6.2]) because of its common usage in all adaptive controller arrangements. This is consistent with the conclusions reached in [6.2] and represents the common interpretation of the plant error that must be satisfied to ensure convergence for filtered-X LMS control.

The filter preceding the LMS algorithm (the second term in [6.8]) is the conventional reference signal filter when employing the filtered-X control strategy of Figures 6.2 and 6.3. Conventional thinking dictates that as long as [6.9] is satisfied, convergence to the optimal solution (minimum MSE) will continue. The instance when $\hat{G}_p$ is exactly equal to G_p satisfies this constraint because the feedback path is eliminated from the actual control-to-error path of Figure 6.3. However, when $\hat{G}_p$ is not precisely equal to G_p, a feedback path is introduced that is a function of the adaptive filter W. We will now consider the case during adaptation, when

$\hat{G}_p$ has an arbitrarily small amount of phase estimation error with respect to G_p, causing the feedback loop to exist.

As before, the LMS algorithm updates the weights based on the negative gradient as in [6.1]. For simplicity we examine the error vector gradient which defines the filter used to filter the reference signal in the filtered-X algorithm. The *actual* error gradient of the filtered-E system is now computed based on the nonzero feedback path in the physical control-to-error transfer function of Figure 6.3.

$$E(z) = D(z) - X(z) - \frac{G_p(z)W(z)X(z)}{1-(G_p(z)-\hat{G}_p(z))W(z)}$$
$$\nabla E(z) = \frac{dE(z)}{dW(z)} = \frac{-G_p(z)}{1-2(G_p(z)-\hat{G}_p(z))W(z)+(G_p(z)-\hat{G}_p(z))^2 W(z)^2} X(z) \quad \textbf{[6.10]}$$

The filter used to filter the reference signal in [6.10] must now be compared to what is conventionally used by the filtered-X in Figure 6.3 to estimate the gradient (without the explicit dependence on z) as

$$\angle\left(\frac{G_p}{1-2(G_p-\hat{G}_p)W+(G_p-\hat{G}_p)^2W^2}\right) - \angle\left(\frac{\hat{G}_p}{1-(G_p-\hat{G}_p)W}\right) < 90^\circ \quad \textbf{[6.11]}$$

Equation [6.11] represents the difference in the filter that should be used to filter the reference based on the actual gradient estimate, and the filter that is conventionally used in the filtered-X formulation of Figure 6.2.

The well-known 90° phase limitation between the physical control-to-error path and the plant estimate has historically been derived only for a single sinusoid [40, 41, 39]. Assumptions made for these derivations rely on a filtered-X problem formulation where there is no dependence of the control-to-error path dynamics on the adaptive filter. An examination of Figure 6.3 shows

that unlike the feedforward situation, where we adapt an FIR filter W(z) that linearly affects the control signal, the filtered-E structure is essentially adapting an IIR filter H(z) given by

$$H(z) = \frac{G_p(z)W(z)}{1-(G_p(z)-\hat{G}_p(z))W(z)} \qquad \textbf{[6.12]}$$

where the parameters to be adapted are contained in the FIR transfer function W(z). To minimize the mean square error, the gradient is still computed as in [6.10] and can be expressed as the partial derivative of H(z) with respect to W(z)

$$\frac{\partial H(z)}{\partial W(z)} = \frac{G_p(z)}{1-2(G_p(z)-\hat{G}_p(z))W(z)+(G_p(z)-\hat{G}_p(z))^2 W(z)^2} \qquad \textbf{[6.13]}$$

Clearly, this is much different than the transfer function used in the filtered-E algorithm, which is the lower left block of Figure 6.3, and shown as the second term in [6.11]. The question then arises as to how much can the gradient used by the filtered-E algorithm differ from the true gradient and yet still produce convergence to the optimal? It would seem to be extremely difficult to answer this question globally, since the equations describing nominal trajectories in the weight space are nonlinear. Certainly near the optimum, W_{opt}, the cost will be quadratic and we can approximate H(z) in a neighborhood of the optimum as a transfer function that is affine in the parameters W as a Taylor's Series expansion about the optimal:

$$H(z) = H(z)\big|_{W_{opt}} + \left.\frac{\partial H(z)}{\partial W(z)}\right|_{W_{opt}} (W - W_{opt}) \qquad \textbf{[6.14]}$$

The first and last terms of [6.14] are moved to the forward (disturbance) path between the reference and error sensor in Figure 6.3, while the control path containing W is altered by the linearized control-to-error dynamics of $\partial H(z)/\partial W(z)\big|_{W_{opt}}$. Because this filter is not a function of the changing adaptive filter, the standard 90° phase error analysis for the filtered-X algorithm

now applies. The conclusion is that as long as the phase of the gradient filter does not depart from the phase of $\partial H(z)/\partial W(z)\big|_{W_{opt}}$ by more than 90° at the frequency of interest, the algorithm will converge to the optimal solution. If the phase difference is greater than 90°, then the optimal cannot be approached, and the algorithm will diverge from the optimal. Since we have no idea *a priori* as to the value of W_{opt}, it makes sense to use [6.13] as the gradient filter. It should be noted that in the simulations, divergence over a wide range of the weight space occurred whenever the gradient filter used by the filtered-E algorithm differed from [6.13] by more than 90°. This would seem to imply that a more global conclusion could be drawn concerning the acceptable plant phase error with respect to broadband input signals. Thus far such a proof has not been made. (Note that the negative sign computed in [6.10] cancels with the negative sign of [6.1] when the FX-LMS algorithm is implemented so that the sign of the filter agrees with the physical control-to-error path predicted by [6.14] from [6.13]).

Returning to the conventional implementation of the filtered-E controller, the inequality expressed by [6.11] defines the difference in the actual plant estimation filter and the conventional plant estimation filter that is typically used. It should be clear that when comparing [6.11] and [6.9], the errors will result in different predictions of algorithmic stability as a function of conventional plant error. It is therefore conceivable that a small plant estimation error in *conventional* terms that satisfies [6.9], could produce a large error that violates the *actual* estimation constraint [6.11], causing an unexpected algorithm divergence, but one that is predicted by [6.11].

Given this result, one might assume that since the actual gradient filter is known, it can be used in place of the conventional filter to ensure that the plant estimate is accurate enough to satisfy [6.11]. Since the actual plant estimation filter of [6.10] is a function of the difference in the actual plant dynamics (G_p) and the estimate of the dynamics ($\hat{G}_p$), this is impossible. If the actual dynamics were known exactly, they could be used to eliminate the feedback path resulting in a strictly feedforward system. The tacit assumption in conventional adaptive feedback control is that the estimate exactly equals the actual plant and there is no error, thereby turning [6.11] and [6.4] into [6.9] and the numerator of [6.4]. In practice there always

exists some finite error between the estimate and the actual control-to-error path. However, this can only be analyzed in a simulation where the error can be explicitly controlled and the "actual" plant is known exactly.

It is interesting to examine the behavior of [6.11] as a function of the adaptive filter W. Evaluating [6.11] when W=0, results in

$$\angle\left(\frac{G_p}{1-2(G_p-\hat{G}_p)W+(G_p-\hat{G}_p)^2W^2}\right)-\angle\left(\frac{\hat{G}_p}{1-(G_p-\hat{G}_p)W}\right)\Bigg|_{W=0}=\angle G_p-\angle\hat{G}_p<90^\circ$$

[6.15]

Also noteworthy is the result when [6.11] is evaluated when the adaptive filter reaches the optimal solution of [6.6].

$$\angle\left(\frac{G_p}{1-2(G_p-\hat{G}_p)W+(G_p-\hat{G}_p)^2W^2}\right)-\angle\left(\frac{\hat{G}_p}{1-(G_p-\hat{G}_p)W}\right)\Bigg|_{W=-\frac{1}{\hat{G}_p}}=0$$

[6.16]

Therefore at the inception of control, assuming a zero initial condition on the adaptive filter, the conventional gradient error estimation is valid. In addition, when the adaptive filter reaches the optimal solution, there is no estimation error, regardless of the choice of $\hat{G}_p$! As a result, divergence of the adaptive algorithm due to inaccurate plant estimation should only be expected *during* adaptation. Although, practically speaking, a finite length FIR filter will not likely have the ability to invert the control-to-error path estimate at every frequency in the controllable bandwidth. Therefore gradient divergence as predicted by [6.11] will always remain a practical concern when implementing adaptive feedback controllers like the filtered-E.

6.2 PRACTICAL APPLICATIONS AND CONSIDERATIONS

6.2.1 INTERRELATED INSTABILITIES

The two instability modes presented above are connected to each other after an initial transient. Each instability can initiate independently, but because of the inherent dependence on W in the gradient estimate, they will eventually influence each other.

Suppose that a conventional control-to-error path estimation error exists, but that [6.11] is satisfied and the adaptive filter is converging toward the optimal solution. Because an error exists, the poles of [6.4] exist and are moving as a function of the error and the adaptive filter. It is possible for one of these poles to leave the unit circle during adaptation and create a feedback loop instability. This can happen independent of violating [6.11]. However, as the loop instability grows in magnitude, the mean squared error will increase and cause the adaptive filter to respond. In view of [6.11], a changing adaptive filter will affect the actual gradient filter error, and potentially cause it to exceed 90°. Therefore a feedback loop instability can cause the phase error to exceed the 90° criterion established by [6.11] resulting in algorithm divergence. Alternatively, the adaptation could potentially re-stabilize the system! It is also important to note that because of the dependence of the control-to-error path on the adaptive filter, it is possible that the phase estimation error defined by [6.11] could be self-correcting during adaptation. In other words initial error in excess of 90° may not guarantee algorithm divergence if the adaptive filter changes the control-to-error path in such a manner that the actual phase error is reduced.

Although each instability mechanism can initiate independent of the other, they are ultimately codependent through the adaptive filter magnitude. That is, if one grows without bound, the other will follow. For this reason, it is virtually impossible to ascertain the mechanism of instability in experimental applications because the time scales are typically too fast. The simulations to follow will illustrate these phenomena.

6.2.2 FILTERED-U LMS ALGORITHM

The filtered-E controller examined above can be viewed as a special case of the more generalized filtered-U LMS algorithm [42]. The filtered-U algorithm, often employed in duct noise control problems, is illustrated in Figure 6.4.

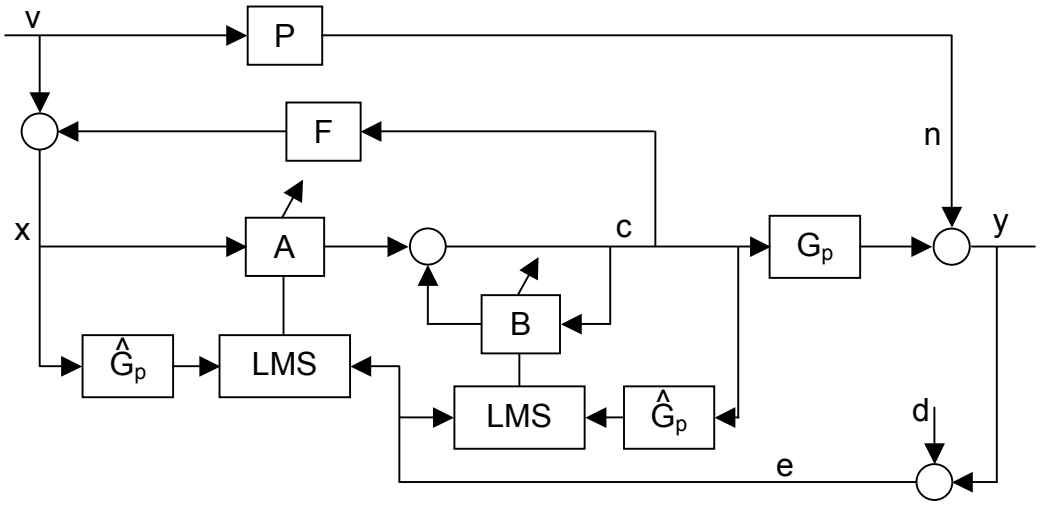

FIGURE 6.4 FILTERED-U CONTROL

Here there are two control sensors: the "upstream" reference microphone detects the original source disturbance (v) and generates the input to the algorithm (x) while the downstream error microphone senses the noise (n) after being altered by the duct acoustics existing between those two sensors, represented by P. Because the two sensors are in the same duct, when the control signal (c) is applied to the system it influences the error signal through the control-to-error path dynamics (G_p) as well as the upstream reference sensor through a feedback path, F.

To see the similarities between the filtered-U and filtered-E structures we need to consider the case when the reference and error signals are identical. When this occurs, physically, there is only one microphone in the duct and therefore no reference signal "v". The transfer function F disappears, P becomes unity, and the reference signal, x, is the same as the error microphone measurement, y. The disturbance now appears as an exogenous input to the error sensor. These changes and the resulting system are depicted in Figure 6.5.

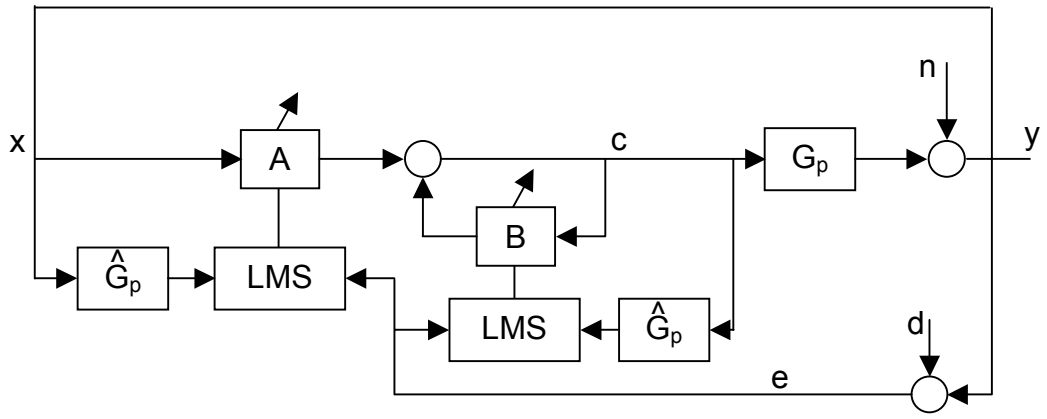

FIGURE 6.5 FILTERED-E ADAPTIVE IIR CONTROL

Comparing Figure 6.2 and Figure 6.5, an obvious difference exists in the controller structure. Figure 6.2 (the filtered-E) uses a fixed estimate of the control-to-error dynamics to compensate for the feedback path created by using the error signal as the reference. Figure 6.5 illustrates a filtered-E controller structure as well, where the feedback path is compensated adaptively by the adaptive IIR form. Equating the transfer functions of Figure 6.2 and Figure 6.5, we see that the two systems are identical when A = W and B = $-W\hat{G}_p$. However, because of the adaptive IIR structure there is no guarantee that these will be the optimal filters or that they will ever be reached [48].

As with the adaptive feedback analysis, the filtered-U system of Figure 6.4 has the same loop stability limitations. Because the reference signal is controllable and the adaptive feedback component does not begin at the optimal solution, the possibility for feedback instabilities exists. In addition, because of the feedback to the reference signal and the existence of an adaptive feedback filter (B), the conventional gradient estimate cannot be accurate during adaptation as shown next.

Block diagram algebra of Figure 6.4 reveals:

$$E(z) = D(z) - P(z)V(z) - \frac{G_p(z)A(z)}{1 - B(z) - A(z)F(z)}V(z) \qquad \textbf{[6.17]}$$
$$V(z) = X(z) - F(z)C(z)$$

Examining the actual gradient of the error signal (which is proportional to the gradient of the cost function) with respect to the forward path filter (A) results in

$$\frac{dE}{dA} = \frac{BG_p - G_p}{(1 - B - AF)^2}V = \frac{-G_p(1-B)}{(1-B-AF)^2}X + \frac{FG_p(1-B)}{(1-B-AF)^2}C \qquad \textbf{[6.18]}$$

Conventional application of the filtered-U algorithm uses an estimate of the control-to-error dynamics ($\hat{G}_p$) to filter the input of the adaptive filter for updating the weights. In the case of the forward component of the IIR filter employed here, the input is x and it would typically be filtered by $\hat{G}_p$. In fact, the actual gradient estimation includes the feedback path and is also a function of the output signal y as shown in [6.18]. A similar analysis can be performed for the partial derivative of the error signal with respect to the feedback adaptive filter B, yielding similar results. It is therefore clear from [6.18] that the conventional and actual gradient estimation errors can differ quite significantly, and may unpredictably result in algorithm divergence even when [6.9] is satisfied.

6.2.3 ONLINE SYSTEM IDENTIFICATION

6.2.3.1 Conventional Identification Methods

Online system identification is typically employed to track changes in the control-to-error dynamics over time. For adaptive feedforward systems with time varying control-to-error transfer functions, this technique may be required to maintain the correct gradient estimate in the LMS algorithm. Figure 6.6 [48] illustrates one possible technique for performing the online system identification for a filtered-X feedforward system. It is assumed that the plant G_p is time varying and must be estimated by continually updating $\hat{G}_p$.

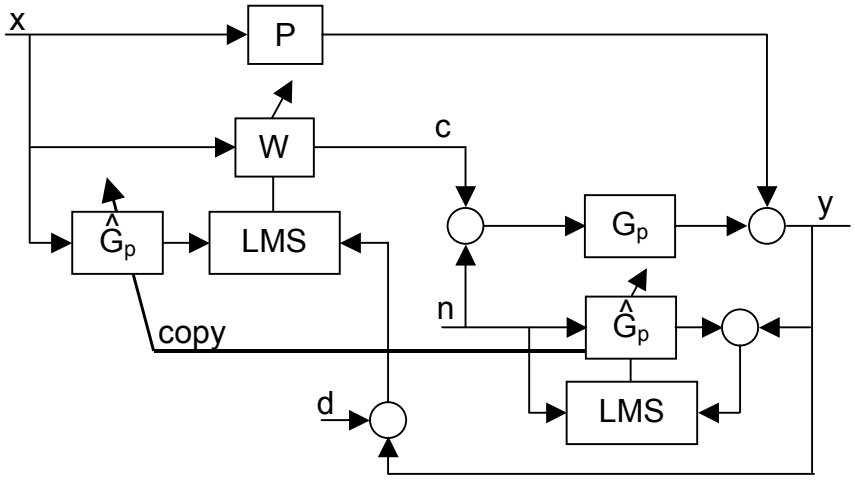

FIGURE 6.6 ONLINE SYSTEM IDENTIFICATION

As shown above for filtered-E control, the actual control-to-error path is a function of the adaptive filter, and is therefore changing with time. The transfer function coefficient of X in [6.10] represents the actual control-to-error path estimate that should be used to filter the input to the LMS algorithm. The question then arises, "if the actual gradient equation is known, why can't it be used in the filtered-X update algorithm". Upon inspection of [6.10], it should be clear that G_p is never known exactly. $\hat{G}_p$ is used to estimate G_p; and if the assumption is that there is no estimation error $\hat{G}_p = G_p$ and [6.11] becomes [6.9]. However, in practice there is always an estimation error, no matter how small, that makes [6.11] the correct gradient error criteria. Therefore, without knowing G_p exactly, the $(G_p - \hat{G}_p)$ terms of [6.10] cannot be computed directly.

Another alternative for generating a more accurate estimate of the actual gradient is the online identification of the gradient filter. Once the loop is closed (the adaptive filter becomes nonzero), an online identification procedure will take into account the feedback loop and the adaptive filter. However, it should also be obvious that a linear system identification of any input/output relationship of Figure 6.2, will never result in the required transfer function coefficient in [6.10]. This is shown clearly by considering that the characteristic equation of Figure 6.2 is the denominator of [6.4]. Therefore any attempt at an online linear system

identification cannot result in the transfer function of the first term in [6.11] which has a quadratic denominator.

A similar argument can be made for an online system identification employed in the filtered-U system of Figure 6.4. The quadratic denominators of [6.18] prevent an online system identification procedure from ever yielding the proper frequency response. [48] and [37] proposed that the feedback terms resulting from F and B in [6.18] were negligible. In this case the gradient estimates for both adaptive filters become $\hat{G}_p = G_p$; a result that ignores the recursion of both B and F. However, an online system identification procedure cannot avoid identifying the physical feedback paths, F and B, in Figure 6.4. Therefore the frequency response resulting from the online identification process (Figure 6.6) of the filtered-U algorithm (Figure 6.4) is

$$\frac{G_p}{(1 - B - AF)} \qquad \textbf{[6.19]}$$

which is not an accurate representation of their proposed gradient filter *approximation*, G_p.

6.2.3.2 A New On-Line Identification Technique

There is one possible solution that can be proposed for reducing the detrimental effects of the $(G_p - \hat{G}_p)$ terms on the gradient estimate and the potential for unstable feedback loops. Consider again the block diagram of Figure 6.3 illustrating the dependence of the loop stability and gradient filter on the plant estimate error and the adaptive filter. Let

$$F = \frac{1}{1 - (G_p - \hat{G}_p)W} \qquad \textbf{[6.20]}$$

Assuming W is an FIR filter and G_p is a stable plant, the loop stability requirement can be restated as: F must have stable poles.

The gradient filter error criteria expressed by [6.11] can also be restated as

$$\begin{aligned} &\angle(G_p F^2) - \angle(\hat{G}_p F) < 90^\circ \\ &(\angle G_p - \angle \hat{G}_p) + (\angle F^2 - \angle F) < 90^\circ \\ &(\angle G_p - \angle \hat{G}_p) + (\angle F) < 90^\circ \end{aligned} \qquad \textbf{[6.21]}$$

so that the phase error to consider is the sum of the phase error in the original plant estimate plus the phase of the feedback term, F.

Addressing the stability of F (and thus the closed loop system) first, consider the block diagram of Figure 6.7 below

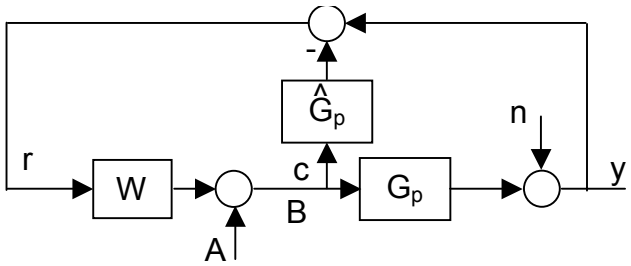

FIGURE 6.7 ONLINE SYSTEM IDENTIFICATION

The transfer function between the output B and the input A is equal to [6.20], and thus F. At locations in the frequency response of [6.20] where the amplitude is high, or increasing, a pole is nearing the axis. Continual monitoring of this transfer function, identified periodically during adaptation, will indicate stability. Ideally, [6.20] will remain low, or near unity to ensure that no poles are nearing the axis. This is also an ideal scenario for ensuring gradient convergence of the LMS algorithm.

In [6.10] we showed that the ideal gradient filter is represented by G_pF^2. *Conventional* implementation of the Filtered-X LMS algorithm uses $\hat{G}_p F$ as the gradient filter, creating the estimation phase error described by [6.11]. An available alternative is to use the identification of B/A represented by Figure 6.7 to generate an online estimate of F while the adaptive filter,

W is held constant, thereby generating an $\hat{F}$. If we multiply our estimate, $\hat{F}$, by the existing conventional gradient filter, the new phase error criterion of concern can then be expressed as

$$\begin{aligned} &\angle(G_p FF) - \angle(\hat{G}_p F\hat{F}) < 90^\circ \\ &(\angle G_p - \angle\hat{G}_p) + (\angle F - \angle F) + (\angle F - \angle\hat{F}) < 90^\circ \\ &(\angle G_p - \angle\hat{G}_p) + (\angle F - \angle\hat{F}) < 90^\circ \end{aligned} \qquad \textbf{[6.22]}$$

where the first term of the first line is the *ideal* gradient filter and the second term is the proposed *estimate* of the ideal gradient filter. Here we can conceivably identify both the open loop plant and the closed loop control system within enough accuracy to ensure less than ninety degrees of total phase error for the criterion of [6.22]. As the adaptive filter changes, identification of $\hat{F}$ should be periodically updated to prevent algorithm divergence. While this approach can theoretically help some of the stability and gradient problems identified earlier in this chapter, continual monitoring is required in order to ensure loop and gradient stability.

An alternative online identification technique can also be proposed. Consider that

$$\frac{A}{B} = \frac{1}{F} = 1 - (G_p - \widehat{G}_p)W \qquad \textbf{[6.23]}$$

can be obtained from an inverted system identification of Figure 6.7. When A = B, F = 1 requiring that $(G_p - \hat{G}_p) = 0$ when W is non-zero. An effective way to ensure that A and B are equal is by using an LMS based adaptive controller as shown in Figure 6.8.

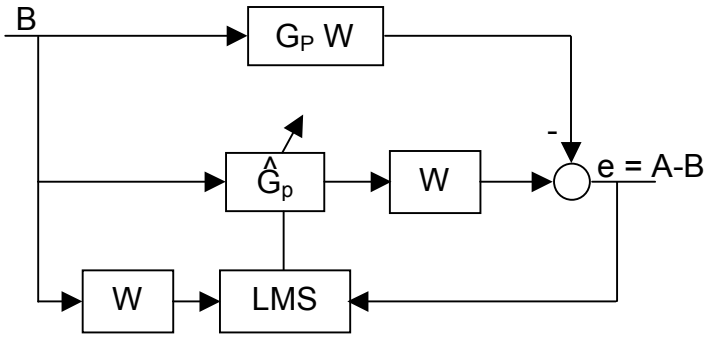

FIGURE 6.8 MODIFIED ONLINE IDENTIFICATION

A significant benefit of this formulation, as seen in [6.23], is that G_p approaches $\hat{G}_p$ most effectively at frequencies where W is high; i.e. the plant estimation error is weighted by the adaptive filter magnitude, corresponding to frequencies requiring significant control. These are also the frequencies where gradient convergence is most critical because they are the frequencies with the highest MSE.

Now suppose that the gradient filter in the adaptive feedback LMS algorithm is NOT modified as suggested by [6.22], but instead the online identification of Figure 6.8 is periodically carried out while W remains fixed. The original system identification of G_p is used in the conventional Filtered-X formulation and does not require a weighted or biased estimate, since we want to ensure convergence for unknown disturbances over the entire bandwidth of the plant. Therefore that original estimate will be called $\hat{G}_{p1}$ and will remain fixed during all adaptations. The identification carried out in Figure 6.8 provides a weighted estimate of the feedback compensation filter which is critical in affecting loop stability and gradient filter errors. That resulting estimate will be known as $\hat{G}_{p2}$. Following [6.11], and since the gradient filter will not be modified, the actual gradient error can be expressed as

$$\angle\left(\frac{G_p}{1-2(G_p-\hat{G}_{p2})W+(G_p-\hat{G}_{p2})^2W^2}\right)-\angle\left(\frac{\hat{G}_{p1}}{1-(G_p-\hat{G}_{p2})W}\right)<90^\circ$$

$$\angle(G_pF_2F_2)-\angle(\hat{G}_{p1}F_2)<90^\circ \qquad \textbf{[6.24]}$$

$$(\angle G_p-\angle\hat{G}_{p1})+(\angle F_2)+(\angle F_2-\angle F_2)=(\angle G_p-\angle\hat{G}_{p1})+(\angle F_2)<90^\circ$$

where F_2 is [6.20] using $\hat{G}_{p2}$ in place of $\hat{G}_p$. Now, the phase error amounts to the error in the original estimate plus the phase associated with the feedback path using the second weighted plant estimate. When F = 1, the phase of F will approach zero as desired. It can also be easily shown that when the adaptive filter approaches its optimal, the angle of F is the difference in the plant and the second online estimate.

There will always be some amount of error attributable to a least squares system identification. However, it is now possible to place some heuristic bounds on how much error can be tolerated based on 6.24. For instance, assume that the initial online identification of $\hat{G}_{p1}$ is carried out with an error of less than 45 degrees at every frequency. Based on [6.24] the remainder of the allowable phase will come from F_2, containing the secondary online identification procedure that updates the feedback plant estimate $\hat{G}_{p2}$. Examining [6.20] we can place a bound on the *magnitude* of the term $(G_p - \hat{G}_p)W$ (such that it cannot be above 0.707) to ensure that the phase of F is never greater than 45 degrees. (If it is never greater than unity, the phase angle of F will always be below 90 degrees). Using the weighted least squares adaptation of Figure 6.8, this represents a realistic tolerance for broadband system identification.

In practical applications there will always be some error associated with an adaptive system identification procedure. This section provided some bounds that can be placed on that error to ensure stable convergence. However, periodic identification as required by this online identification procedure, may not be an acceptable solution for real world applications.

6.2.4 EXTENSION TO SELF-EXCITED SYSTEMS

All previous analyses and discussions in this Chapter have focused on systems having exogenous disturbances from stable plants. The thermoacoustic instability can generate disturbances through the nonlinear limit cycling behavior of an unstable plant. Chapter 5 discusses the experimental application of adaptive feedback control to the thermoacoustic instability. In Chapter 5 it is shown that the most appropriate choice for a control-to-error path estimate is the stable acoustic dynamics plus actuator dynamics so that $\hat{G}_p = G_{act}$; exact estimation capability is assumed throughout Chapter 5. Here it is assumed that the plant estimate is not able to exactly model the desired transfer function.

Figure 6.9 illustrates the adaptive feedback controller applied to a self-excited instability in the form of a thermoacoustic instability just as in Chapter 5.

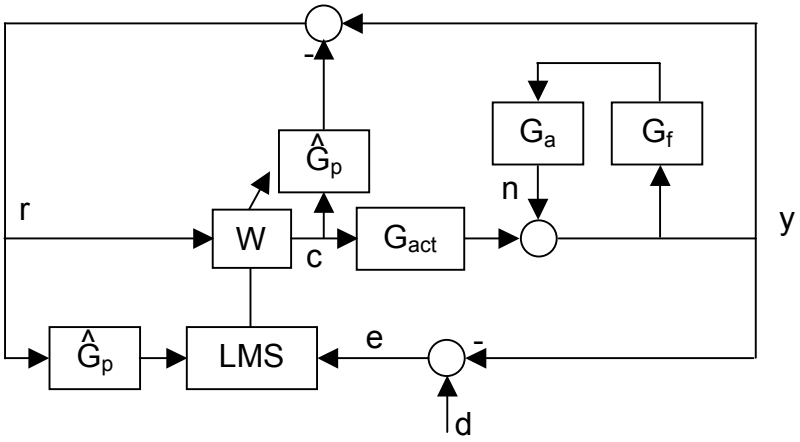

FIGURE 6.9 SELF-EXCITED SYSTEM FILTERED-E CONTROL

Adaptive feedback and filtered-U controllers have been applied to the thermoacoustic instability in an attempt to reduce the pressure oscillation that may change with changing operating conditions [25, 22, 23, 28].

Unfortunately, the same instability mechanisms for the stable plant control exist for the unstable plant control. The characteristic equation for the adaptive feedback control system of Figure 6.9 is represented by

$$1 - G_a G_f - W(G_{act} + \hat{G}_p - G_a G_f \hat{G}_p) \qquad \textbf{[6.25]}$$

There are no guarantees on the stability of the roots of [6.25]. The adaptive filter could easily cause a root of this equation to become unstable during adaptation, regardless of the choice of $\hat{G}_p$. This is unlike the stable plant control where the feedback loop is canceled if $\hat{G}_p = G_p$. Without accurate knowledge of the self-excited system dynamics, it is impossible to limit the roots of [6.25] to strictly stable values. It should be noted that when $W = W_{opt}$ the roots of [6.25] are the roots of the denominator of G_{act}. But no guarantees can be made on reaching the optimal solution if the gradient estimate is incorrect.

The gradient of the cost function is even more complex for the self-excited case. The filter to which the input to the LMS algorithm should be applied will be a function of the adaptive filter, plant estimate and actual plant as before, but will also be influenced by the self-excited system dynamics. Computation of the actual gradient of the filtered-E self-excited system should not be required in order to recognize that the conventional estimate of G_{act} will be inaccurate with respect to the actual gradient.

6.3 SIMULATION

Three simulations have been designed that illustrate the two specific instability mechanisms independently. Each simulates the stable disturbance rejection system of Figure 6.2 using different plants and plant estimates. As set forth in the previous discussions, the *conventional* plant error refers to the criterion of [6.9] which was shown to be inaccurate for adaptive feedback controllers. Equation [6.11] represents the *actual* estimation error criterion.

6.3.1 FEEDBACK LOOP INSTABILITIES

This simulation illustrates a case where the conventional plant error is in excess of 90° at many frequencies, but no algorithm divergence is observed. Instead, an unstable feedback loop is generated due to a pole of [6.4] leaving the unit circle.

The plant shown in Figure 6.2 was chosen to have unity magnitude and a linear delay of 25 samples while the plant estimate was chosen to have unity magnitude and 19 samples of delay at a sample rate of 2000 Hz. The exogenous disturbance was chosen to be a single sinusoid at 32 Hz with additive white noise at a lower level at every other frequency. The adaptive filter was a 2-weight FIR filter with a convergence parameter of 0.00003.

The difference in phase between the plant and estimate increased almost linearly, reaching an excess of 1000° of phase error by 1000 Hz, thus allowing for the possibility of divergence of the weights due to a conventionally inaccurate system identification. Figure 6.10 illustrates the uncontrolled (solid) and controlled (dotted) power spectra of the tonal disturbance from the stable plant at 32 Hz.

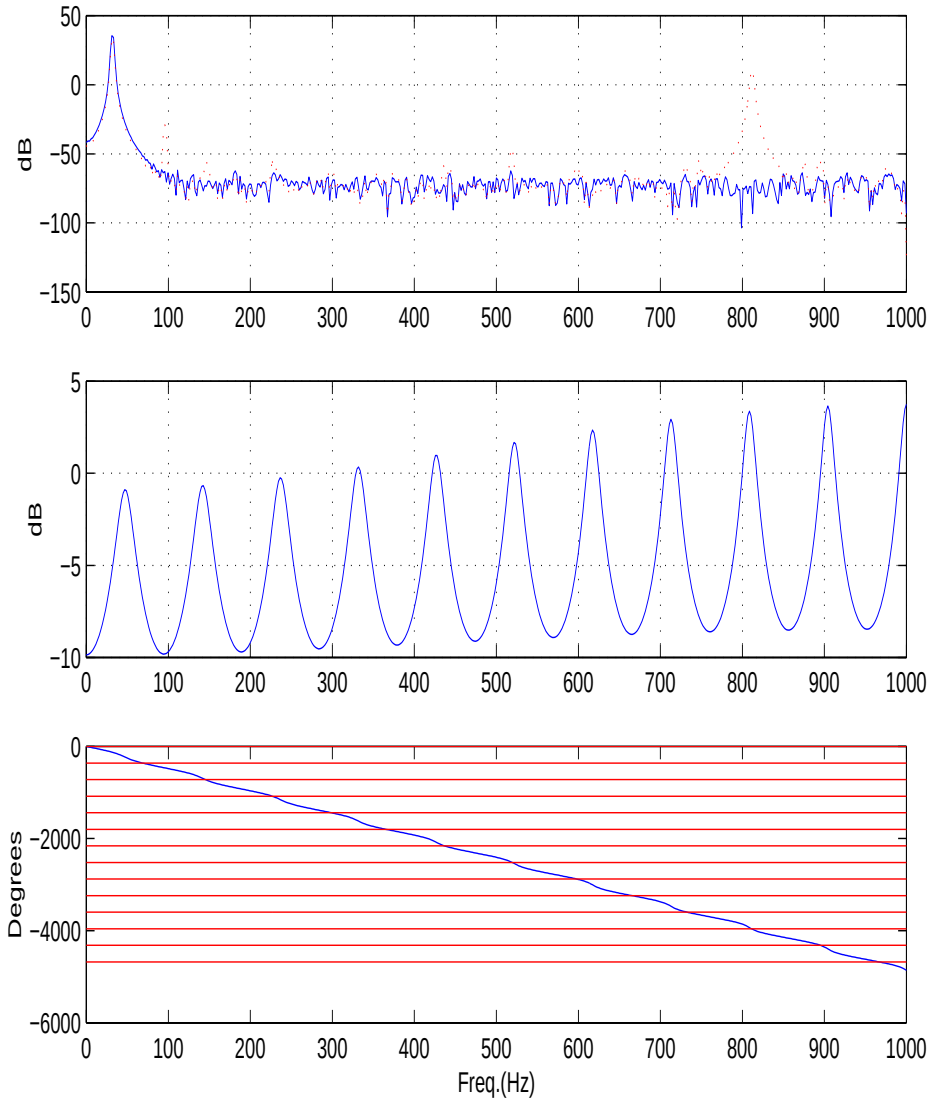

FIGURE 6.10 FEEDBACK LOOP INSTABILITY AND BODE PLOT PREDICTION

Initially, the tone is suppressed with only two adaptive filter weights but the loop gain that accompanies the optimal adaptive filter causes a loop instability at 810 Hz. This is accurately predicted by the Bode gain/phase relationship in that the open loop frequency response magnitude is in excess of 0 dB at the 810 Hz phase crossover frequency.

This adaptive feedback controller diverges because of the feedback loop instability, not divergence of the algorithm. Increasing the number of adaptive filter weights reduces the gain of the adaptive filter at 810 Hz thus eliminating that loop instability. However, the added

phase and filter complexity causes poles at other frequencies, away from the disturbance, to become unstable before convergence is achieved. For this simulation, the *conventional* phase error between the plant and estimate is still in excess of 90° at many frequencies throughout the control bandwidth but the algorithm *never* diverges because the actual phase error is less than 90°.

A second simulation was developed that illustrates a feedback loop instability independent of algorithm instability. The primary difference in this simulation is that *no* phase error between the plant and plant estimate was created. Instead, a modest DC gain difference in the two dynamic models was created. With a (digital) zero at 0.696 and a pole at 0.97, the control-to-error path had a gain of 1.3 while the estimate of that path was given a gain of 1.0. Figure 6.11 illustrates the actual and estimated control-to-error path frequency responses as well as the difference in phase between them (lowest plot).

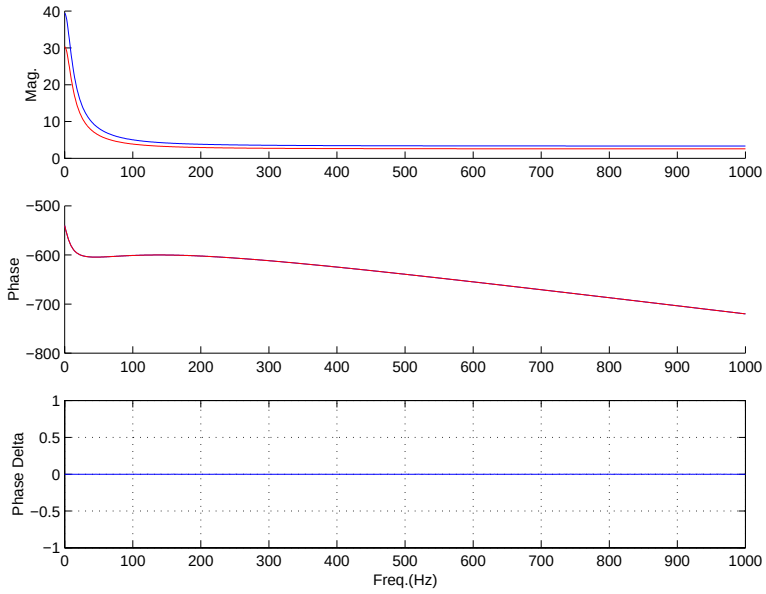

FIGURE 6.11 CONTROL-TO-ERROR PATH AND ESTIMATE

This simulation illustrates two interesting behaviors. First, a feedback loop instability prevents convergence to the optimal solution of [6.6] because a pole is leaving the unit circle at 1000 Hz, half the sample rate. Stated differently, the optimal solution to this problem results in an unstable pole because of the amplitude difference in the estimate creates the denominator of

[6.4] which is a function of the adaptive filter. Second, a searching behavior not unlike that described in the previous chapter is witnessed. The time response of this adaptive feedback simulation is shown in Figure 6.12.

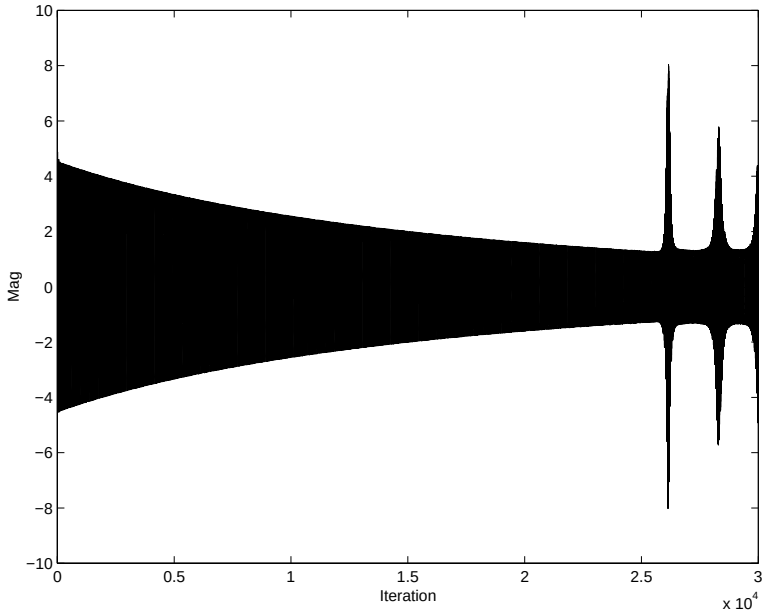

FIGURE 6.12 LOOP INSTABILITY SEARCHING BEHAVIOR

Because of the adaptive nature of the controller, once the increase in MSE is detected, the weights are corrected. However, since the optimal solution for a two weight adaptive filter requires that the loop contain an unstable pole, the algorithm continues to drive toward that solution. A searching behavior begins that is a function of the convergence parameter μ. To see this more clearly, consider the closed loop poles of Equation [6.4]. Since we are in the z-domain, an absolute magnitude of the complex pole coordinates that is greater than unity indicates an unstable pole. Figure 6.13 shows the path of the absolute magnitude of the poles of [6.4] over time.

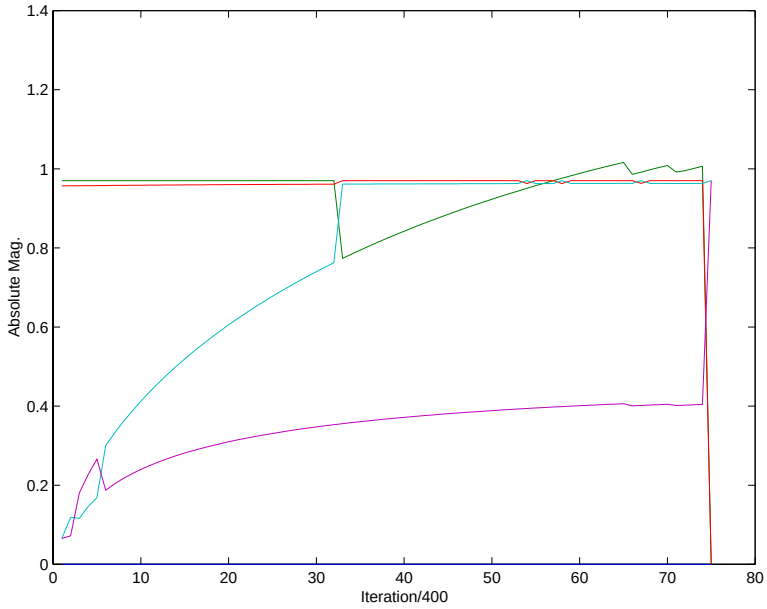

FIGURE 6.13 POLE MOVEMENT WITH TIME

It is clear that as the system adapts toward the optimal solution, one pole has a trajectory leading out of the unit circle. The adaptive filter corrects it but the intermittency continues as the pole moves in and out of the unit circle.

The optimal solution requires an unstable pole in this situation because of the adaptive filter order. While any phase and magnitude can be obtained using a two weight FIR filter, this is only true at a single frequency. Because of the limited control over the entire bandwidth, the optimal solution of [6.6] cannot be effectively inverted at *every* frequency, only the frequency generating the greatest MSE. This results in excess out of bandwidth magnitude and eventually an unstable pole at half the sampling rate. This problem is easily remedied by increasing the adaptive filter order where more precise inversion of the estimate of the control-to-error path can occur over the entire bandwidth. Nevertheless, this simulation effectively illustrates the limitations of the adaptive feedback controller in terms of loop stability even when a very accurate system model is available.

6.3.2 ALGORITHM DIVERGENCE

When the adaptive filter is at zero or its optimal solution, the *actual* plant error is either equivalent to the *conventional* error [6.15] or is degenerate [6.16]. Therefore we are only concerned with the times during adaptation when neither of these conditions are satisfied. In addition, we are interested in illustrating a case where the *conventional* plant estimation error is arbitrarily small but the *actual* plant estimation error exceeds the constraints of [6.11]. Finally, it is important to continue to differentiate the gradient based algorithm divergence from the loop instability presented above. This simulation accomplishes each of these goals.

Because the actual plant estimation error [6.11] established herein is a function of the plant estimation error as well as the adaptive filter, it is impossible to generalize the expected gradient error. For this particular simulation the plant estimate was chosen to be unity so that the optimal adaptive filter was –1. The control-to-error path was chosen to be a complex zero at 200 Hz with a damping ratio of .025 combined with a complex pole at 300 Hz with a damping ratio of .016. Due to the way the simulation was designed an additional delay was imparted to both the control-to-error path and it's estimate (with a sample frequency of 2000Hz). These choices resulted in a *conventional* phase difference in the plant and plant estimate that was less than 4° at the disturbance frequency of 150 Hz. Therefore in a conventional interpretation where the tolerable error satisfies [9], there is no chance for gradient divergence at 150 Hz.

In a user controlled simulation environment, we have access to both the actual plant and the plant estimate. Therefore it is possible to compute the phase difference described by [6.11] directly for a variety of adaptive filters. In order to effectively visualize the weight space, a two weight adaptive filter was chosen. This is also typically sufficient to control a single tone disturbance. Figure 6.14 illustrates the *actual* gradient error as computed by [6.11], as a function of the two adaptive weights, at 150 Hz. The *'s represent the weight combinations that result in a gradient error of greater than 90° at 150 Hz; the absence of *'s represent areas where the *actual* estimation error is less than 90°. Recall that the *conventional* gradient error for the entire weight space, at 150 Hz, is less than 4°. The optimal adaptive solution of [6.6] is shown as a

star at coordinates (0.98,-1.77). Note that the *actual* gradient error at (0,0) and the optimal, is within the 90 degree specification.

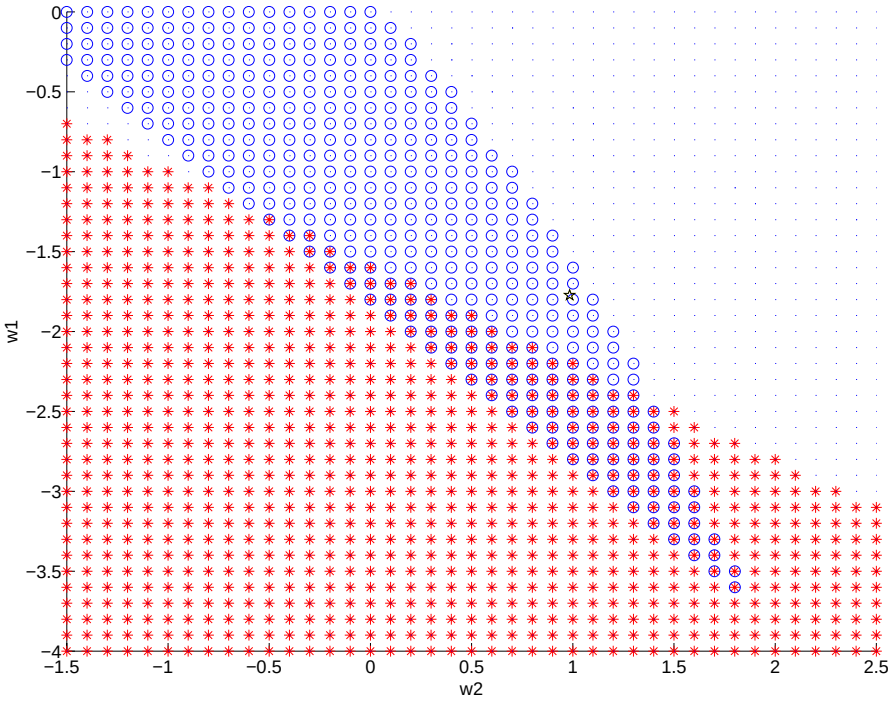

FIGURE 6.14 GRADIENT AND STABILITY IN THE WEIGHT SPACE

Figure 6.14 also illustrates loop stability. For every weight combination shown, [6.4] was evaluated for unstable roots. The O's represent areas in the weight space where the loop has no unstable roots; areas without O's have at least 1 unstable root. By inspection, it is possible to see a union where the feedback loop is stable but the actual gradient is greater than 90° at 150 Hz ([6.11] is not satisfied) while the *conventional* gradient is less than 4° ([6.9] is satisfied). If we choose an initial condition of the weights in this region (-2.8 and 1.3 for example), the algorithm diverges at 150 Hz but the feedback loops remain stable for some time. The upper portion of Figure 6.15 illustrates the error signal with time while the lower portion shows the increase in amplitude of the 150 Hz tone after control has been applied.

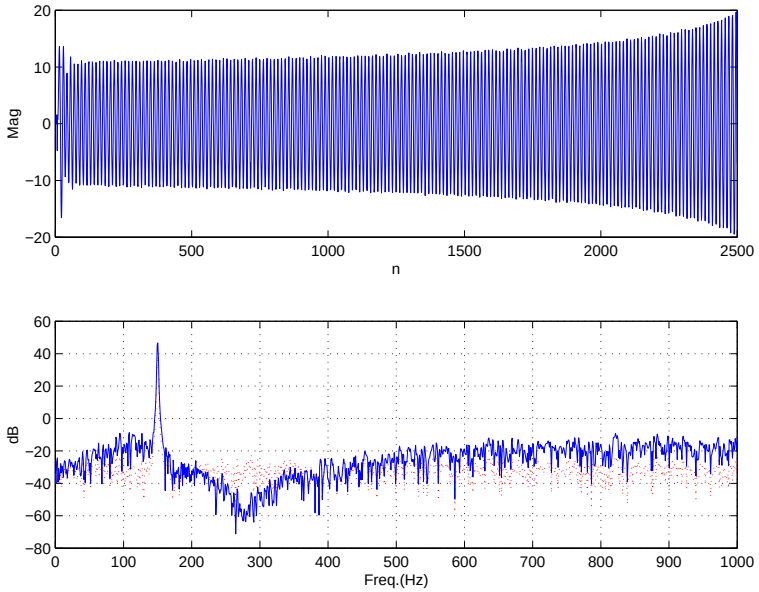

FIGURE 6.15 GRADIENT DIVERGENCE FOR 4 DEGREES OF PLANT ESTIMATION ERROR

This example illustrates that the conventional interpretation of the plant phase error of [6.9] is insufficient to ensure convergence to the optimal solution during adaptation. Equation [6.11] accurately predicts the *actual* phase error that can be expected during adaptation.

6.4 CONCLUSIONS

Filtered-E control and filtered-U control have been implemented in the past with varying degrees of success. Some systems illustrate stable and repeatable convergence while others diverge, even with accurate (in a conventional sense) plant estimates. This chapter presents two distinct reasons for such divergence: feedback loop instabilities and inaccurate gradient estimation. Both modes of instability are heavily dependent on the form of the plant, plant estimate, and the adaptive filter. For this reason it is difficult to predict the onset of instability outside of a simulation environment since the actual plant can never be known exactly.

It is obvious that any time an feedback loop exists, it has the potential of becoming unstable. Using an adaptive controller in a feedback system structure is no exception. For an inaccurate plant estimation in the control of a stable plant, the controller can become unstable. In addition, in controlling an unstable plant, no choice of the plant estimate will guarantee a stable

system during adaptation. The recognition and prediction of these unstable feedback loops for adaptive feedback and filtered-U control of both stable and unstable plants has not been previously discussed.

Simplifying assumptions have led researchers to adopt a conventional plant estimate for the filtered-X LMS algorithm that estimates the open loop control-to-error dynamics. It was shown for both stable and unstable plants that this estimate can be insufficient during adaptation, and may generate enough error in the actual gradient to cause the algorithm to diverge. Therefore the *conventional* interpretation of the gradient was differentiated from the *actual* gradient error to provide a method to accurately predict the correct gradient during adaptation. It was then shown that for an arbitrarily small amount of *conventional* phase error, the *actual* phase error could exceed the 90° criterion and cause divergence.

Despite the difficulties shown here in guaranteeing stable performance of filtered-U and filtered-E algorithms, they have performed effectively in certain applications. An *exact* estimation of the control-to-error dynamics will eliminate feedback loops and result in an accurate gradient estimation for the filtered-X LMS algorithm. Limitations on the tolerable error in the plant estimation and actual plant are entirely system dependent, and cannot be evaluated in general. Therefore it is conceivable that a sufficiently accurate estimate is physically achievable for certain applications such that feedback instabilities and algorithm divergence are avoided. This can only be determined experimentally, on a case-by-case basis.

Chapter 7

Time Averaged Gradient Control

7.1 INTRODUCTION

Many algorithmic approaches to active control of thermoacoustic instabilities have been investigated, and they are all hindered by significant limitations. As we have seen previously, manually adjustable feedback controllers cannot effectively track changes in plant dynamics or combustor operating conditions. Model-based controller designs such as H-infinity and LQG require accurate knowledge of the plant to be controlled. Prior discussion of filtered-X LMS-based adaptive controllers has shown them to be an impractical solution to the thermoacoustic control problem. Some gradient-based methods, such as extremum-seeking control and the triangular search algorithm, do not require system models, but are not easily adapted to multi-parameter controllers.

Here, a simple and versatile algorithm for suppressing instabilities is described. The TAG adaptive control algorithm requires no detailed knowledge of the plant or system dynamics. Generally, time-averaged gradient (TAG) control algorithms automatically determine the direction of the local gradient and adapts control parameters to minimize the mean-squared error of the input signal. Because the gradient is computed on-line, no *a priori* information regarding the detailed behavior of the thermoacoustic instability is required. The algorithm searches the performance surface, which is a function of the control parameters, and finds a solution that locally minimizes the mean-squared error. The algorithm is versatile enough to update any type of control parameters (FIR filter coefficients, gain and time-delay parameters, etc.) and operate with a wide variety of actuation schemes (proportional, on-off, subharmonic, etc.) with few or no algorithmic modifications.

The efficacy of such a simple control algorithm for the thermoacoustic instability problem is due largely to the simple nature of this particular control problem. Although the thermoacoustic feedback loop is extraordinarily complicated with regard to the detailed physics, we have seen that the control problem is dominated in practice by a single pair of acoustic poles crossing the imaginary axis due to the gain of the flame dynamics subsystem. Stabilizing the system can usually be accomplished with extremely simple control structures. To maintain control over widely varying conditions, the controller must be made adaptive and the general TAG scheme is ideally suited for modifications that allow it to be successfully used for active combustion control.

7.2 TIME-AVERAGED GRADIENT CONTROL

Time-averaged gradient control uses a gradient search to update control parameters so as to reach the minimum mean-squared error of the given input. The gradient descent algorithms and time-averaged gradient controllers presented here have many notable advantages over previously investigated algorithms for ACC. The controller does not require any prior knowledge of the plant dynamics and no system identification is required. Since the algorithm continually seeks the minimum mean-squared error, it can adapt to changing operating conditions and prevent controller-induced feedback instabilities. Finally, the TAG control method can be applied to any controller parameterization and actuation scheme and is ideally suited to single frequency control because of its inherent simplicity.

Figure 7.1 illustrates the TAG controller applied to the combustion plant. The control filter, W, is updated by a gradient descent algorithm (GDA). The output of the control experiences the control-to-error path dynamics indicated here by G_{ACT}. This controller design is differentiated from previous embodiments in that it does not require a separate measure of the noise (reference signal) and therefore does not require a control-to-error path estimate. The control filter, W, does not have any strict implementation requirements. As will be shown it can take on a variety of parameterizations such as an FIR filter, a constrained IIR filter, or a subharmonic actuation signal generator. The GDA seeks to minimize the error signal in all

cases, by updating the control parameters to find the minimum on the performance surface defined by the mean squared error and the control parameters.

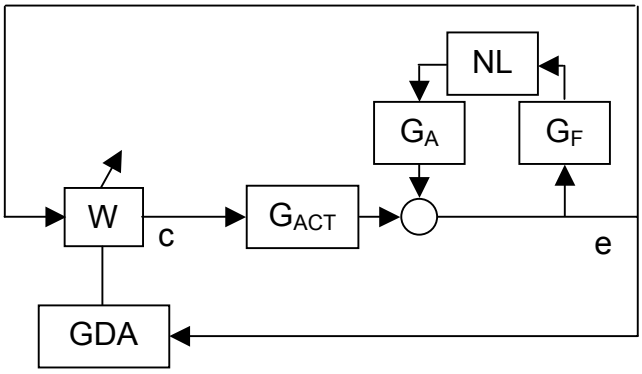

FIGURE 7.1 TAG CONTROL OF SELF-EXCITED PLANT

Gradient descent algorithms, such as Newton's method and the method of steepest descent, are capable of searching a performance surface and locally minimizing multi-dimensional functions. Their primary limitation is that the higher order filters necessary to control large bandwidths require longer adaptation times than their LMS driven counterparts of lower order. Recalling that the thermoacoustic instability problem is very narrowband, the following discussion presents these algorithms.

Gradient descent algorithms measure the gradient of a cost function and continually update the independent parameters to move in the direction of the minimum cost. The method of steepest descent is a simple implementation of this concept and can be represented by the following weight update equation:

$$w_{n+1} = w_n - \mu\xi'(w_n) \qquad \textbf{[7.1]}$$

where the convergence parameter μ controls the speed of the weight update. Equation [7.1] represents the update for a single weight at iteration n, but can be extended to the multi-weight case by replacing the scalar parameters with vectors. (It is also clarified that the weights of [7.1] can form the coefficients of the adaptive filter W in Figure 7.1, or some other controller

parameterization.) The gradient of the cost function for a given update is computed using a measurement of the cost at the current weight location and a perturbed weight location by the formula

$$\xi'(w) = \frac{\xi(w) - \xi(w - \delta)}{\delta} \qquad \textbf{[7.2]}$$

where the cost is given by the mean-squared error (MSE) of some signal *e:*

$$\xi(w) = \frac{1}{N}\sum_{n=0}^{N} e^2(n) \qquad \textbf{[7.3]}$$

This method minimizes the cost as a function of each filter weight so the computational complexity increases with the number of weights, resulting in a lengthy convergence time for large filter sizes. In the case of the thermoacoustic instability, it may be sufficient to adapt as few as two weight parameters to attain a stable operating point and cost minimization. 2N samples are collected before a single weight update can occur. For a two-weight adaptive filter, 3N samples are collected after two separate perturbations in order to update the entire filter.

Newton's method is an alternative gradient descent method that finds a zero of an arbitrary function. In the case of cost minimization, the minimum mean-squared error may never become zero. However, the *gradient* of the cost will become zero at the local minimum. Newton's method derives from the definition of the derivative and can be expressed as

$$x_{n+1} = x_n - \frac{f(x)}{f'(x)} \qquad \textbf{[7.4]}$$

In general applications, we are only concerned with the multi-parameter case where the weight update becomes

$$W_{n+1} = W_n - [\xi''(W)]^{-1}\xi'(W) \qquad \textbf{[7.5]}$$

and ξ'' is the matrix of second partial derivatives, referred to as the Hessian matrix. Computing and inverting this matrix greatly increases the computational complexity of the algorithm. The potential for singularity of the Hessian matrix also introduces complications.

Each of the weight-update algorithms has advantages and disadvantages. Computationally, the steepest descent is able to update the weights much faster than Newton's method. However, Newton's method can converge to the optimal solution faster than the steepest descent algorithm. This is because the steepest descent algorithm moves in the direction of the steepest local gradient, which is only in the direction of the optimal solution if the initial condition is on a principle axis of the error surface. But faster convergence, which implies larger parameter steps, can be a liability when dealing with the non-quadratic cost surface generated by the feedback nature of the ACC control architecture shown in Figure 7.1. This fact, coupled with the increased computational complexity and potential singularity problems of Newton's method, makes the steepest descent technique a better choice for the thermoacoustic instability control solution.

There are two limitations inherent to the TAG control structure shown in Figure 7.1: 1) feedback loops can generate instabilities and 2) the cost function may contain local minima. Although the gradient descent algorithm may drive the weights in the direction of the negative gradient, there is no assurance that a global minimum will be reached. There is also no guarantee that the minimum that is found will result in a stabilized system. Even with these constraints, the gradient descent algorithm has outperformed its filtered-X counterpart in comparable simulations where the control-to-error path G_p may change from trial to trial. It should also be noted that the two limitations are fairly easily dealt with in practical implementations. If a parameter step results in the control feedback loop going unstable, this instability can be sensed, the parameter step undone, and a smaller step size chosen. To alleviate the local minimum problem, the highly scheduled nature of real-world controllers will allow control gains near the global minimum to be swapped in as operating points are changed. In addition, some amount of random probing can be incorporated in the algorithm when the

current operating cost is viewed as too high. This random probing will eventually cause the controller to find a better parameter set and extract itself from a local minimum condition.

Widrow and Stearns [49] examine the stability constraints of the steepest descent algorithm in detail. The convergence parameter μ must be less than the inverse of the maximum eigenvalue of the input correlation matrix to ensure stable convergence. In a practical setting, the maximum eigenvalue can be approximated by the tap input power. The other parameters that will affect the convergence of the TAG controller are the perturbation size δ and the average duration N. After the weight vector has converged to the optimal solution, the perturbation will ensure continual tracking of plant changes. Small perturbations may cause slow convergence to the optimal but will reduce the minimum mean squared error after convergence. Alternatively, relatively large values of the perturbation may provide more accurate estimates of the local gradient permitting faster convergence; this is at the expense of an increased minimum mean squared error after convergence. The appropriate average duration, N, is largely dependent on the noise present in the system. For non-noisy systems, low average durations can generate accurate estimates of the local mean squared error, and thus accurate computation of the gradient. Longer average durations will lead to longer convergence times because the weight cannot be updated until the gradient is computed. More detailed observations on the effects of these parameters on convergence and performance of the control of a thermoacoustic instability are presented in conjunction with simulations and experiments described next.

7.3 SIMULATION

The thermoacoustic instability and TAG controller using the steepest descent algorithm were simulated using MATLAB. The simulation is included in the Appendix. The acoustic portion of the combustion plant was modeled as a lightly damped single acoustic mode while the flame dynamics were modeled as a low pass filter. The modeled acoustic and flame dynamics were

$$G_A = \frac{-300000}{s^2 + 43.98s + 1.21e6} \qquad G_f = \frac{1500}{s + 1257} \qquad \textbf{[7.6]}$$

A saturation nonlinearity was approximated using a hyperbolic tangent function. While this is a crude model from a physical standpoint, it is sufficient to illustrate the controller performance because the spectrum and RMS pressure of the physical system is typically dominated by a single frequency limit cycle and its harmonics. The gain for the self-excited loop was chosen such that the limit cycle was established after only one second.

The actuator dynamics, G_{ACT} in Figure 7.1, include all dynamics associated with A/D and D/A conversion, the dynamics of the actuator, and the acoustic pressure response due to actuation. Two different actuator paths were chosen to illustrate different convergence behaviors of the TAG algorithm. Both contained the acoustic dynamics while one was a high gain, delayed version and the other used a lower gain without delays; both are shown here:

$$G_{ACT} = \frac{-0.11z - 0.11}{z^7 - 1.525z^6 + 0.973z^5} \qquad G_{ACT} = \frac{-0.011z - 0.011}{z^2 - 1.525z + 0.9729} \qquad \textbf{[7.7]}$$

For most experiments discussed here, the TAG controller was a two-weight FIR filter whose coefficients were updated using the steepest descent algorithm. Deviations from this are explicitly noted.

Figure 7.2 illustrates how the feedback loop stability varies with a two-weight feedback controller. The stable region (darker) is surrounded by a larger region where at least one closed loop pole is unstable. The TAG controller drives the weights to the stable region as long as it does not encounter a local minimum. In addition, it will adapt away from higher amplitude limit cycles that may be present in the unstable region of Figure 7.2, thereby preventing controller-induced instabilities.

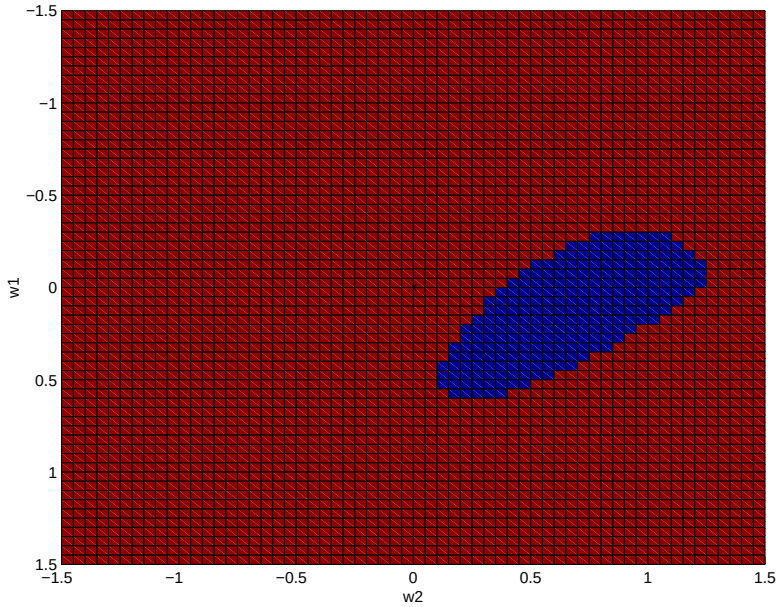

FIGURE 7.2 HIGH HEAT RELEASE STABILITY MAP

Figure 7.3 illustrates a segment of the normalized performance surface of the system of Figure 7.1 when the actuator path contains delays. This corresponds to the same system for which the stability map of Figure 7.2 was generated. It is apparent that a local minimum does exist on this performance surface. It is therefore possible that a small perturbation size might result in the algorithm settling to a local minimum.

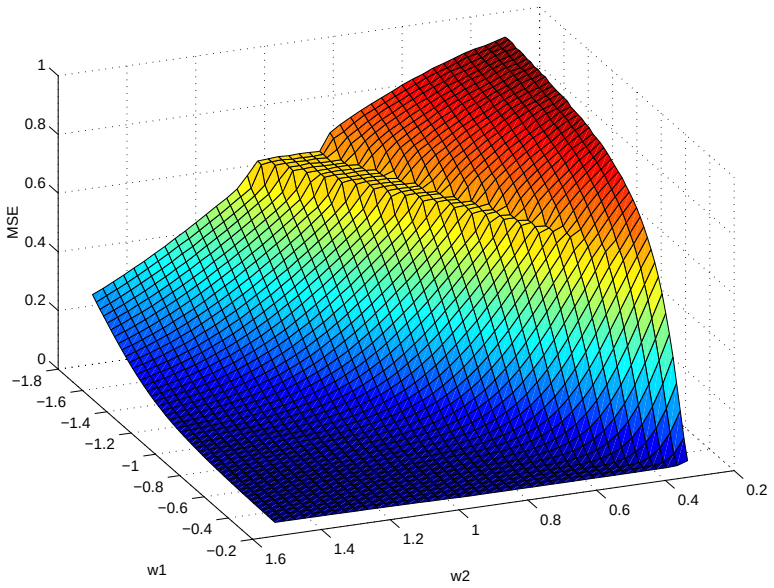

FIGURE 7.3 MSE PERFORMANCE SURFACE

As discussed above, there are three algorithmic parameters that affect the convergence of the steepest descent algorithm to a stable solution: the convergence parameter μ (controls the speed of the weight update), the perturbation size δ (controls the step size used in computing the gradient), and the average duration N (controls accuracy of cost estimate). Large convergence parameters may result in faster convergence or possible divergence depending on the shape of the MSE surface. The appropriate perturbation size also depends on the shape of the MSE surface and may add noise to the overall spectrum because it continually changes in a square wave fashion even after convergence. The average duration should be increased as noise pollutes the spectrum. However, simulations indicate that 0.0625s worth of average time is sufficient to provide convergence for very high noise levels and a 175 Hz instability sampled at 1600 Hz.

Figure 7.4 illustrates the simulated TAG control of the limit cycle where the actuator dynamics included phase delay and added gain. For a non-optimized choice of the perturbation size and convergence parameter (upper trace), the error signal is seen to initially increase in response to the perturbation. After the weights are corrected by the steepest descent algorithm, the controller attenuates the limit cycle and begins driving it toward the minimum. The cycling amplitude seen in the error signal represents the weight perturbation and subsequent re-

evaluation of the gradient and weight update. The slow convergence and initial misdirection are corrected as seen in the lower trace, by changing the perturbation direction (adding a minus sign to δ) and increasing the magnitude of the convergence parameter μ.

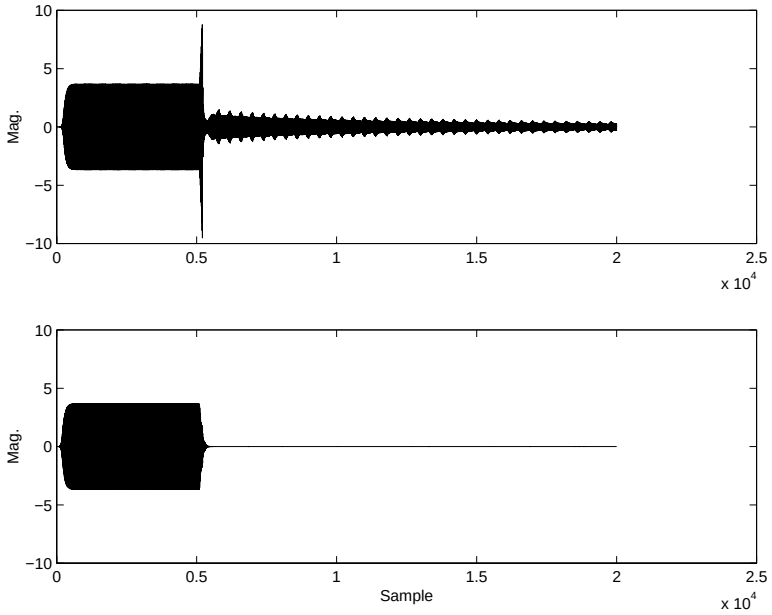

FIGURE 7.4 SLOW AND FAST TAG CONVERGENCE

As mentioned earlier, the convergence parameter size is limited by the stability of the algorithm. It is generally desirable to have a slightly overdamped response for noisy systems and gradient estimates to ensure continual convergence toward a minimum. Therefore the size of the convergence parameter is governed by the input power and the system noise and consequently controls the rate of convergence. The perturbation size is predominantly system dependent. The amplitude of the perturbation must be sufficiently large so as to affect the RMS level of the input signal in a measurable manner. If the perturbation is too small, the system will not be affected, no gradient will be computed and the weights will not be updated. This is equivalent to finding a local minimum on the gradient surface, where sufficient weight excitation is not available to significantly alter the gradient estimation.

Figure 7.5 represents another simulation result where the actuator dynamics were a scaled version of the acoustic plant without additional delays. Here we see that for a non-optimized

choice of the convergence parameter and perturbation, a new limit cycle (at a slightly lower frequency) is found. In this case, significant adaptation stops and the system has not been stabilized; a local minimum is found on the cost function. To remedy this (result shown in lower trace), the perturbation size was doubled and the convergence parameter was increased. Larger perturbations in the weights permit more global gradient estimates and the increased convergence parameter amplifies the gradient estimate to affect the weights more significantly. The result is a stabilized system.

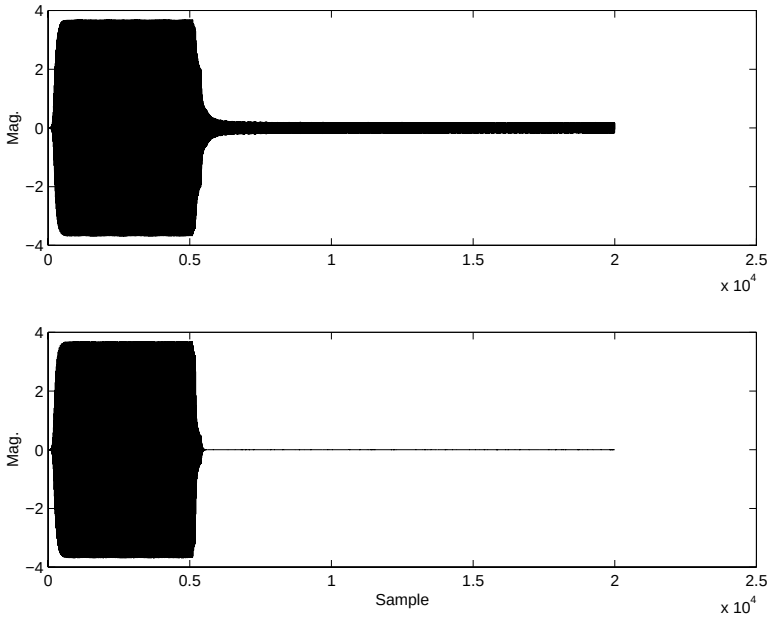

FIGURE 7.5 LOCAL MINIMUM AND OPTIMIZED CONVERGENCE

The effects of the perturbation size and convergence parameter seen in simulation can be categorized into a set of rules that can adaptively control the convergence behavior of the TAG controller. These are summarized as follows:

- If the MSE increases after the first perturbation, change the sign of the perturbation.
- If the MSE increases after changing the sign, reduce the magnitude of the perturbation.

- If the gradient is zero after the first several perturbations, increase the magnitude of the perturbation until a change in gradient is detected.
- If the MSE is near the minimum MSE, decrease the magnitude of the perturbation to reduce the misadjustment noise.
- If the system continually diverges, reduce the convergence parameter.
- If the gradient is too small to change subsequent MSE calculations, and the perturbation size has been increased, increase the convergence parameter.

Clearly these rules will interact with each other and care must be taken when applying them in actual experimental settings so as to avoid local minima and divergence. A subset of these rules has been implemented in conjunction with the TAG controller in a quasi-experimental setting. The rule based TAG was employed on a TI-C31 DSP and used to control an analog electronics version of the single mode simulation described above. All of the rules described above result in the desired effect of faster and more repeatable convergence. However, once a perturbation size was chosen, simply changing the direction of the perturbation when an increase in MSE was detected, resulted in stabilization for every trial. A maximum tap input power was determined based on the initial limit cycle amplitude and the control actuator authority. This governed the choice of μ to guarantee stable convergence. This value was then reduced to limit the speed of convergence.

7.4 EXPERIMENTAL RESULTS

The Rijke tube combustor described previously was used as the experimental test bed. Recall that the 2nd acoustic mode is unstable when the burner is placed at the mid-length of the tube, in accordance with the Rayleigh criterion. At low heat release operating conditions, the frequency of the 2nd mode is nominally 178 Hz and the limit cycle frequency is approximately the same. The control actuator was a three-inch acoustic driver (speaker) coupled to the tube through a plenum and attached just above the flame. The actuator power was sufficient to achieve control at low heat-release conditions, corresponding to low equivalence ratios. At higher equivalence ratios, however, the increased unsteady heat release rate caused the self-excited loop gain to increase to the point that no controller could stabilize the system, although

the limit cycle amplitude could be reduced to some degree. As described in earlier sections, this was due to the actuator power limitations and eventually resulted in a dynamic searching between stable and unstable regimes.

The Rijke tube combustor was set to operate with an equivalence ratio of 0.54 and a total volume flow of 130 cc/sec. The two-weight TAG controller using the steepest descent algorithm was then employed using a TI-C31 DSP control system. The uncontrolled input level of the pressure signal measurement was adjusted external to the DSP. Based on the input signal level, the convergence parameter was chosen as 0.4 to ensure gradient convergence. The perturbation value of 0.4 was found to be small enough to prevent excessive noise after convergence, yet large enough to provide a measurable change in the gradient. Typically this can be determined experimentally, or algorithmically as described above. Figure 7.6 illustrates the converged TAG controlled power spectrum of the pressure signal (solid) compared to the uncontrolled pressure spectrum (dotted). The TAG controller converged to a stabilizing solution within approximately 0.25s and maintained control of the low-heat release case indefinitely.

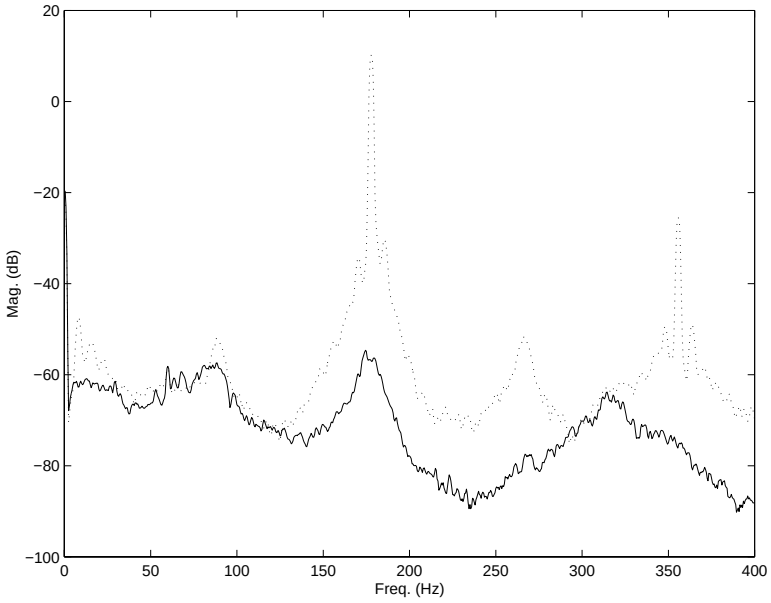

FIGURE 7.6 LOW HEAT RELEASE RIJKE TUBE TAG CONTROL

The TAG controller is a very versatile method for controlling the combustion instability and can be applied in a variety of formats and parameterizations. Several different algorithm variants were investigated experimentally including the multi-weight TAG (FIR filter using four weights) and the direct adaptation of gain and phase. The IIR all pass filter form of the gain and phase controller in the z-domain is

$$H(z) = b\frac{z^{-2} + 2az^{-1} + a^2}{1 + 2az^{-1} + a^2 z^{-2}} \qquad \textbf{[7.8]}$$

This represents two first order all-pass filters in series where the control parameter "a" controls the phase delay and "b" controls the gain. Two all-pass filter sections permit 360 degrees of phase adjustment at 175 Hz (the instability frequency) when sampled at 1600 Hz. If "a" is limited to remain between +1 and –1, H(z) is guaranteed to be stable while allowing controller poles to adapt. The gain and phase of the controller are perturbed and updated directly without altering the shape of the control filter's frequency response.

Both methods stabilized the Rijke tube combustor after brief transients, resulting in performances nearly identical to Figure 7.6. The steepest descent formulation of the weight

update equation in no way limits the number of weights that can be updated or the form of the control filter. In the case of the Rijke tube combustor, two control weights were found to be sufficient to achieve stabilizing control. A notable benefit for additional weights is that they can more readily control the frequency response, preventing control loop instabilities induced by the feedback controller. There is no specific advantage of choosing the gain and phase parameterization of [7.8] for the control of the Rijke tube combustor, as the performance was identical to that of the FIR filter control update. However, there may be instances where it is more advantageous to update controller parameters other than FIR filter coefficients; the TAG formulation can easily accommodate such changes.

To illustrate the versatility of the algorithm, it was also used to adapt a subharmonic controller to achieve stabilization of the Rijke tube. The output of a TAG-controlled two weight FIR filter was frequency divided to produce an output with half the frequency of the input and with a duty cycle of 50% that was used as the control signal. The second harmonic of the sub-harmonic control signal serves to attenuate the limit cycle in a linear system sense while the cycle stress on the actuator is reduced. The TAG controller requires no *a priori* information of this change since its only concern is to minimize the RMS pressure of the error signal. The subharmonic application of the TAG algorithm (transient convergence shown in Figure 7.7) led to limit cycle amplitude reductions that were identical to those shown for the standard TAG implementation in Figure 7.6.

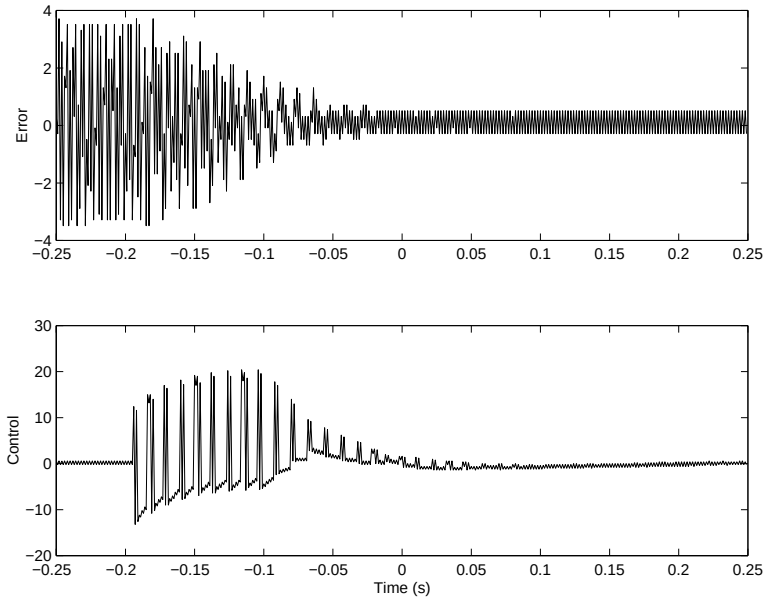

FIGURE 7.7 SUBHARMONIC TAG CONVERGENCE

Higher equivalence ratios, corresponding to higher self excited loop gains, were not stabilizable using the low-power acoustic actuator employed in these experiments. However, it is informative to examine the performance of the TAG controller when compared to other controllers for this operating condition. Figure 7.8 illustrates three controlled time responses at the high heat release condition.

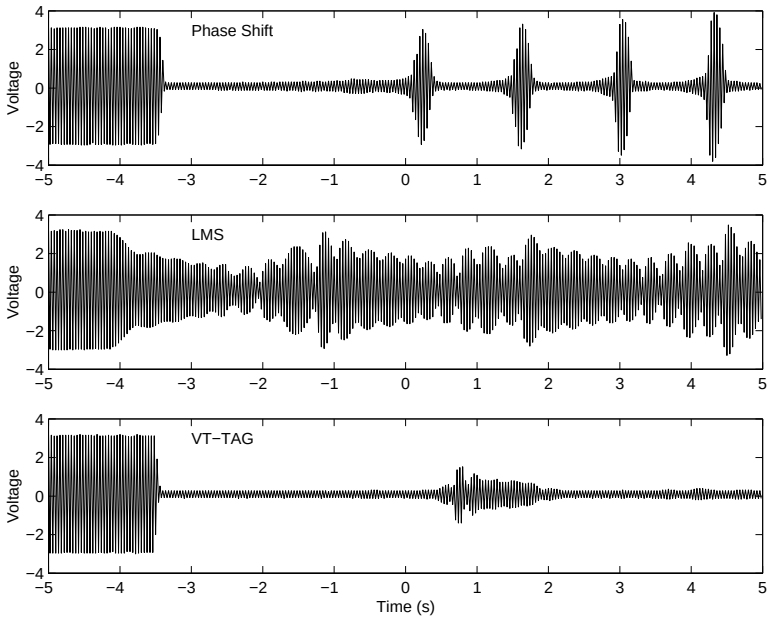

FIGURE 7.8 HIGH HEAT RELEASE CONVERGENCE COMPARISON

The upper trace represents a manually-tuned fixed feedback controller. The intermittent behavior is a result of the actuator power limitations and changing plant dynamics in response to the control as described earlier. The second time response represents an adaptive feedback controller of the type shown in Figure 5.2, employed at the same operating conditions. In both the fixed gain and adaptive feedback controllers, the intermittency amplitude was approximately the same as the original limit cycle amplitude. However, when the TAG controller was used at these operating conditions, the intermittency period increased and the amplitude decreased significantly. In this case, the TAG controller represents a more robust adaptive control solution, even in the presence of actuator authority limitations.

The performance of the TAG controller was extended to a more practical setting when it was tested using a liquid fuel combustor actuated with fuel injectors at Louisiana State University; shown in Figure 7.9.

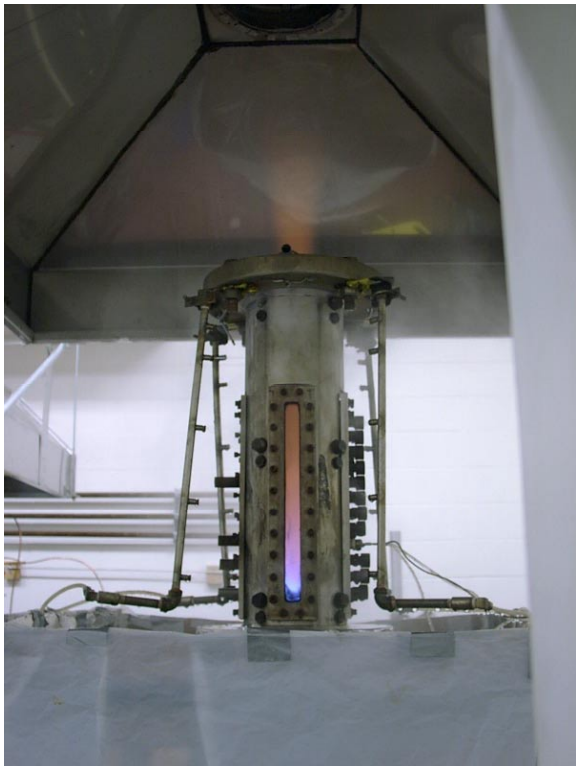

FIGURE 7.9 LSU LIQUID FUEL COMBUSTOR

The two weight TAG controller used in the Rijke tube experiments and sub-harmonic control experiments, was not significantly altered when employed on the liquid fuel combustor. The perturbation size was changed slightly in order to affect the plant enough to measure the local gradient. The output signal was converted from a sinusoid to a square wave using a threshold detector at a fixed amplitude to appropriately drive the fuel injector valve. The TAG controller performed very well as shown in Figure 7.10, reducing the limit cycle and its harmonics by approximately 20 dB.

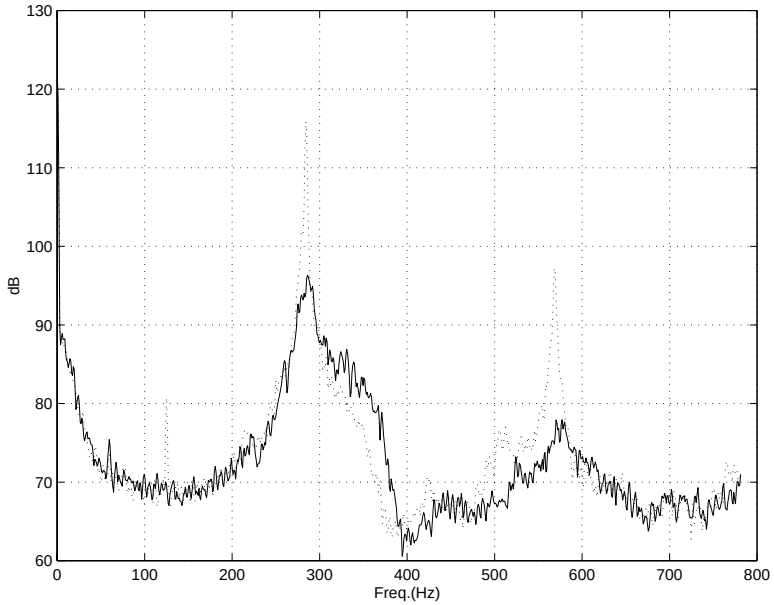

FIGURE 7.10 LSU LIQUID FUEL COMBUSTOR, TAG CONTROL

7.5 CONCLUSIONS

The time-averaged gradient controller presented here was shown to be an effective and versatile method for controlling thermoacoustic instabilities. Requiring no plant estimate or model, the steepest descent algorithm effectively moves a wide variety of control parameters toward a solution that consistently minimizes the mean-squared error of the input signal.

Effective control of a Rijke tube combustor was achieved experimentally when the TAG controller was a two-weight FIR filter, an all-pass IIR filter, a four-weight FIR filter, and a sub-harmonic frequency division of the output of a two-weight FIR filter.

Because of its ease of implementation, control effectiveness, and versatility, it holds many advantages over other controllers previously discussed. Fast and repeatable convergence of the TAG controller is dependent upon several algorithmic parameters. Certain observations, simulations, and experimental results presented here, help define the effects of these parameters on the overall performance. Initial investigation into automatic selection of these parameters was presented and shown to be effective. Future work will include more

investigation of algorithms for automatically selecting the convergence parameter, averaging-interval, and perturbation of the TAG controller in order to make it more system independent.

Chapter 8

Conclusions

8.1 SUMMARY AND CONCLUSIONS

Disturbance rejection for *stable* systems can be accomplished using both feedforward and feedback control techniques. Feedforward control modifies the zeros of the plant, minimizing its response at specific frequencies. Feedforward control relies on the ability to sense a coherent but uncontrollable representation of the disturbance to be cancelled. Feedback control achieves disturbance rejection by altering the poles and zeros of a plant to minimize the disturbance to output transfer function at specific frequencies.

Control of *unstable* limit cycling systems can only be accomplished using *feedback* control. The disturbance to be canceled is a result of an exponentially increasing transient response that has been limited by a saturation nonlinearity. (The unstable transient response can be initiated by any small disturbance that enters the plant or noise in the plant itself; for physically realizable, open loop unstable systems, initiation of the unstable transient always occurs). Attempting feedforward control of self-excited systems reveals two distinct limitations: an uncontrollable, coherent reference is not available and the system cannot be stabilized by modifying only zeros. Since the disturbance exists due to unstable dynamics, stabilizing those dynamics is required to ensure global control. Only feedback control can alter system poles.

The specific self-excited system examined throughout this work was the thermoacoustic instability. Feedback interaction of unsteady heat release rate and acoustic pressure can cause the combustion plant to become unstable. The dynamics of the flame transfer function influence the acoustic dynamics as heat increases or decreases in the combustion chamber. In addition, operating conditions and external power load can affect the flame dynamics and unsteady heat release rate. For these reasons self-adapting control technologies are preferred

over fixed gain active or passive control approaches. The goal of this research was to examine existing and new adaptive control approaches for controlling the self-excited thermoacoustic instability. To this end, the following approaches were investigated.

- Loopshaping feedback controller design to minimize controller induced instabilities and maximize control performance.
- Artificial neural network plant estimation and automatic feedback controller update.
- Adaptive feedback control employing Filtered-X LMS based approaches to system stabilization.
- Time averaged gradient control of self-excited systems.

Numerous implementation and stability issues were addressed for each of these controller designs. The following paragraphs summarize the key findings from each design approach.

The most rudimentary control approach previously examined was termed "phase shifting feedback control". This approach involved simply measuring the acoustic pressure in the combustion chamber and modulating an actuator (acoustic or fuel injector) with that signal after a manual phase shift was applied. Many researchers reported problems with this approach that were not adequately explained. So before proceeding with adaptive approaches, this research investigated the source and solution to the "secondary peaks" experienced by fixed gain control approaches previously investigated.

Anytime a feedback controller is implemented, the risk of creating instabilities exists. Careful design of the frequency response of the controller in conjunction with the open loop plant is required in order to apply the most open loop gain for disturbance rejection, and the least gain at phase crossovers to limit new instabilities. A unique system identification method was developed that accurately predicts the creation of controller induced instabilities for specific controller designs. Predicting the frequency and magnitude of these instabilities greatly reduced the mystique behind manual phase shifting controller "design"; although, the approach is a well known classical implementation of Bode gain and phase margin criteria. This precursor is important to all other contributions made herein because the general

feedback control structure for the self-excited system is similar in all controller implementations.

The fixed gain controller design made possible by the system identification procedure resulted in a stabilized thermoacoustic instability on a Rijke tube experimental setup. However, this design was only applicable for the operating conditions for which it was designed. New operating conditions and new flame dynamics changed the plant enough to require a different controller design. Armed with a controller design tool, and a method of system identification, it was conceived that a feedback controller could be designed for every operating condition for a specific combustor.

An artificial neural network was trained to predict the self-excited plant frequency response as a function of operating conditions and temperature profile. This neural network was then used in conjunction with a controller design algorithm to update feedback controller parameters in real-time. Because the control of the plant can change the dynamics of the plant, the frequency response had to be estimated by the neural network *during* control. It was shown that the neural network/fuzzy controller update could maintain stabilizing control over a wide range of operating conditions within the capabilities of the three inch diameter acoustic actuator. This control method holds promise for specific combustor control, but is difficult to generically port to a multitude of platforms.

In addition to fixed gain feedback controller design, prior research has also examined adaptive control approaches to thermoacoustic instability control. While the examined approaches were typically Filtered-X based controllers, their configurations have been adaptive IIR or "Filtered-U". The adaptive feedback controller examined in this work can be classified as a special case of Filtered-U control, but has not been previously examined by the combustion control community. The feedback filter in adaptive IIR control attempts to adaptively compensate the feedback path generated from the *controllable* reference signal used in self-excited system control. In adaptive feedback control, a fixed FIR filter is placed in the feedback path to compensate the controllable reference signal. In addition, because the reference signal *is* the error signal, the Filtered-X algorithm employs the same fixed FIR filter as the gradient filter.

The stability analysis and performance of the adaptive feedback architecture is much more straightforward than for the adaptive IIR controller.

Using a newly proposed, stable control-to-error path estimate including the actuator dynamics and hot acoustics, the thermoacoustic instability was stabilized using the adaptive feedback controller. Because the plant estimate was fixed, a new estimate had to be generated for each operating condition. In general, this is undesirable for an adaptive controller but the adaptation proved to be effective for specific operating conditions, converging to the same solution found with a manually tunable feedback controller.

The stability analysis for adaptive feedback control was conducted for control of *stable* plants. The results can be heuristically extended to unstable plant control, but the analysis becomes significantly more complicated. Conventional implementation of feedforward Filtered-X algorithms require that the plant estimate is within 90 degrees of the actual plant to ensure gradient convergence. It was shown here that when employed in a feedback arrangement, these criteria do not hold. Feedback loop instabilities and algorithm divergence can occur for arbitrarily small errors in both magnitude and phase in the control-to-error path estimate. Therefore the robust implementation of the adaptive feedback controller cannot be guaranteed for any general plant.

In addition to loop and algorithm instabilities, a third intermittent instability was identified when attempting to control relatively high heat release operating conditions. This intermittency was shown to be a function of the actuator authority in conjunction with the changing plant dynamics under the action of the controller. When the system was stabilized, the gain in the flame dynamics transfer function increased, causing the stabilized pole to move back toward the right half plane. At higher heat release conditions, near the limits of actuator saturation, enough gain was not present in the control loop to maintain stabilizing control and the system began to limit cycle again. During oscillation, the loop gain decreased allowing stabilizing control. This recurring phenomenon caused an intermittent oscillation when using all control approaches, including fixed gain feedback, and time averaged gradient control.

All prior approaches examined here, and in previous research, have relied on a model of the control-to-error path, or some knowledge of the unstable plant dynamics. The thermoacoustic instability is a very complicated plant and modeling efforts have been ongoing for years. The model accuracy required to ensure robust controller design may never be achieved. In addition, the changing plant dynamics, both under the action of the controller and in response to operating and load conditions, make a fixed plant estimate impractical. Therefore a need exists for a feedback controller that can adapt to changing conditions and does not rely on any prior knowledge of the plant to be controlled. The time averaged gradient algorithm as presented here, begins to fit that need.

The time averaged gradient algorithm uses an estimate of the local gradient to dynamically update the parameters of a controller. As each parameter is perturbed in a specific direction, the local gradient is computed and the parameter is updated so that the mean squared error is reduced. This simple approach was shown to be very versatile, controlling both the Rijke tube with acoustic actuation and a full-scale liquid fuel combustor using fuel injector actuation. FIR filter, IIR filter and subharmonic control parameters were all investigated with success. The TAG algorithm does not require any prior knowledge of the plant to be controlled, and can be easily ported to a variety of combustor platforms.

The most promising of all control approaches for the thermoacoustic instability seems to be the TAG algorithm. Its limitations include significantly increased computation and convergence time for a large number of control parameters and system dependent convergence characteristics. However, supervisory controls can be added that will ensure robust performance. The artificial neural network also performs admirably over a wide variety of operating conditions, but is designed specifically for a single combustor/actuator arrangement. This limited portability may limit its perceived effectiveness. The Filtered-X based adaptive approaches seem to hold the least promise for ensuring robust control performance. While the adaptive feedback controller was shown to effectively control the simple Rijke tube, the requirement for continual system identification and lack of guaranteed robustness make this a particularly unattractive option for control of thermoacoustic instabilities and self-excited systems in general.

8.2 FUTURE WORK

While all research seeks to answer questions, it inevitably poses new ones. In a finite period of time, all questions cannot be answered. This final section offers several new research and development opportunities that were generated during the course of this work.

Thermoacoustic instabilities have recently become a more significant problem due to restrictions placed on acceptable pollutant levels. Lean air/fuel ratios improve emissions but can exacerbate thermoacoustic instabilities. The goal of active (or passive) control of these instabilities is to ensure that dangerous noise and vibration levels are not reached while *simultaneously* limiting emissions. The effects of these control approaches on emissions has not been carefully addressed by this work. For acoustic actuation, it is assumed that no significant changes will occur because the amount of fuel has not been affected. However, acoustic actuation is not typically considered to be a viable practical solution and secondary (or primary) fuel injectors are typically used as the preferred form of control actuation for full scale combustors. The effects that the control approaches have on pollutant emissions should be carefully examined.

Conventional application of the Filtered-X LMS algorithm has always maintained that no more than a 90 degree phase error in the control-to-error path estimate is tolerable to prevent divergence of the algorithm. In simulation and experiment this author has found this to be a true bound for broadband and tonal control alike. However, the literature only supports this bound for tones and does not directly relate the gradient direction to the gradient filter phase. Given the overwhelming experimental evidence, it seems plausible that the 90 degree criteria can be proven for broadband disturbance rejection without any specific limitations on sampling or plant structure.

Chapter 6 presented a theoretical online system identification technique that may remedy some of the plant estimation problems for adaptive feedback control. However, this fix was never simulated or tested in an experimental setting. Before adaptive feedback control of stable or unstable systems is completely abandoned, it may be useful to investigate this online system identification technique and quantify the expected performance for real systems. If stabilizing

control can be achieved as shown in Chapter 5, the plant to be identified by the proposed online identification technique will be stable, making the task much easier. Continual identification of the appropriate transfer function may yield an adaptive feedback controller that is robust to plant changes and will not become unstable due to gradient divergence or feedback loop instabilities.

The TAG algorithm as presented here provides the framework for a valuable controller that is implemented independent of the system dynamics to which it is applied. Because it is an adaptive controller, and is in a feedback loop, the risk of controller induced instabilities is always present. In addition, the update of the weights relies upon the ability to accurately estimate the local change in MSE due to a specific weight perturbation. During transients in the system response, the computed MSE will not be accurate and will not be based strictly on the weight perturbation. Finally, for a complex, non-quadratic performance surface, it is possible that a single weight perturbation may immediately generate a controller induced instability that saturates the actuator before the next weight can measure the MSE. In this instance any perturbation of any control parameter will not detect any change in the MSE because the system is in a new controller induced limit cycle. Each of these problems can be remedied using supervisory control where the MSE is continually monitored for such changes. Some suggested rules were presented and implemented in the previous chapter. Careful and thorough implementation of these rules and other safeguards against the phenomenon discussed above, is recommended to ensure that the TAG controller is a robust and repeatable solution for the generic combustion control problem

Research for the sake of research is not a profitable prospect. The end goal of any funded research should be to *solve* a real problem. For extremely complex problems, it may be necessary to approach a potential solution from first principles. In many such cases, the problem becomes so abstract it is difficult to even relate it to the original goal. When this occurs, it is easy to become so immersed in core research, that the original problem is never solved. It is important to continue to consider that the goal of this particular research effort has been to deliver a robust controller solution to the thermoacoustic instability – i.e. to solve a real problem. While efforts have been made throughout this text to keep the problem in focus

and to consider real-world issues, the end result is still only a controller algorithm implemented on prototype hardware with no failsafe features to prevent a variety of potential catastrophic failures. The practical issues of robust implementation, productization, packaging, user interface, and performance safeguards must be addressed by future work before a final solution can be offered.

REFERENCES

[1] K. Kailasanath and E. Gutmark, "Combustion Instability," Chapter 5 in Propulsion Combustion: Fuels to Emissions Taylor and Francis, 1997.

[2] A. Annaswamy., M. Fleifil, J. Hathout, and A. Ghoneim, "Impact of Linear Coupling on the Design of Active Controllers for the Thermoacoustic Instability," Combustion Science and Technology, 128, 1997, pp. 131-181.

[3] J. Keller, "Thermoacoustic Oscillations in Combustion Chambers of Gas Turbines," AIAA Journal, 33, no. 12, 1995, pp. 2280-2288.

[4] F. Culick, "Short Communication: A Note on Rayleigh's Criterion," Combustion Science and Technology, 56, 1987, pp. 159-166.

[5] T. Lieuwen and B. Zinn, "Theoretical Investigation of Combustion Instability Mechanisms in Lean Premixed Gas Turbines,"AIAA 98-0641, 36th Aerospace Sciences Meeting and Exhibit, Reno, NV, Jan. 1998.

[6] R. Murray, C. Jacobson, R. Casas, A. Khibnik, C. Johnson, R. Bitmead, A. Peracchio, and W. Proscia, "System Identification for Limit Cycling Systems: A Case Study for Combustion Instabilities," Proceedings of the 1998 ACC, June, 1998.

[7] M. Macquisten and A. Dowling, "Low-frequency Lombustion Oscillations in a Model Afterburner," Combustion and Flame, 94, 1993, pp. 253-264.

[8] K. Yu, K. Wilson, and K. Schadow, "Liquid –Fueled Active Instability Suppression," , Paper No. P098, 27th Symposium (International) on Combustion, Boulder, CO, 1998.

[9] K. Yu, K. Wilson, and K. Schadow, "Liquid-Fueled Combustion Control: Scale-Up Experiments and Effect of Fuel Droplet Size," AiAA-99-0328, 37th AIAA Aerospace Sciences Meeting, Reno, NV, 1999.

[10] A. Dowling, "Combustion Noise and Active Control," VKI Lecture, September, 1997.

[11] A. Annaswamy and A. Ghoniem, "Active Control in Combustion Systems," IEEE Control Systems Magazine, 15, no. 6, 1995, pp. 49-63.

[12] B.S. Hong, V. Yang, and A. Ray, "Robust Feedback Control of Combustion Instability with Model Uncertainty," AIAA Paper 98-0354, 1998.

[13] K.R. McManus, J.C. Magill, and M.F. Miller, "Closed-Loop System for Stability Control in Gas Turbine Combustors," AIAA Paper 97-0463, 1997.

[14] P. Langhorne, A. Dowling, and N. Hooper, "Practical Active Control System for Combustion Oscillations," Journal of Propulsion and Power, 6, no. 3, 1990.

[15] J. Rumsey, M. Fleifil, A. Annaswamy, J. Hathout, and A. Ghoniem, "The Role of Active Control in Suppressing Thermoacoustic Instability," Proceedings of the American Control Conference, Albuquerque, NM, 1997.

[16] M.A. Vaudrey, W.R. Saunders, and B. Eisenhower, "Control Of Combustion Instabilities A Test-Based Methodology For Apriori Selection Of Gain/Phase Relationships In Proportional, Phase-Shifting," ASME Turbo Expo Conf., Munich, Germany, May 2000.

[17] W.R. Saunders, M.A. Vaudrey, B.A. Eisenhower, U. Vandsburger, and C.A. Fannin, "Perspectives on Linear Compensator Designs for Active Control," AIAA 99-0717**,** 37th AIAA Aerospace Sciences Meeting, Reno, NV, Jan. 11-14, 1999.

[18] M. Fleifil, A.M. Annaswamy, J.P. Hathout, and A.F. Ghoneim, "The Origin of Secondary Peaks with Active Control of Thermoacoustic Instability," Proceedings of the AIAA Joint Propulsion Conference, Seattle, WA, July 1997.

[19] M.A. Vaudrey, and W.R. Saunders, "Control Of Combustor Instabilities Using An Artificial Neural Network," ASME TurboExpo Conf., Munich, Germany, May 2000.

[20] R. Blonbou and A. Laverdant, "Control of Combustion Instabilities on a Rijke Tube by a neural Network," AVT Symposium on Active Control Technology for Enhanced Performance Operational Capabilities of Military Aircraft, Land Vehicles and Sea Vehicles, Braunschweig, Germany, May 8-11, 2000.

[21] K. McManus, T. Poinsot, and S. Candel, "A Review of Active Control of Combustion Instabilities," Prog. Energy Combust. Sci. 19, 1993, pp. 1-29.

[22] G. Billoud, M.A. Galland, C.H. Huu, and S. Candel, "Adaptive Active Control of Combustion Instabilities," Combust. Sci. and Tech., 81, 1992, pp.257-283.

[23] A. Kemal and C. Bowman, "Active Adaptive Control of Combustion," Proceedings of the IEEE Conference on Control Applications, 1995, pp.667-672.

[24] S. Evesque, A. Dowling, and A. Annaswamy, "Adaptive Algorithms for Control of Combustion," AVT Symposium on Active Control Technology for Enhanced Performance Operational Capabilities of Military Aircraft, Land Vehicles and Sea Vehicles, Braunschweig, Germany, May 8-11, 2000.

[25] A.M. Annaswamy, O.M. El Rifai, M. Fleifil, J.P. Hathout, and A.F. Ghoneim, "A Model-based Self-tuning Controller for Thermoacoustic Instability," *Combustion Science and Technology,* 135, 1998, pp. 213-239.

[26] M. Kristic, A. Krupadanam, and C. Jacobson, "Self-Tuning Control of a Nonlinear Model of Combustion Instabilities," Proceedings of the 1997 IEEE International Conference on Control Applications, Hartford, CT, 1997.

[27] S. Evesque, Y. Chu, A. Dowling, and K. Glover, "Feedback Control of a Premixed Ducted Flame," AIAA, 1999.

[28] S. Koshigoe, T. Komatsuzaki, and V. Yang, 'Adaptive Control of Combustion Instability with On-Line System Identification,' Journal of Propulsion and Power, 15, 1999, pp.383-389.

[29] M. Mettenleiter and S. Candel, "Developments of Adaptive Methods for Active Instability Control," AVT Symposium on Active Control Technology for Enhanced Performance

Operational Capabilities of Military Aircraft, Land Vehicles and Sea Vehicles, Braunschweig, Germany, May 8-11, 2000.

[30] R. Mohanraj and B.T. Zinn, "Numerical Study of the Performance of Active Control Systems for Combustion Instabilities," AIAA 98-0356, 36th Aerospace Sciences Meeting & Exhibit, Reno, NV, Jan., 1998.

[31] S. Ziada and H. Graf, "Feedback Control of Combustion Oscillations," Journal of Fluids and Structures, 12, 1998, pp. 491-507.

[32] E. Chang and K. Kailasanath, "Active Control of combustions Instabilities Using Timed Injection of High Energy Fuels," AIAA-98-3765, 34th Joint Propulsion Conference and Exhibit, Cleveland, OH, 1998.

[33] C. Johnson, Y. Neumeier, E. Lubarsky, J. Lee, M. Neumaier, and B. Zinn, "Suppression of Combustion Instabilities in a Liquid Fuel Combustor Using a Fast Adaptive Control Algorithm," AiAA-2000-0476, 38th Aerospace Sciences Meeting and Exhibit, Reno, NV, 2000.

[34] A. Banaszuk, Y. Zhang, and C. Jacobson, "Active Control of Combustion Instabilities in Gas Turbine Engines for Low Emissions. Part II: Adaptive Control Algorithm Development, Demonstration and Performance Limitations," AVT Symposium on Active Control Technology for Enhanced Performance Operational Capabilities of Military Aircraft, Land Vehicles and Sea Vehicles, Braunschweig, Germany, May 8-11, 2000.

[35] M.A. Vaudrey, W.R. Saunders, and W.T. Baumann, "An Investigation of Adaptive Signal Processing Approaches to Active Combustion Control," AVT Symposium on Active Control Technology for Enhanced Performance Operational Capabilities of Military Aircraft, Land Vehicles and Sea Vehicles, Braunschweig, Germany, May 8-11, 2000.

[36] Y. Zhang, "Stability and Performance Tradeoff with Discrete Time Triangular Search Minimum Seeking," Proceedings of the American Control Conference, Chicago, 2000.

[37] P. Feintuch, "An Adaptive Recursive LMS Filter," Proceedings of the IEEE, 1976, pp. 1622-1624.

[38] L. Eriksson and M. Allie, "Correlated Active Attenuation System with Error and Correction Signal Input," U.S. Patent Number 5206911, 1993.

[39] S.J. Elliott, I.M. Stothers, and P.A. Nelson, "A Multiple Error LMS Algorithm and Its Application to the Active Control of Sound and Vibration," IEEE Transactions on Acoust., Speech, and Sig.Proc., Vol.ASSP-35, No.10, Oct., 1987.

[40] D. Morgan, "An Analysis of Multiple Correlation Cancellation Loops with a Filter in the Auxiliary Path," IEEE Trans. Acoust. Speech, Signal Processing, ASSP-28, 1980, pp. 454-467.

[41] S. Snyder and C. Hansen, "The Effect of Transfer Function Estimation Errors on the Filtered-X LMS Algorithm," IEEE Transactions on Signal Processing, 42, no. 4, 1994, pp. 950-953.

[42] A. Wang and W. Ren, "Convergence Analysis of the Filtered-U Algorithm for Active Noise Control," Signal Processing, 73, 1999, pp. 255-266.

[43] M. Rupp and A. Sayed, "A Time-domain Feedback Analysis of Filtered-Error Adaptive Gradient Algorithms," IEEE Transaction on Signal Processing, 44, no. 6, 1996, pp. 1428-1439.

[44] G. Gibbs and R. Clark, "Feedforward Higher Harmonic Control Using the H-TAG Algorithm," Noise-Con 93, Williamsburg, VA, 1993, pp. 541-546.

[45] D. Kewley, R. Clark, and S. Southward, "Feedforward Control Using the Higher Harmonic, Time-Averaged Gradient Descent Algorithm," Journal of the Acoustical Society of America, 97, no. 5, 1995, pp. 2892-2905.

[46] P. A. Nelson and S. J. Elliot, *Active Control of Sound*, Academic Press Ltd., London, England, 1992.

[47] S.Haykin, *Adaptive Filter Theory*, 3rd ed, Prentice-Hall, Upper Saddle River, N. J., 1996.

[48] S.M. Kuo and D.R. Morgan, *Active Noise Control Systems, Algorithms and DSP Implementations*, John Wiley and Sons, Inc., New York, NY, 1996.

[49] B. Widrow and S.D. Stearns, *Adaptive Signal Processing*, Prentice-Hall, Inc., Englewood, N.J., 1985.

[50] G. Franklin, J. Powell, and A. Emami-Naeini, *Feedback Control of Dynamic Systems*, 3rd Edition. Addison-Wesley Publishing Company, Inc., Reading, Massachusetts, 1994.

[51] P. Regalia, *Adaptive IIR Filtering in Signal Processing and Control*, Marcel Dekker, Inc., New York, NY, 1995.

[52] R. Clark, W. Saunders, and G. Gibbs, *Adaptive Structures: Dynamics and Control*, John Wiley and Sons, Inc., New York, NY, 1998.

[53] E. Leboucher, P. Micheau, and A. Berry, "An Index to Predict the Stability of Decentralized Adaptive Feedback Active Noise Control System," Canadian Acoustics, 28, Part 3, 2000, pp. 60-61.

[54] Y. Chu, A. Dowling, K. Glover, and S. Evesque, "Algorithms for Feedback Control of Combustion Oscillations," Proceedings of the IEEE Conference on Decision and Control, v. 3, 1999, pp. 2863-2868.

[55] K. Nishikawa and K. Hitoshi, "LS Based New Gradient Type Adaptive Algorithm – Least Squares Gradient," Proceedings – ICASSP, part 3, 1994, pp. III 413-416.

[56] Eriksson, L.J., "Recursive algorithms for active noise control," Proc. Int. Symp. Active Control of Sound Vib., 1991, pp. 137-146.

[57] M.A. Vaudrey, W.T. Baumann, and W.R. Saunders, "Applying Adaptive LMS to Feedback Control of Thermoacoustic Instabilities," Submitted to IEEE Transactions on Control Systems Technology, June 2001.

[58] M.A. Vaudrey, W.T. Baumann, and W.R. Saunders, "Stability and Operating Constraints of Adaptive LMS-Based Feedback Control," Submitted to Automatica, June 2001.

[59] M.A. Vaudrey., W.T. Baumann, and W.R. Saunders, "Time Averaged Gradient Control of Thermoacoustic Instabilities," Submitted to the Journal of Propulsion and Power, June 2001.

[60] Khanna, V. "A Study of the Dynamics of Laminar and Turbulent Fully and Partially Premixed Flames," Ph.D. Dissertation, Virginia Tech, 2001.

APPENDIX

A NEURAL NETWORK DSP C-FILE

Not included here is the training procedure where the weights of the neural network are determined based on data collected on the combustor. There are sufficient references that provide the necessary background for creating and training a neural network. Therefore the explicit description of that process is not included here for brevity. However, the c-file used in the real time implementation of the neural network is presented. It is assumed that the 6-20-20 neural network has been trained using actual tube data over the desired operating conditions. This is most easily accomplished in a MATLAB type of simulation environment. The coefficients for the ANN must then be inserted into the following c-file which does the following:

- Receives as inputs the temperatures and operating conditions,
- Generates a complex valued FRF and converts that to magnitude and phase,
- Computes the gain and phase margins for the closed loop system,
- Computes the required gain and phase delay to apply to the feedback controller to ensure optimum performance, and
- Performs feedback control.

This is carried out in two different sampling routines where the ANN is updated once every second and the feedback controller operates at 11,000 times per second. This program was designed to run on a dSpace DS1003 with a DS2201 A/D, D/A daughter board.

```
/*********************************************************************/
#include <brtenv.h>
#include <ensigdsp.h>
#include <math.h>

float NET_SampFreq = 1.0;
float cont_SampFreq = 11000.0;

#define MAX_VEC_SIZE 55
```

```
float cont_inp_vec[2][MAX_VEC_SIZE + 2];

float ts = 0.0;
float freqin = 180.0;
float actual_delay = 0.0;
float actual_phase = 0.0;
float in_1, net_output;
int not_current = 1;
int current_row = 0;
int ind = 0;
int manual_mode = 1;
float real_fb_gain = 0.0;
float manual_gain = 0.0;
int manual_delay = 47.0;
float u, out_1;
float tt,uu,vv,ww;
float input_test = 0.0;
float output_test = 0.0;
float output_test2 = 0.0;
float junk = 0.0;
float check_out = 0.0;
float T_scale = 0.001639344;
float F_scale = 0.006666666;
float net_samp_period;
float con_samp_period;
float in_2, in_3, in_4, in_5;
float T_4,T_6,Phi,Flow,T_5,T_7;
float desired_gain_margin = -8.0;
float desired_phase_margin = -20.0;
int pha_cross_ind1,  pha_cross_ind2, mag_cross_ind1, mag_cross_ind2;
float gain_margin1, gain_margin2, gain_margin, fb_gain, fb_gaindb;
int delay_samples1, delay_samples2, cont_delay_samples;
int delay_samples = 0;
float check_pha1, check_pha2, phase_delay, actual_phase;
int mc1, mc2, pc1, pc2;
float pm1, pm2, atmag1, atmag2, gm1,gm2,atpha1,atpha2;
int index = 0;
int index_1 = 0;
int crap_ind = 0;
int crap_ind2 = 0;

#define OUT_LAY_NODE 20
#define INP_LAY_NODE 7

float odd_space_freq[OUT_LAY_NODE] = {150.0,152.0,154.0,156.0,158.0,160.0,162.0,164.0,166.0,168.0,
        170.0,174.0,188.0,190.0,192.0,194.0,196.0,198.0,200.0};
float inp_vec[INP_LAY_NODE];

#define HID_LAY_NODE 20

/*MUST INSERT ANN TRAINED DATA - GET FROM MATLAB TRAINING*/
float w_lay1_re[HID_LAY_NODE][INP_LAY_NODE] =
float w_lay1_im[HID_LAY_NODE][INP_LAY_NODE] =
```

```
float lay1_out_re[HID_LAY_NODE];
float lay1_out_im[HID_LAY_NODE];
float lay2in_re[HID_LAY_NODE+1];
float lay2in_im[HID_LAY_NODE+1];

/*MUST INSERT ANN TRAINED DATA - GET FROM MATLAB TRAINING*/
float w_lay2_re[OUT_LAY_NODE][HID_LAY_NODE+1] =
float w_lay2_im[OUT_LAY_NODE][HID_LAY_NODE+1] =

float lay2_out_re[OUT_LAY_NODE];
float lay2_out_im[OUT_LAY_NODE];
float net_out_re[OUT_LAY_NODE];
float net_out_im[OUT_LAY_NODE];
float net_out_mag[OUT_LAY_NODE];
float net_out_pha[OUT_LAY_NODE];
float modified_mag[OUT_LAY_NODE];
float modified_pha[OUT_LAY_NODE];
float mag1, mag2, mag3, mag4, mag5, mag6, mag7, mag8, mag9, mag10, mag11, mag12, mag13, mag14, mag15,
        mag16, mag17, mag18, mag19, mag20;
float pha1, pha2, pha3, pha4, pha5, pha6, pha7, pha8, pha9, pha10, pha11, pha12, pha13, pha14, pha15,
        pha16, pha17, pha18, pha19, pha20 ;

/* Variables for execution time profiling */
#define TMR0 0                          /* timer0 definition */
#define TMR1 1
float exec_time0, exec_time1;                       /* execution time */
unsigned long count0, count1;                   /* timer0 time count */

/* error flag for CHKERR at last dual-port memory location */
volatile int *error = (int *) (DP_MEM_BASE + DP_MEM_SIZE - 1);

/* Input macros via DS2201 ADC channels 1 */

 #define Input_Chan1(u)     \
 start_ds2201ad(DS2201_1_BASE);   \
 u = ds2201ad(DS2201_1_BASE, 1)

/* Input macros via DS2201 ADC channels 2-5 */

 #define Input_LabViews(tt,uu,vv,ww)   \
 start_ds2201ad(DS2201_1_BASE);   \
 tt = ds2201ad(DS2201_1_BASE, 2);     \
 uu = ds2201ad(DS2201_1_BASE, 3);      \
 vv = ds2201ad(DS2201_1_BASE, 4);      \
 ww = ds2201ad(DS2201_1_BASE, 5)

/* Output via DS2201 DAC channel valid channels from 21 to 28 (1-8)*/
#define Output_Chan1(out_1) ds2201da(DS2201_1_BASE, 21, out_1);

/*---------------------------------------------------------------------*/
void main()
{
 float NET_DT = 1.0/NET_SampFreq;
 float CONT_DT = 1.0/cont_SampFreq;
```

```
 net_samp_period = 1.0/NET_SampFreq;
 con_samp_period = 1.0/cont_SampFreq;

 init();

 inp_vec[0] = 1.0;
 inp_vec[1] = T_scale*450.0;
 inp_vec[2] = T_scale*276.0;
 inp_vec[3] = T_scale*191.0;
 inp_vec[4] = T_scale*124.0;
 inp_vec[5] = F_scale*130.0;
 inp_vec[6] = 0.55;

 for(index = 0; index < MAX_VEC_SIZE+1; index ++)
 {
  cont_inp_vec[0][index] = 0.0;
  cont_inp_vec[1][index] = 0.0;
 }

 *error = NO_ERROR;
 start_isr_t0(CONT_DT);
 start_isr_t1(NET_DT);

 while (*error == NO_ERROR)
  service_cockpit();
}

/*---------------------------------------------------------------------*/
void isr_t0()
{
 /*begin_isr_t0(*error);*/

 service_trace();
 count0 = count_timer(TMR0);

 if(manual_mode == 0)
 {
  cont_delay_samples = 47 + delay_samples;
  real_fb_gain = fb_gain;
 }
 else
 {
  cont_delay_samples = manual_delay;
  real_fb_gain = manual_gain;
 }

 actual_phase = 360.0*178.0*cont_delay_samples*(1.0/cont_SampFreq);

 Input_Chan1(in_1);
 cont_inp_vec[current_row][0] = in_1;

            for(ind = 0; ind < MAX_VEC_SIZE; ind++)
            {
            cont_inp_vec[not_current][(ind+1)] = cont_inp_vec[current_row][ind];
```

```
            }

            if (current_row == 0)
            {
            current_row = 1;
            not_current = 0;
            }
            else
            {
            current_row = 0;
            not_current = 1;
            }

 net_output = real_fb_gain*cont_inp_vec[not_current][cont_delay_samples];
 Output_Chan1(net_output);

 exec_time0 = time_elapsed(TMR0, count0);  /* calculate execution time */

 /*end_isr_t0();                  /*  end of interrupt service routine */
}

/*-------this does the neural network and controller update----------------------*/
void isr_t1()
{
 begin_isr_t1(*error);

 count1 = count_timer(TMR1);

 Input_LabViews(in_2,in_3,in_4,in_5);

 T_4 = (11.45*10.0*in_2) + 489.5;
 T_6 = (3.55*10.0*in_3)  + 191.5;
 Phi = (0.0175*10.0*in_4) + 0.645;
 Flow = (1.9*10.0*in_5) + 126.0;
  T_5 = 2.1417*T_6 - 112.593;
 T_7 = 0.5401*T_6 + 19.9476;

 inp_vec[0] = 1.0;
 inp_vec[1] = T_scale*T_4;
 inp_vec[2] = T_scale*T_5;
 inp_vec[3] = T_scale*T_6;
 inp_vec[4] = T_scale*T_7;
 inp_vec[5] = F_scale*Flow;
 inp_vec[6] = Phi;

/*COMPUTES REAL LAYER 1 NET OUTPUT */
 for(index_1 = 0; index_1 < HID_LAY_NODE; index_1++)
 {
  junk = 0.0;
  for(index = 0; index < INP_LAY_NODE; index++)
   {
    junk = inp_vec[index]*w_lay1_re[index_1][index] + junk;
   }
  lay1_out_re[index_1] = junk;
```

```
 }

/*COMPUTES IMAGINARY LAYER 1 NET OUTPUT */
 for(index_1 = 0; index_1 < HID_LAY_NODE; index_1++)
 {
  junk = 0.0;
  for(index = 0; index < INP_LAY_NODE; index++)
   {
    junk = inp_vec[index]*w_lay1_im[index_1][index] + junk;
   }
  lay1_out_im[index_1] = junk;
 }

 lay2in_re[0] = 1.0;
 lay2in_im[0] = 1.0;

 for(index = 1; index < HID_LAY_NODE+1; index++)
  {
   lay2in_re[index] = (2.0/(1.0 + exp(-lay1_out_re[index-1]))) - 1.0;
   lay2in_im[index] = (2.0/(1.0 + exp(-lay1_out_im[index-1]))) - 1.0;
  }

/*COMPUTES REAL LAYER 2 NET OUTPUT */
 for(index_1 = 0; index_1 < OUT_LAY_NODE; index_1++)
 {
  junk = 0.0;
  for(index = 0; index < HID_LAY_NODE+1; index++)
   {
    junk = lay2in_re[index]*w_lay2_re[index_1][index] + junk;
   }
  lay2_out_re[index_1] = junk;
 }

/*COMPUTES IMAGINARY LAYER 2 NET OUTPUT */
 for(index_1 = 0; index_1 < OUT_LAY_NODE; index_1++)
 {
  junk = 0.0;
  for(index = 0; index < HID_LAY_NODE+1; index++)
   {
    junk = lay2in_im[index]*w_lay2_im[index_1][index] + junk;
   }
  lay2_out_im[index_1] = junk;
 }

/* THIS IS THE NEURAL NET OUTPUT (OLFRF) */
 for(index = 0; index < OUT_LAY_NODE; index++)
  {
   net_out_re[index] = (2.0/(1.0 + exp(-lay2_out_re[index]))) - 1.0;
   net_out_im[index] = (2.0/(1.0 + exp(-lay2_out_im[index]))) - 1.0;

   net_out_mag[index] = 4.0 + 10.0*log10((net_out_re[index]*net_out_re[index]) +
(net_out_im[index]*net_out_im[index]));
   net_out_pha[index] = -(180.0/3.14159)*atan2(net_out_im[index],net_out_re[index]);
```

```
            if (index >= 13)
              net_out_pha[index] = net_out_pha[index] - 360.0;
  }

  output_test = net_out_im[crap_ind];
  output_test2 = inp_vec[crap_ind2];

  mag1 = net_out_mag[0]; mag2 = net_out_mag[1]; mag3 = net_out_mag[2]; mag4 = net_out_mag[3]; mag5 =
net_out_mag[4];
  mag6 = net_out_mag[5]; mag7 = net_out_mag[6]; mag8 = net_out_mag[7]; mag9 = net_out_mag[8]; mag10 =
net_out_mag[9];
  mag11 = net_out_mag[10]; mag12 = net_out_mag[11]; mag13 = net_out_mag[12]; mag14 = net_out_mag[13];
mag15 = net_out_mag[14];
  mag16 = net_out_mag[15]; mag17 = net_out_mag[16]; mag18 = net_out_mag[17]; mag19 = net_out_mag[18];
mag20 = net_out_mag[19];

  pha1 = net_out_pha[0]; pha2 = net_out_pha[1]; pha3 = net_out_pha[2]; pha4 = net_out_pha[3]; pha5 =
net_out_pha[4];
  pha6 = net_out_pha[5]; pha7 = net_out_pha[6]; pha8 = net_out_pha[7]; pha9 = net_out_pha[8]; pha10 =
net_out_pha[9];
  pha11 = net_out_pha[10]; pha12 = net_out_pha[11]; pha13 = net_out_pha[12]; pha14 = net_out_pha[13]; pha15
= net_out_pha[14];
  pha16 = net_out_pha[15]; pha17 = net_out_pha[16]; pha18 = net_out_pha[17]; pha19 = net_out_pha[18]; pha20
= net_out_pha[19];

/* FIND PHASE CROSSOVER INDICES */

index = 0;
while (net_out_pha[index] > desired_phase_margin)
  {
  pha_cross_ind1 = index;
  index = index + 1;
  }

index = 0;
while (net_out_pha[index] > (-360.0 - desired_phase_margin))
  {
  pha_cross_ind2 = index;
  index = index + 1;
  }

  gain_margin1 = net_out_mag[pha_cross_ind1] - desired_gain_margin;
  gain_margin2 = net_out_mag[pha_cross_ind2] - desired_gain_margin;

  if (gain_margin1 > gain_margin2)
   gain_margin = gain_margin1;
  else
   gain_margin = gain_margin2;

  fb_gain = pow(10.0,(-gain_margin/20.0));
  fb_gaindb = 20.0*log10(fb_gain);

/*FIND THE GAIN CROSSOVER POINTS WITH THE FBGAIN APPLIED */
index = 0;
```

```
while ((fb_gaindb + net_out_mag[index]) < desired_gain_margin)
  {
  mag_cross_ind1 = index;
  index = index + 1;
  }

index = 19;
while ((fb_gaindb + net_out_mag[index]) < desired_gain_margin)
  {
  mag_cross_ind2 = index;
  index = index - 1;
  }

/*DETERMINES THE NEEDED DELAY SAMPLES FOR EACH CROSSOVER POINT AND
AVERAGES DELAY */
delay_samples1 = 0;

if (net_out_pha[mag_cross_ind1] > desired_phase_margin)
  {
  check_pha1 = net_out_pha[mag_cross_ind1];
  while(check_pha1 > desired_phase_margin)
            {
            delay_samples1 = delay_samples1 - 1;
            phase_delay = delay_samples1*360.0/(cont_SampFreq/odd_space_freq[mag_cross_ind1]);
            check_pha1 = net_out_pha[mag_cross_ind1] + phase_delay;
            }
  }
else
  {
  check_pha1 = net_out_pha[mag_cross_ind1];
  while(check_pha1 < desired_phase_margin)
            {
            delay_samples1 = delay_samples1 + 1;
            phase_delay = delay_samples1*360.0/(cont_SampFreq/odd_space_freq[mag_cross_ind1]);
            check_pha1 = net_out_pha[mag_cross_ind1] + phase_delay;
            }
  }

delay_samples2 = 0;

if (net_out_pha[mag_cross_ind2] > (-360-desired_phase_margin))
  {
  check_pha2 = net_out_pha[mag_cross_ind2];
  while(check_pha2 > (-360-desired_phase_margin))
            {
            delay_samples2 = delay_samples2 -1;
            phase_delay = delay_samples2*360.0/(cont_SampFreq/odd_space_freq[mag_cross_ind2]);
            check_pha2 = net_out_pha[mag_cross_ind2] + phase_delay;
            }
  }
else
  {
  check_pha2 = net_out_pha[mag_cross_ind2];
  while(check_pha2 < (-360-desired_phase_margin))
```

```
            {
            delay_samples2 = delay_samples2 + 1;
            phase_delay = delay_samples2*360.0/(cont_SampFreq/odd_space_freq[mag_cross_ind2]);
            check_pha2 = net_out_pha[mag_cross_ind2] + phase_delay;
            }
  }

  delay_samples = ((delay_samples1 + delay_samples2)/2) + 3;

  for(index = 0; index < OUT_LAY_NODE; index++)
    {
            modified_mag[index] = net_out_mag[index] + fb_gaindb;
            modified_pha[index] = net_out_pha[index] +
delay_samples*360.0/(cont_SampFreq/odd_space_freq[index]);
    }

index = 0;
while(modified_mag[index] < desired_gain_margin)
  {
  mc1 = index;
  index = index + 1;
  }
index = 19;
while(modified_mag[index] < desired_gain_margin)
  {
  mc2 = index;
  index = index -1;
  }
pm1 = modified_pha[mc1];
pm2 = (-360-modified_pha[mc2]);
atmag1 = modified_mag[mc1];
atmag2 = modified_mag[mc2];

index = 0;
while(modified_pha[index] > 0 )
  {
  pc1 = index;
  index = index + 1;
  }
index = 19;
while(modified_pha[index] < -360)
  {
  pc2 = index;
  index = index - 1;
  }
gm1 = modified_mag[pc1];
gm2 = modified_mag[pc2];
atpha1 = modified_pha[pc1];
atpha2 = modified_pha[pc2];

  exec_time1 = time_elapsed(TMR1, count1);  /* calculate execution time */
  end_isr_t1();
}
```

B ADAPTIVE FEEDBACK SIMULATION M-FILES

This simulation is carried out in two parts via two separate m-files. The first m-file sets up the self excited system and then simulates the multi-tone identification procedure just as it occurs in the experiment. The resulting identification is then saved to a *.mat file and used by the second part of the simulation. The second m-file loads the identified control-to-error path and performs adaptive feedback control on the limit cycling system. Both files are included below.

```
clear
close all

%THIS FILE STARTS BY CREATING A PLANT THAT IS CALLED Gp AND IS THE ACOUSTIC
%PLUS ACTUATOR PATH THAT COMES BEFORE THE CONTROL PRESSURE MEETS THE SELF EXCITED PRESSURE

%THE ACOUSTIC PART OF THE PLANT MENTIONED ABOVE IS USED IN A SELF EXCITED LOOP THAT
CONTAINS
%A BANDPASS FILTER (FOR AVOIDING ALIASING) THE FLAME DYNAMICS ( A LOW PASS FILTER) AND
%A NONLINEARITY (tanh)

%AFTER THE SYSTEM LIMIT CYCLES, A SYSTEM ID ROUTINE IS USED TO GET GpHAT.
%FIRST A SET OF TONES ARE INJECTED INTO THE SYSTEM ANDTHE INPUT FFT IS DIVIDED BY THE
OUTPUT
%FFT GIVING THE MAG AND PHASE OF THE TF INCLUDING THE NONLINEARITY
%THEN INVFREQZ IS USED TO GENERATE THE PLANT MODEL FROM THE DATA ABOVE.
%I THEN CHECK THE PLANT MODEL AGAINST THE LINEAR PART OF THE CLOSED LOOP SYSTEM???
%USED IN THE FESE5 SIMULATION

samp_freq = 1600;
max_iter = 20000;
fft_size = 4096;
freq = [0:samp_freq/fft_size :(samp_freq/2)];
omega = 2*pi*freq;

tspace = 1/samp_freq;
tinit = 0.00;
tfinal = max_iter/samp_freq;
time_vec = [tinit:tspace:tfinal];

%NOW MAKE A Ga THAT SEEMS REASONABLE BASED ON WHAT WILL SAID
%HOT TUBE IS AT A RES. OF ABOUT 175 AND 2% DAMPING
Ga_zeros = 2*pi*[];
Ga_poles = 2*pi*[-3.5-175*i;-3.5+175*i];
Ga_gain = -300000;
[Ga_num,Ga_den] = zp2tf(Ga_zeros, Ga_poles, Ga_gain);
[Gad_num,Gad_den] = c2dm(Ga_num,Ga_den,tspace,'zoh');
    PGA = length(Gad_den);
    PGAN = length(Gad_num);

[Gad_mag,Gad_phase] = dbode(Gad_num,Gad_den,1/samp_freq,2*pi*freq);
figure
subplot(211),plot(freq,20*log10(Gad_mag))
title('Ga')
subplot(212),plot(freq,Gad_phase)

%MAKE THE "PLANT" WHICH IS THE ACOUSTICS ABOVE (ALSO USED IN THE SE LOOP)
%BUT WITH ACTUATOR DYNAMICS ADDED, IN THE FORM OF A DELAY
%CALLING IT CONTROL TO ERROR

num_c2e = [0 0 Gad_num];
NN = length(num_c2e);
den_c2e = [Gad_den 0 0];
N = length(den_c2e);
```

```
[c2e_mag,c2e_phase] = dbode(num_c2e,den_c2e,1/samp_freq,2*pi*freq);
figure
subplot(211),plot(freq,20*log10(c2e_mag))
title('c2e =  acoustics + delay')
subplot(212),plot(freq,c2e_phase)

%THIS IS THE FLAME DYNAMICS.  A LOW PASS FILTER AT 200 HZ
Gf_zeros = 2*pi*[];
Gf_poles = 2*pi*[-200];
Gf_gain = 500;
[Gf_num,Gf_den] = zp2tf(Gf_zeros, Gf_poles, Gf_gain);
[Gfd_num,Gfd_den] = c2dm(Gf_num,Gf_den,tspace,'zoh');
    NGF = length(Gfd_den);
    NGFN = length(Gfd_num);

[Gfd_mag,Gfd_phase] = dbode(Gfd_num,Gfd_den,1/samp_freq,2*pi*freq);
figure
subplot(211),plot(freq,20*log10(Gfd_mag))
title('GF')
subplot(212),plot(freq,Gfd_phase)

%OPEN LOOP AND CLOSED LOOP SYSTEM
[OLd_num,OLd_den] = series(Gad_num,Gad_den,Gfd_num,Gfd_den);
[OLd_mag,OLd_phase] = dbode(OLd_num,OLd_den,tspace,omega);
figure
subplot(211),plot(freq,20*log10(OLd_mag))
title('digital open loop bode self excited')
grid
subplot(212),plot(freq,OLd_phase)
grid

[CL_num,CL_den] = feedback(Gad_num,Gad_den,Gfd_num,Gfd_den,1);

figure
pzmap(CL_num,CL_den)
zgrid
title('digital closed loop dynamics')

%CREATE THE MULTI-SIN INPUT SIGNAL AND FILTER IT WITH THE PLANT
%BEFORE INJECTING IT INTO THE
start_id = 3500;

n = [1:max_iter+1];
idsins = 20000*( ...
sin(2*pi*(150/samp_freq)*n)' + ...
sin(2*pi*(152/samp_freq)*n)' + ...
sin(2*pi*(154/samp_freq)*n)' + ...
sin(2*pi*(156/samp_freq)*n)' + ...
sin(2*pi*(158/samp_freq)*n)' + ...
sin(2*pi*(160/samp_freq)*n)' + ...
sin(2*pi*(162/samp_freq)*n)' + ...
sin(2*pi*(164/samp_freq)*n)' + ...
sin(2*pi*(166/samp_freq)*n)' + ...
...
sin(2*pi*(178/samp_freq)*n)' + ...
sin(2*pi*(180/samp_freq)*n)' + ...
sin(2*pi*(182/samp_freq)*n)' + ...
sin(2*pi*(184/samp_freq)*n)' + ...
sin(2*pi*(186/samp_freq)*n)' + ...
sin(2*pi*(188/samp_freq)*n)' + ...
sin(2*pi*(190/samp_freq)*n)' + ...
sin(2*pi*(192/samp_freq)*n)' + ...
sin(2*pi*(194/samp_freq)*n)' + ...
sin(2*pi*(196/samp_freq)*n)' + ...
sin(2*pi*(198/samp_freq)*n)' + ...
sin(2*pi*(200/samp_freq)*n)');

idsins(1:start_id) = 0;
```

```
%-------------------------------------------------------------------------

dig_in = zeros(length(time_vec),1);
dig_in(1) = 100;

%d IS THE NONLIN AMPLITUDE, f IS THE SEVERITY
d = 4e5;
f = .2e-5;
noise_gain = 5000;

Gad_Pout(length(time_vec),1) = 0;
Gfd_Qout(length(time_vec),1) = 0;
input_Gfd(length(time_vec),1) = 0;
input_Gad(length(time_vec),1) = 0;
plant(length(time_vec),1) = 0;

input_Gad(PGA+1,1) = 1000;

for index = (PGA+NN+1):length(time_vec),

      plant(index) = (-den_c2e(1,2:N)*flipud(plant(index-N+1:index-1))) +
num_c2e*flipud(idsins(index-NN+1:index));

      Gad_Pout(index) = (-Gad_den(1,2:PGA)*flipud(Gad_Pout(index-PGA+1:index-1))) +
Gad_num*flipud(input_Gad(index-PGAN+1:index));
      input_Gfd(index) = Gad_Pout(index) + plant(index);

      Gfd_Qout(index) = (-Gfd_den(1,2:NGF)*flipud(Gfd_Qout(index-NGF+1:index-1))) +
Gfd_num*flipud(input_Gfd(index-NGFN+1:index));
       input_Gad(index+1) = d*tanh(f*Gfd_Qout(index)) + noise_gain*(rand-0.5);

end

figure
plot(Gad_Pout)
title('time response of digital simulation')

figure
psd(Gad_Pout(start_id:length(time_vec)),fft_size,1/tspace)
title('digital simulation of same closed loop system')

%-------------------------------------------------------------------------

figure
cohere(idsins(start_id:length(time_vec)),Gad_Pout(3500:length(time_vec)),fft_size,samp_fre
q)

%NOW COMPUTE A FRF AT 2 HZ INTERVALS CORRESPONDING TO THE IDSINS FREQUENCIES
%BY DIVIDING THE OUTPUT FFT BY THE INPUT FFT.
mod_fft_size = 800;

[Gphat_data,freq_mod] =
tfe(idsins(start_id:length(time_vec)),input_Gfd(start_id:length(time_vec)),mod_fft_size,sa
mp_freq);

figure
subplot(211),plot(freq_mod,20*log10(Gphat_data),'*')
title('')
subplot(212),plot(freq_mod,(180/pi)*unwrap(angle(Gphat_data)),'*')

%-------------------------------------------------------------------------

%GENERATE PIECES OF DATA THAT HAVE HIGH COHERENCE THAT OCCURED
%AT THE ID SINS
%MAKE THESE INDICES MATCH THE TONES I'M PUTTING IN IN IDSINS

id_freq_vec = [freq_mod(76:83)' freq_mod(91:101)'];
c2e_dat=[Gphat_data(76:83).' Gphat_data(91:101).'];

%CHANGE THESE THINGS AS NEEDED TO GET A BETTER FIT
```

```
[mod_num,mod_den] = invfreqz(c2e_dat, 2*pi*id_freq_vec/samp_freq,4,4);
[test_mag,test_phase,omega] = dbode(mod_num,mod_den,1/samp_freq,2*pi*[120:240]);

mod_freq = omega/(2*pi);
figure
subplot(211),plot(mod_freq,20*log10(test_mag),'r')
hold on
subplot(212),plot(mod_freq,mod(test_phase,-360),'r')
hold on
subplot(211),plot(id_freq_vec,20*log10(abs(c2e_dat)),'*')
title('sin sweep data model in red')
subplot(212),plot(id_freq_vec, mod((180/pi)*angle(c2e_dat),-360),'*')
hold off

[z,p,k] = tf2zp(mod_num,mod_den);
figure
pzmap(p,z)
title('model dynamics')
zgrid

num_c2e_hat = mod_num;
den_c2e_hat = mod_den;

save tfs5 Gad_num Gad_den Gfd_num Gfd_den num_c2e den_c2e num_c2e_hat den_c2e_hat d f
```

The following begins the second portion of the simulation.

```
clear
close all

%FILTERED E ALG. SIMULATION

%THIS SIMULATION STARTS TO REALLY SIMULATE WHAT GOES ON IN THE REAL SYSTEM
%I USE (IN ANOTHER FILE) A STABLE SYSTEM ID OF THE SELF EXCITED LOOP
%WHERE THE ACOUSTIC PLANT IS MORE HEAVILY DAMPED THAN THE MODEL SYSTEM BECAUSE
%THE MODEL SYSTEM IS CLOSED LOOP AND LIMIT CYCLING

samp_freq = 1600;
max_iter = 20000;
dist_freq = 173;
noise_gain = 5000;

tinit = 0.0;
tfinal = max_iter/samp_freq;
tspace = 1/samp_freq;
time_vec = [tinit:tspace:tfinal];

fft_size = 2048;
no_avgs = 2;
freq_vec = [0:samp_freq/fft_size :(samp_freq/2)];
omega = 2*pi*freq_vec;

n = [1:max_iter];

%LOAD IN THE FILE THAT IS CREATED BY MODSIM5
%IT CONTAINS THE GA, GF, NUM-C2E AND NUM-C2E-HAT AND NONL. PARAMS
load tfs5

%CREATE SELF EXCITED SYSTEM

%GA BASED ON KNOWLEDGE OF TUBE (manually enter this if we want to change it)
shift_hz = 0;

oldGad_num = Gad_num;  oldGad_den = Gad_den;
[z,p,k] = tf2zp(Gad_num,Gad_den);
freq_shift = shift_hz*((2*pi)/samp_freq);
```

```
    p(1) = abs(p(1))*(cos(angle(p(1))+freq_shift) + i*sin(angle(p(1))+freq_shift));
   p(2) = abs(p(1))*(cos(angle(p(1))+freq_shift) - i*sin(angle(p(1))+freq_shift));
[Gad_num,Gad_den] = zp2tf(z,p,k);

PGA = length(Gad_den);
PGAN = length(Gad_num);

NGF = length(Gfd_den);
NGFN = length(Gfd_num);

%d IS THE NONLIN AMPLITUDE, f IS THE SEVERITY

%CONTROL TO ERROR PATH - NEED TO CHANGE THIS IF gA IS SHIFTING HZ ABOVE
if shift_hz ~= 0
   old_num_c2e = num_c2e;
   old_den_c2e = den_c2e;
    num_c2e = [0 0 Gad_num];
    den_c2e = [Gad_den 0 0];

    NN = length(num_c2e);
    N = length(den_c2e);
else
    NN = length(num_c2e);
    N = length(den_c2e);
end

%CONTROL TO ERROR PATH ESTIMATE
%CAN TRY TO FIX THE ID BY SHIFTING IT
fix_shift = 0;
old_num_c2e_hat = num_c2e_hat;  old_den_c2e_hat = den_c2e_hat;
[z,p,k] = tf2zp(num_c2e_hat,den_c2e_hat);
freq_shift = fix_shift*((2*pi)/samp_freq);
   p(1) = abs(p(1))*(cos(angle(p(1))+freq_shift) + i*sin(angle(p(1))+freq_shift));
   p(2) = abs(p(1))*(cos(angle(p(1))+freq_shift) - i*sin(angle(p(1))+freq_shift));
   p(3) = abs(p(3))*(cos(angle(p(3))+freq_shift) + i*sin(angle(p(3))+freq_shift));
   p(4) = abs(p(3))*(cos(angle(p(3))+freq_shift) - i*sin(angle(p(3))+freq_shift));
[num_c2e_hat,den_c2e_hat] = zp2tf(z,p,k);

PN = length(num_c2e_hat);
P = length(den_c2e_hat);

%ADAPTIVE FILTER
start_at = 5000;
mu = 0.00;
real_mu = 0.00001;
M = 2;
w_hats = [zeros(size(1:M))]';

%INITIALIZE AND POPULATE
desir = 0;
ref_hat(max_iter,1) = 0;
filt_x(1,max_iter) = 0;
cont(max_iter,1) = 0;
plant(max_iter,1) = 0;
y(max_iter,1) = 0;
plant_hat(max_iter,1) = 0;
Pout_vec(max_iter) = 0;
Gad_Pout(max_iter,1) = 0;
Gfd_Qout(max_iter,1) = 0;
input_Gfd(max_iter,1) = 0;
input_Gad(max_iter,1) = 0;
wt_spc = 10;
w_hats_matrix(M,max_iter/wt_spc) = 0;
w_hats_matrix_freq(fft_size,max_iter/wt_spc) = 0;
mat_ind = 1;

scale_factor = 1.4e-6;
input_Gad(M+N+P,1) = 10000;

%-----------------------------------------------------------------
```

```
for index = (M+N+P):max_iter,

  Gad_Pout(index) = (-Gad_den(1,2:PGA)*flipud(Gad_Pout(index-PGA+1:index-1))) +
Gad_num*flipud(input_Gad(index-PGAN+1:index));
  Pout_vec(index) = Gad_Pout(index);

  dist(index) = Pout_vec(index)*scale_factor;

  if index == start_at
     mu = real_mu;
  end

   plant(index) = (-den_c2e(1,2:N)*flipud(plant(index-N+1:index-1))) +
num_c2e*flipud(cont(index-NN:index-1));
    y(index) = dist(index) + plant(index);
    err(index) = desir - y(index);
   plant_hat(index) = (-den_c2e_hat(1,2:P)*flipud(plant_hat(index-P+1:index-1))) +
num_c2e_hat*flipud(cont(index-PN:index-1));
    ref_hat(index) = y(index) - plant_hat(index);
    cont(index) = w_hats'*flipud(ref_hat(index-M+1:index));
   filt_x(index) = (-den_c2e_hat(1,2:P)*flipud(filt_x(index-P+1:index-1)')) +
num_c2e_hat*flipud(ref_hat(index-PN+1:index));

   w_hats = w_hats + mu*flipud(filt_x(index-M:index-1)')*err(index);


  input_Gfd(index) = y(index)/scale_factor;

  Gfd_Qout(index) = (-Gfd_den(1,2:NGF)*flipud(Gfd_Qout(index-NGF+1:index-1))) +
Gfd_num*flipud(input_Gfd(index-NGFN+1:index));
  input_Gad(index+1) = d*tanh(f*Gfd_Qout(index)) + noise_gain*(rand-0.5);


  if rem(index-1,wt_spc)==0
     w_hats_matrix(:,mat_ind) = w_hats;
     mat_ind = mat_ind + 1;
  end

  if abs(y(index))>500
     max_iter = index
     break
  end

  if abs(y(index))> 8;
     mu = 0.00;
  end

end


%-------------------------------------------------------------

% CORRECT FOR ALGORITHM DELAYS IN DISPLAYING OF THE DBODE PLOTS
num_c2e = [0 num_c2e];
den_c2e = [den_c2e 0];
N = length(den_c2e);
num_c2e_hat = [0 num_c2e_hat];
den_c2e_hat = [den_c2e_hat 0];
P = length(den_c2e_hat);
Gad_num = [0 Gad_num];
Gad_den = [Gad_den 0];
PGA = length(Gad_den);
PGAN = length(Gad_num);

%W, GP and GPHAT IN FREQ DOMAIN
w_hats_freq = fft(w_hats,fft_size);
[c2e_mag,c2e_phase] = dbode(num_c2e,den_c2e,tspace,omega);
[c2e_mag_hat,c2e_phase_hat] = dbode(num_c2e_hat,den_c2e_hat,tspace,omega);
    c2e_complex = c2e_mag.*cos(c2e_phase*(pi/180)) + i*c2e_mag.*sin(c2e_phase*(pi/180));
    c2e_hat_complex = c2e_mag_hat.*cos(c2e_phase_hat*(pi/180)) +
i*c2e_mag_hat.*sin(c2e_phase_hat*(pi/180));
```

```
w_hats_num = w_hats';
w_hats_den = [1 zeros(1,length(w_hats)-1)];

%FORM OF ADAPTIVE FILTER REQUIRED FOR "OPTIMAL" CONTROL
    [temp5_num,temp5_den] = series(Gad_num,Gad_den,Gfd_num,Gfd_den);
   [temp6_num,temp6_den] = series(temp5_num,temp5_den,den_c2e,num_c2e);
   [temp_num,temp_den] = feedback(temp6_num,temp6_den,num_c2e_hat,den_c2e_hat,-1);
afopt_num = -temp_num;
afopt_den = temp_den;
[afopt_mag,afopt_phase] = dbode(afopt_num,afopt_den,tspace,omega);

%ANOTHER WAY TO LOOK AT OPTIMAL (UPPER LOOP EQUALS NEGATIVE OF LOWER LOOP)
[temp2_num,temp2_den] = feedback(w_hats_num,w_hats_den,num_c2e_hat,den_c2e_hat,-1);
[temp4_num,temp4_den] = series(num_c2e,den_c2e,temp2_num,temp2_den);
[check_mag,check_phase] = dbode(-temp4_num,temp4_den,1/samp_freq,omega);

%LOOK AT THE OPEN LOOP CONTROL SYSTEM TO SEE IF BODE PREDICTS APPROPRIATE GAIN/PHASE
%THIS MAY OR MAY NOT BE RIGHT
[seOL_num,seOL_den] = series(Gad_num,Gad_den,Gfd_num,Gfd_den);
[seCL_num,seCL_den] = feedback(1,1,seOL_num,seOL_den,1);

[conCL_num,conCL_den] = feedback(1,1,temp4_num,temp4_den,1);
disp('control poles')
abs(roots(conCL_den))

[sysOL_num,sysOL_den] = series(seOL_num,seOL_den,conCL_num,conCL_den);
[sysCL_num,sysCL_den] = feedback(1,1,sysOL_num,sysOL_den,1);


[seOL_mag,seOL_phase] = dbode(seOL_num,seOL_den,tspace,omega);
[sysOL_mag,sysOL_phase] = dbode(sysOL_num,sysOL_den,tspace,omega);
[sysCL_mag,sysCL_phase] = dbode(sysCL_num,sysCL_den,tspace,omega);

%[seCL_mag,seCL_phase] = dbode(seCL_num,seCL_den,tspace,omega);
%[temp3_num,temp3_den] = series(seCL_num,seCL_den,num_c2e,den_c2e);
%[OL_num,OL_den] = series(temp2_num,temp2_den,temp3_num,temp3_den);
%[CL_num,CL_den] = feedback(1,1,OL_num,OL_den,1);
%[OL_mag,OL_phase] = dbode(OL_num,OL_den,tspace,omega);
%[CL_mag,CL_phase] = dbode(CL_num,CL_den,tspace,omega);

%PLOTTING
figure
subplot(211),plot(freq_vec,20*log10(sysOL_mag))
title('open loop system bode - use only if control poles are stable')
subplot(212),plot(freq_vec,sysOL_phase)

figure
subplot(211),pzmap(1,seCL_den)
zgrid
title('self excited poles - no control')
subplot(212),pzmap(sysCL_num,sysCL_den)
title('closed loop dynamics')
zgrid

%CHECK CONVERGENCE
figure
plot(n,y)
title('PERFORMANCE: Error Microphone')
ylabel('Mag')
xlabel('n')
tax = axis;

%CHECK CONTROL PERFORMANCE WITH ORIGINAL PLANT VS. CONTROLLED PLANT (LAST X ELEMENTS)
fft_start = 1000;
    figure
   dist_psd = psd(dist(fft_start:start_at),fft_size,samp_freq);
   plot(freq_vec,10*log10(dist_psd),'b:')

    y_psd = psd(dist((max_iter - no_avgs*fft_size):max_iter),fft_size,samp_freq);
    hold on
    plot(freq_vec,10*log10(y_psd),'r')
```

```
    hold off
   title('')
   ylabel('dB')
   xlabel('Freq.(Hz)')
   grid

%CHECK DEGREE THAT THE SYS_ID WAS OFF FROM THE ACTUAL
figure
    subplot(311)
    hold on
   plot(freq_vec, (c2e_mag));
   ylabel('linear units')
   title('SYS ID : red is c2e_hat from sin sweep yellow is actuator only')
   hold off
    subplot(312)
    hold on
    plot(freq_vec, (180/pi)*unwrap(c2e_phase*(pi/180))-720);
    hold off

    subplot(311)
    hold on
    plot(freq_vec, (c2e_mag_hat), 'r');
    hold off
    subplot(312)
    hold on
    plot(freq_vec, (180/pi)*unwrap(c2e_phase_hat*(pi/180))+360-1080, 'r');
   hold off

   subplot(313),plot(freq_vec, (180/pi)*unwrap(c2e_phase_hat*(pi/180)) -
((180/pi)*unwrap(c2e_phase*(pi/180))))
   grid

%OPTIMAL ADAPTIVE FILTER IN FREQ DOMAIN COMPARED TO ACTUAL
figure
subplot(211),plot(freq_vec,abs(w_hats_freq(1:(fft_size/2)+1)),'y')
hold on
plot(freq_vec,afopt_mag,'r')
ylabel('linear units')
title('yellow is actual AF, red is predicted optimal')
hold off
subplot(212),plot(freq_vec,(180/pi)*(angle(w_hats_freq(1:(fft_size/2)+1))),'y')
hold on
plot(freq_vec,afopt_phase,'r')
hold off

%try looking at optimal another way (control loop frf compared to SE loop frf witha minus
sign)
figure
subplot(211),plot(freq_vec,seOL_mag,'r')
hold on
plot(freq_vec,check_mag,'y')
title('red is self excited open loop, yellow is -Gp*w/(1+gphat*W)')
hold off
subplot(212),plot(freq_vec,seOL_phase,'r')
hold on
plot(freq_vec,check_phase,'y')
title('phase')
hold off

%3-D PLOTS THE ADAPTIVE FILTER WITH TIME COMPARED TO THE OPTIMAL ADAPTIVE FILTER
%for crap_ind = 1:(max_iter/wt_spc)
%   crap_mat(:,crap_ind) = afopt_mag;
%end
%w_hats_matrix_freq = fft(w_hats_matrix,fft_size);
%figure
%surf([1:wt_spc:max_iter],freq_vec,abs(w_hats_matrix_freq(1:(fft_size/2)+1,:)))
%hold on
%mesh([1:wt_spc:max_iter],freq_vec,crap_mat)
%hold off
%view(130,40)
%xlabel('time')
```

```
%ylabel('freq')

%SHOW PATH THE MAG AND PHASE TAKES TO THE OPTIMAL SOLUTION
%YOU MUST MANUALLY ENTER THE LIMIT CYCLE FREQ
freq_ind = round((dist_freq/(samp_freq/fft_size))+1);

for crap_ind = 1:(max_iter/wt_spc)
   w_hats = w_hats_matrix(:,crap_ind)';
   w_hats_freq = fft(w_hats,fft_size);
   w_hats_mag = abs(w_hats_freq(1:(fft_size/2)+1));
   w_hats_phase = (180/pi)*(angle(w_hats_freq(1:(fft_size/2)+1)));
   mag_vec(crap_ind) = w_hats_mag(freq_ind);
   phase_vec(crap_ind) = w_hats_phase(freq_ind);

end
opt_mag = afopt_mag(freq_ind);
opt_phase = afopt_phase(freq_ind);

figure
subplot(211),plot(max_iter/wt_spc,opt_phase,'rp',max_iter/wt_spc,opt_phase+360,'rp',max_it
er/wt_spc,opt_phase-360,'rp')
hold on
text(1650,200,'Opt. Phase')
plot(phase_vec)
title('')
ylabel('Phase')
subplot(212),plot(max_iter/wt_spc,opt_mag,'rp')

hold on
text(1700,.075,'Opt. Mag.')
plot(mag_vec)
title('')
ylabel('Mag.')
xlabel('Iteration/10')

%WEIGHTS WITH TIME
figure
plot(w_hats_matrix(1,:))
hold on
plot(w_hats_matrix(2,:))
ylabel('Mag.')
xlabel('Iteration/10')
hold off
```

C TIME AVERAGED GRADIENT SIMULATION M-FILES

The following is one simulation of the time averaged gradient (TAG) algorithm as applied to a limit cycling system. The TAG in the simulation below is implemented as a consecutive weight update where each weight is updated immediately after the local gradient is computed. Alternatively, a vector update can be implemented where the vector of adaptive parameters is updated after all perturbations occur. To achieve this simulation, simply follow the commented directions. Additional weights can also be added.

```
clear
close all

%TAG ALGORITHM AND SIMULATION CREATED BY MIKE VAUDREY AT
%VIRGINIA TECH (VIRGINIA ACTIVE COMBUSTION CONTROL GROUP)
```

```
%COPYRIGHT JUNE 2000

%THIS IS THE TAG ALGORITHM BASED ON THE STEEPEST DESCENT
%METHOD OF GRADIENT SEARCHING - NEWTON'S METHOD IS ALSO
%VIABLE BUT MORE COMPUTATIONALLY INTENSIVE
%IMPLEMENTED ON A SELF EXCITED PLANT WHERE
%THE ALGORITHM UPDATES THE WEIGHTS OF THE CONTROLLER
%WHICH IS AN FIR FILTER, W1 AND W2
%NOTE THAT THIS SIMULATION ILLUSTRATES SEQUENTIAL UPDATING OF
%THE WEIGHT PARAMETERS - IT IS ALSO POSSIBLE TO UPDATE ALL
%WEIGHTS AT THE SAME TIME AFTER THE COST IS DETERMINED FROM
%EACH PERTURBATION - LOOK AT THE C-CODE FOR THE DSPACE TO
%SEE THE DIFFERENCES.

%GENERAL TIME A FREQ INFO.
samp_freq = 1600;
max_iter = 15000;
fft_size = 2048;
freq = [0:samp_freq/fft_size :(samp_freq/2)];
omega = 2*pi*freq;
tspace = 1/samp_freq;
tinit = 0.00;
tfinal = max_iter/samp_freq;
time_vec = [tinit:tspace:tfinal];

%Ga - THE (DIGITAL) ACOUSTICS OF THE SELF EXCITED LOOP
Ga_zeros = 2*pi*[];
Ga_poles = 2*pi*[-3.5-175*i;-3.5+175*i];
Ga_gain = -300000;
[Ga_num,Ga_den] = zp2tf(Ga_zeros, Ga_poles, Ga_gain);
[Gad_num,Gad_den] = c2dm(Ga_num,Ga_den,tspace,'zoh');
    PGA = length(Gad_den);
    PGAN = length(Gad_num);

%Gf - THE FLAME DYNAMICS.  A LOW PASS FILTER AT 200 HZ
Gf_zeros = 2*pi*[];
Gf_poles = 2*pi*[-200];
Gf_gain = 500;
[Gf_num,Gf_den] = zp2tf(Gf_zeros, Gf_poles, Gf_gain);
[Gfd_num,Gfd_den] = c2dm(Gf_num,Gf_den,tspace,'zoh');
    NGF = length(Gfd_den);
   NGFN = length(Gfd_num);

%MAKE A CONTROL TO ERROR PATH
%WILL TYPICALLY CONTAIN THE ACOUSTICS AS WELL AS SOME DELAY
num_c2e = 2*[0 0 0 0 0 Gad_num];
NN = length(num_c2e);
den_c2e = [Gad_den 0 0 0 0 0];
N = length(den_c2e);

%ADAPTIVE FILTER PARAMETERS
%NO_SAMP CONTROLS AVERAGE LENGTH
%DELTA CONTROLS PERTURBATION SIZE
%MU CONTROLS CONVERGENCE SPEED
no_samp = 100;
delta = -.1 %-0.1;
mu = .01*(1.4e-6)^2 % 0.01;
w_hats = [0;0];
delta_w1 = [delta;0];
delta_w2 = [0;delta];

%INITIALIZE SIMULATION VARIABLES
scale_factor = 1; % 1.4e-6;
turn_on = 5000;
M = 2;
state = 0;
temp_iter = 1;
cost1 = 0;
cost2 = 0;
vec_ind = 1;
wt_spc = 10;
```

```
w_hats_matrix(M,max_iter/wt_spc) = 0;
w_hats_matrix_freq(fft_size,max_iter/wt_spc) = 0;
mat_ind = 1;

%d IS THE NONLINEARITY AMPLITUDE (USING TANH), f IS THE SEVERITY
d = 4e5;
f = .2e-5;
noise_gain = 5000;

%POPULATE VECTORS
Gad_Pout(length(time_vec),1) = 0;
Gfd_Qout(length(time_vec),1) = 0;
input_Gfd(length(time_vec),1) = 0;
input_Gad(length(time_vec),1) = 0;
plant(length(time_vec),1) = 0;
cont(length(time_vec),1) = 0;
y(length(time_vec),1) = 0;
input_Gad(PGA+1,1) = 1000;

%-------------------------------------------------------------------------
%RUN SIMULATION LOOP

for index = (N+PGA+1):length(time_vec),

    %I.C. ON ACOUSTICS
      Gad_Pout(index) = (-Gad_den(1,2:PGA)*flipud(Gad_Pout(index-PGA+1:index-1))) +
Gad_num*flipud(input_Gad(index-PGAN+1:index));
     % input_Gfd(index) = Gad_Pout(index);

       dist(index) = Gad_Pout(index)*scale_factor;

         %CONTROL SIGNAL FILTERED BY PLANT AND ADDED TO ACOUSTIC SYSTEM OUTPUT
         plant(index) = (-den_c2e(1,2:N)*flipud(plant(index-N+1:index-1))) +
num_c2e*flipud(cont(index-NN:index-1));
           y(index) = dist(index) + plant(index);

         %ONLY TURN ON THE CONTROLLER AFTER THE INSTABILITY HAS HAD A CHANCE TO DEVELOP
         if index > turn_on

         %TAG CONTROLLER
         %PERTURB, COLLECT, ADJUST FOR EACH WEIGHT, HERE ONLY 2 ARE USED
                %-------------------------------------------------------------
                if (temp_iter == no_samp) & (state == 0)
                   cost_w1 = (1/no_samp)*sum(y((index-no_samp):index).^2);

                   w_hats = w_hats - delta_w1;
                   temp_iter = 0;
                    state = 1;
                end

                if (temp_iter == no_samp) & (state == 1)
                cost_w1minus = (1/no_samp)*sum(y((index-no_samp):index).^2);
                cost1 = (cost_w1 - cost_w1minus)/delta;

                %FOR VECTOR UPDATE REPLACE THE NEXT LINE WITH
                %w_hats = (w_hats + delta_w1) - delta_w2;
                w_hats = (w_hats + delta_w1) - mu*[cost1;0];
                temp_iter = 0;
                state = 2;
                cost_vec(1,vec_ind) = cost1;
            end

               %FOR VECTOR UPDATE, REMOVE THIS IF STATEMENT
            if (temp_iter == no_samp) & (state == 2)
                 cost_w2 = (1/no_samp)*sum(y((index-no_samp):index).^2);

                 w_hats = w_hats - delta_w2;
                 temp_iter = 0;
                 state = 3;
                end
```

```
                if (temp_iter == no_samp) & (state == 3)
                    cost_w2minus = (1/no_samp)*sum(y((index-no_samp):index).^2);

                %FOR VECTOR UPDATE REPLACE THE NEXT TWO LINES WITH
                %cost2 = (cost_w1 - cost_w2minus)/delta;
                %w_hats = (w_hats + delta_w2) - mu*[cost1;cost2];

                cost2 = (cost_w2 - cost_w2minus)/delta;
                w_hats = (w_hats + delta_w2) - mu*[0;cost2];

                temp_iter = 0;
                    state = 0;
                    cost_vec(2,vec_ind) = cost2;
                    vec_ind = vec_ind + 1;
                end

                temp_iter = temp_iter + 1;
            %-------------------------------------------------------------

            %GENERATE CONTROLLER OUTPUT
            cont(index) = w_hats'*flipud(y(index-M+1:index));
        end

        input_Gfd(index) = y(index)/scale_factor;

      %SIMULATE NONLINEAR FLAME DYNAMICS
      Gfd_Qout(index) = (-Gfd_den(1,2:NGF)*flipud(Gfd_Qout(index-NGF+1:index-1))) +
Gfd_num*flipud(input_Gfd(index-NGFN+1:index));
       input_Gad(index+1) = d*tanh(f*Gfd_Qout(index)) + noise_gain*(rand-0.5);

      %COLLECT SOME DATA FOR LATER
      if rem(index-1,wt_spc)==0
           w_hats_matrix(:,mat_ind) = w_hats;
         mat_ind = mat_ind + 1;
       end

      %STOP IF GOES UNSTABLE (LOOP)
      if abs(y(index))>2000000000 %200
          max_iter = index
          break
       end
end


%END SIMULATION LOOP
%-------------------------------------------------------------------------------
%MODIFY TRANSFER FUNCTIONS FOR AN ALGORITHM DELAY
Gad_num = [0 Gad_num];
Gad_den = [Gad_den 0];
num_c2e = [0 num_c2e];
den_c2e = [den_c2e 0];

%MOST OF THESE ARE JUST ANALYSIS PLOTS, UNCOMMENT IF YOU ARE INTERESTED
%BODE PLOTS OF Ga AND Gf
[Gad_mag,Gad_phase] = dbode(Gad_num,Gad_den,1/samp_freq,2*pi*freq);
    %figure
    %subplot(211),plot(freq,20*log10(Gad_mag))
    %title('Ga')
    %subplot(212),plot(freq,Gad_phase)

[Gfd_mag,Gfd_phase] = dbode(Gfd_num,Gfd_den,1/samp_freq,2*pi*freq);
    %figure
    %subplot(211),plot(freq,20*log10(Gfd_mag))
    %title('GF')
    %subplot(212),plot(freq,Gfd_phase)

%OPEN LOOP AND CLOSED LOOP SYSTEM
[OLd_num,OLd_den] = series(Gad_num,Gad_den,Gfd_num,Gfd_den);
[OLd_mag,OLd_phase] = dbode(OLd_num,OLd_den,tspace,omega);
    %figure
    %subplot(211),plot(freq,20*log10(OLd_mag))
```

```
    %title('digital open loop bode self excited')
    %grid
    %subplot(212),plot(freq,OLd_phase)
    %grid

[CL_num,CL_den] = feedback(Gad_num,Gad_den,Gfd_num,Gfd_den,1);

figure
pzmap(CL_num,CL_den)
zgrid
title('digital uncontrolled closed loop dynamics')

%PERFORMANCE PLOTS
figure
plot(y)
title('time response of digital simulation')

    figure
    dist_psd = psd(dist(turn_on-fft_size:turn_on),fft_size,samp_freq);
    plot(freq,10*log10(dist_psd))
    y_psd = psd(y(max_iter-fft_size:max_iter),fft_size,samp_freq);
    hold on
    plot(freq,10*log10(y_psd),'r')
    hold off
   title('PERFORMANCE:  red is controlled plant psd')
   ylabel('dB')
    grid

%LOOK AT HOW THE WEIGHTS MOVE WITH TIME
figure
plot(w_hats_matrix(1,:),'r')
hold on
plot(w_hats_matrix(2,:))
title('weights with time - w1 in red')
hold off

%HOW DOES COST CHANGE WITH TIME
figure
plot(cost_vec(1,:),'r')
hold on
plot(cost_vec(2,:),'b')
title('costs red is one')
```

VITA

Michael A. Vaudrey

Michael Vaudrey was born in Franklin, Virginia in 1972. After moving to Greenville, South Carolina and again to Columbia, he achieved the rank of Eagle Scout and graduated with high honors from Spring Valley High School in 1990. Mike spent his first two summers after high school graduation working as a manufacturing shop hand at Patterson Fan Company. Beginning his Bachelor's degree in Mechanical Engineering at Virginia Tech in 1990, he spent three semesters in school before starting a co-op program with Michelin Americas Research and Development Corporation. After four semesters of work and five more semesters of class, Mike graduated Magna Cum Laude in 1995. Immediately following commencement he began his Master's degree program in Mechanical Engineering also at Virginia Tech. His thesis topic was entitled "A Novel Approach to Multiple Reference Frequency Domain Adaptive Filtering" and it was successfully defended in 1996. Following graduation Mike became an owner and vice-president of Adaptive Technologies, Inc., a high-tech research and development company located in Blacksburg, Virginia. In the Fall of 1998, Mike began his Ph.D. program (part-time) in Mechanical Engineering while concurrently running and working for his business. Following graduation in 2001, Mike plans to continue with Adaptive Technologies, Inc.